SYNTHESIS AND STRUCTURAL CHARACTERIZATION OF VARIOUS INORGANIC PHOSPHATES, BORATES AND BOROPHOSPHATES

by

SEVİM DEMİRÖZÜ ŞENOL

THESIS SUBMITTED TO
THE GRADUATE SCHOOL OF NATURAL AND APPLIED SCIENCES
OF
THE ABANT IZZET BAYSAL UNIVERSITY
IN PARTIAL FULFILLMENT OF THE REQUIREMENTS FOR THE DEGREE
OF
DOCTOR OF PHILOSOPHY
IN
THE DEPARTMENT OF CHEMISTRY

AUGUST 2010

Approval of the Graduate School of Natural and Applied Sciences

Prof.Dr. Nihat ÇELEBİ
Director

I certify that this thesis satisfies all the requirements as a thesis for the degree of Doctor of Philosophy.

Prof.Dr. Çetin BOZKURT
Head of Department

This is to certify that we have read this thesis and that in our opinion it is fully adequate, in scope and quality, as a thesis for the degree of Doctor of Philosophy.

Prof.Dr. Ayşe MORKAN
Supervisor

Examining Committee Members

1. Prof.Dr. Ceyhan KAYRAN .....
2. Prof.Dr. Resul ERYİĞİT .....
3. Prof.Dr. Ayşe MORKAN .....
4. Assoc.Prof.Dr. Halil GÜLER .....
5. Assoc.Prof.Dr. Sefa DURMUŞ .....

ABSTRACT

SYNTHESIS AND STRUCTURAL CHARACTERIZATION OF VARIOUS INORGANIC PHOSPHATES, BORATES AND BOROPHOSPHATES

Demirözü Şenol, Sevim
Ph.D., Department of Chemistry
Supervisor: Prof. Dr. Ayşe Morkan

August 2010, 165 pages

This thesis covers the preparation and characterization of some novel compounds namely magnesium transition metal borates, lithium lanthanide oxyphosphates, lithium sodium lanthanide oxyphosphates, rare earth oxyapatites and lanthanide borate phosphates. Solid state method was employed for the synthesis of the desired materials. The characterization of the products was investigated by X-ray Powder Diffraction (XRPD), Fourier Transform Infrared Spectroscopy (FT-IR), Scanning Electron Microscopy (SEM) and Thermogravimetric Analysis-Differential Thermal Analysis (TG/DTA) methods.

In the first part of this thesis, $MgNi_2(BO_3)_2$, $MgCo_2(BO_3)_2$, $Mg_2Ni(BO_3)_2$ and $Mg_2Co(BO_3)_2$ compounds were prepared through the following solid state reactions at 900^oC for 48h.

$$2M(NO_3)_2\,6.H_2O_{(s)} + MgO_{(s)} + 2H_3BO_{3(s)} \rightarrow \mathbf{MgM_2(BO_3)_{2(s)}} + 4NO_{2(g)} + 15H_2O_{(g)} + O_{2(g)}$$

(M: Ni, Co)

$$M(NO_3)_2.6H_2O_{(s)} + 2MgO_{(s)} + 2H_3BO_{3(s)} \rightarrow \mathbf{Mg_2M(BO_3)_{2(s)}} + 2NO_{2(g)} + 9H_2O_{(g)} + 1/2\ O_{2(g)}$$

(M: Ni, Co)

It was found that all these compounds crystallized in the orthorhombic system and isostructural with the kotoite type of compounds, $M_3(BO_3)_2$ (M: Mg, Ni, Co). It was also detected that these compounds were thermodynamically stable with 20-1000^oC using thermal analysis technique.

In the second part, the synthesis of new oxyphosphates of the type Li_2LnOPO_4 (Ln: Nd, Gd, Dy), which were not reported before have been done through the following solid state reactions at 1000^oC.

$$Ln_2O_{3(s)} + 2Li_2CO_{3(s)} + 2(NH_4)_2HPO_4(s) \rightarrow \mathbf{2Li_2LnOPO_{4(s)}} + 4NH_{3(g)} + 2CO_{2(g)} + 3H_2O_{(g)}$$

Examination of the X-ray powder diffraction data and Infrared spectra of the products showed the existence of Li_2NdOPO_4, Li_2GdOPO_4, Li_2DyOPO_4 compounds which have an orthorhombic crystal structures with the refined unit cell parameters of a=14.865(1), b=10.734(2), c=13.231(1); a=14.686(3), b=10.634(5) c=13.047(9); a=14.554(1), b=10.589(8), c= 12.926(2) Å, respectively.

In the third part of this study, $LiNaNdOPO_4$, $LiNaGdOPO_4$, $LiNaDyOPO_4$, have also been prepared and indexed in orthorhombic system with the refined unit cell parameters a=14.903(8), b=10.861(3), c=13.247(1); a =14.745(0), b=10.651(6), c=13.096(8); a= 14.622(2), b=10.581(0), c= 13.018(2) Å, respectively. The thermal

analysis (TG/DTA) of the compounds, Li_2LnOPO_4 and $LiNaLnOPO_4$ (Ln: Nd, Gd, Dy) showed that all these compounds were stable up to1100^oC.

In the fourth part of this study were investigated using different rare earths to obtain $Ca_8Ln_2(PO_4)_6O_2$ (Ln: Nd, Gd, Dy) the solid state reactions of Ln_2O_3 with $CaHPO_4$ and $CaCO_3$ (ratio:1:6:2) at different temperatures.

In the last part, the attempt to prepare rare earth borate phosphates, Ln_2O_3, (Ln:Nd, Gd, Dy) B_2O_3 and $(NH_4)_2HPO_4$ were done through the solid state reactions of $2Ln_2O_3 + B_2O_3 + 2(NH_4)_2HPO_4 \longrightarrow 2Ln_2(BO_3)(PO_4) + 4NH_3 + 3H_2O$

Key words: X-ray Powder Diffraction, Fourier Transform Infrared Spectroscopy, Scanning Electron Microscopy, Thermogravimetric/Differential Thermal Analysis, Metal Borates, Oxyphosphates, Apatite, Rare Earths, Borophosphates.

ÖZET

ÇEŞİTLİ ANORGANİK FOSFATLARIN, BORATLARIN VE BORFOSFATLARIN SENTEZİ VE YAPISAL KARAKTERİZASYONU

Demirözü Şenol, Sevim
Doktora, Kimya Bölümü
Tez Danışmanı: Prof.Dr. Ayşe Morkan

Ağustos 2010, 165 sayfa

Bu tez, magnezyum geçiş metal boratları, lityum lantanit oksifosfatlar, lityum sodyum lantanit oksifosfatlar, nadir toprak oksiapatitler ve lantanit borat fosfatları olarak adlandırılan bazı yeni bileşiklerin hazırlanması ve karakterizasyonunu kapsamaktadır. Hedeflenen malzemelerin sentezlenmesinde katı hal metodu kullanılmıştır. Ürünlerin karakterizasyonu, X-ışını Toz Kırınımı (XRD), Kızılötesi spektrumu (FT-IR), Taramalı Elektron Mikroskopu (SEM) ve Termogravimetrik analiz-diferansiyal ısısal analiz (TG/DTA) yöntemleri ile incelendi.

Bu tezin ilk bölümünde, $MgNi_2(BO_3)_2$, $MgCo_2(BO_3)_2$, $Mg_2Ni(BO_3)_2$ ve $Mg_2Co(BO_3)_2$ bileşikleri aşağıdaki katı hal reaksiyonları ile 900^oC'de 48 saatte hazırlandı;

$2M(NO_3)_2\,6.H_2O_{(s)} + MgO_{(s)} + 2H_3BO_{3(s)} \rightarrow \mathbf{MgM_2(BO_3)_{2(s)}} + 4NO_{2(g)} + 15H_2O_{(g)} + O_{2(g)}$

(M: Ni, Co)

$M(NO_3)_2.6H_2O_{(s)} + 2MgO_{(s)} + 2H_3BO_{3(s)} \rightarrow \mathbf{Mg_2M(BO_3)_{2(s)}} + 2NO_{2(g)} + 9H_2O_{(g)} + 1/2\ O_{2(g)}$

(M: Ni, Co)

Tüm bileşiklerin ortorombik sistemde kristallendiği ve $M_3(BO_3)_2$ (M: Mg, Ni, Co) kotoit tipi, bileşikleri ile eşyapılı olduğu bulunmuştur. Ayrıca, bu bileşiklerin termal analiz tekniği kullanılarak 20-1000^oC'de termodinamik olarak kararlı olduğu saptanmıştır.

İkinci bölümde, daha önceden rapor edilmeyen Li_2LnOPO_4 (Ln:Nd, Gd, Dy), tipindeki yeni oksifosfatlar 1000^oC'de aşağıda verilen katı hal reaksiyonu ile sentezlenmiştir;

$Ln_2O_{3(s)} + 2Li_2CO_{3(s)} + 2(NH_4)_2HPO_4(s) \rightarrow \mathbf{2Li_2LnOPO_{4(s)}} + 4NH_{3(g)} + 2CO_{2(g)} + 3H_2O_{(g)}$

Ürünlerin X-ışını Toz Kırınımı verileri ve Infrared Spektrumları incelemesi, ortorombik kristal yapıda olan ve sırasıyla a=14.865(1), b=10.734(2), c=13.231(1); a=14.686(3), b=10.634(5) c=13.047(9); a=14.554(1), b=10.589(8), c=12.926(2) Å, birim hücre parametrelerine sahip Li_2NdOPO_4, Li_2GdOPO_4, Li_2DyOPO_4 bileşiklerinin varlığını göstermektedir.

Bu çalışmanın üçüncü bölümünde, bir önceki kısıma ek olarak, $LiNaNdOPO_4$, $LiNaGdOPO_4$, $LiNaDyOPO_4$, bileşikleri hazırlanmış ve birim hücre parametreleri sırasıyla a=14.903(8), b=10.861(3), c=13.247(1); a=14.745(0), b=10.651(6), c=13.096(8); a=14.622(2), b=10.581(0), c=13.018(2) Å olan ortorombik sistemde

indekslenmiştir. Li_2LnOPO_4 ve $LiNaLnOPO_4$ (Ln: Nd, Gd, Dy) bileşiklerinin termal analiz sonuçları, bu bileşiklerin 1000^oC'ye kadar kararlı olduğu gösterdi.

Bu çalışmanın dördüncü bölümünde, $Ca_8Ln_2(PO_4)_6O_2$'i (Ln: Nd, Gd, Dy) elde etmek için farklı nadir toprak metalleri kullanılarak, Ln_2O_3 ile $CaHPO_4$ ve $CaCO_3$ (oran :1:6:2) farklı sıcaklıklarda katı hal reaksiyonu ile incelendi.

Son bölümde ise, Ln_2O_3 (Ln:Nd, Gd, Dy), B_2O_3 ve $(NH_4)_2HPO_4$'ın aşağıda verilen katı hal reaksiyonu ile nadir toprak borat fosfatları hazırlanmaya çalışıldı;

$$2Ln_2O_3 + B_2O_3 + 2(NH_4)_2HPO_4 \longrightarrow 2Ln_2(BO_3)(PO_4) + 4NH_3 + 3H_2O$$

Anahtar kelimeler: X-ışını Toz Difraksiyonu, Fourier Dönüşümlü Kızılötesi Spektrokopisi, Taramalı Elektron Mikroskopu, Termogravimetrik Analiz-Diferansiyal Isısal Analiz, Metal Boratlar, Oksifosfatlar, Apatit, Nadir Toprak Metalleri, Borfosfatlar.

TO MY DAUGHTER ZEYNEP BUSE

ACKNOWLEDGEMENT

I express sincere appreciation to my supervisor Prof. Dr. Ayşe Morkan, who has shared with me many of her ideas on which to pursue research, and encouraged me to learn interesting and valuable ideas, techniques and skills.

I would like to give my special thanks to Prof. Dr. İzzet Morkan, moral support and encouragement all the time.

I would like thank to Prof.Dr. Ahmet Varilci and Mustafa Akdoğan for providing and informing SEM and XRD analysis.

Especially I want to express gratitude to Assist. Prof.Dr. Bahadır Altıntaş who has helped me with technical problems in computing and for programming our X-ray pattern indexing software. I am also grateful to my officemate Dr.Erhan Budak.

I would like to express my thanks to my husband Assit. Prof.Dr. Abdulkadir Şenol for supportive, encouraged and patience.

Finally, I would like to thank to TÜBİTAK-No: 104T083 for supporting my thesis.

LIST OF ABBREVATIONS

EDX	Energy Dispersive X-ray Analysis
FTIR	Fourier-Transform Infrared Spectroscopy
ICDD	International Centre for Diffraction Data
KTP	Potassium titanium oxide phosphate
Ln	Lanthanide
LT	Low Temperature
RTP	Rubidium titanium oxide phosphate
SEM	Scanning Electron Microscope
TG/DTA	Thermogravimetric- Differential Thermal Analysis
TTP	Thallium titanium oxide phosphate

TABLE OF CONTENTS

ABSTRACT iii

ÖZET vi

ACKNOWLEDGEMENT x

LIST OF ABBREVATIONS xi

TABLE OF CONTENTS xii

LIST OF TABLES xviii

LIST OF FIGURES xx

CHAPTER

1. INTRODUCTION 1

1.1 History of Boron 1

1.1.1 Occurrence and Concentration 2

1.1.2. Structure and Polymorphism 4

1.1.3 Application Areas 6

1.2 Crystal Chemistry of Anhydrous Borates 8

1.3 Borates 9

1.4. Rare Earth Orthoborates 12

1.5. Infrared Studies of the Aragonite, Calcite and Vaterite Type Structures in Borates.....19

1.6 Vibrational Spectra of Borates.....20

1.7 Transition Metal Orthoborates.....23

1.8 Borophosphates.....30

1.9 Phosphorus and Phosphates.....33

1.10 Oxyphosphates.....34

1.11 Apatite.....42

2. EXPERIMENTAL TECHNIQUES.....47

2.1. Chemical Substances.....47

2.2 Instrumentation.....47

2.2.1. X-Ray Powder Diffractometer.....47

2.2.2 Infrared Spectrophotometer.....48

2.2.3. Thermogravimetric-Differential Thermal Analyser.....48

2.2.4. Scanning Electron Microscope (SEM)- Energy Dispersive X-Ray (EDX).....48

2.2.5. Camera Furnace.....48

2.3. Experimental Procedure.....49

2.3.1 Solid-State Reactions of $2Ni(NO_3)_2.6H_2O$ with MgO and $2H_3BO_3$. .49

2.3.2 Solid-State Reactions of $2Co(NO_3)_2.6H_2O$ with MgO and $2H_3BO_3$ ..50

2.3.3 Solid-State Reactions of $Ni(NO_3)_2 .6H_2O$ with $2MgO$ and $2H_3BO_3$ ...50

2.3.4 Solid-State Reactions of $Co(NO_3)_2 .6H_2O$ with $2MgO$ and $2H_3BO_3$ ..51

2.3.5 Solid- State Reactions of $Nd_2O_{3(s)} + 2Li_2CO_{3(s)} + 2(NH_4)_2HPO_{4(s)}$.....51

2.3.6 Solid- State Reactions of $Gd_2O_{3(s)} + 2Li_2CO_{3(s)} + 2(NH_4)_2HPO_{4(s)}$.....51

2.3.7 Solid- State Reactions of $Dy_2O_{3(s)} + 2Li_2CO_{3(s)} + 2(NH_4)_2HPO_{4(s)}$.....52

2.3.8 Solid- State Reactions of $Nd_2O_{3(s)} + Li_2CO_{3(s)} + Na_2CO_{3(s)} + 2(NH_4)_2HPO_{4(s)}$ 52

2.3.9 Solid- State Reactions of $Gd_2O_{3(s)} + Li_2CO_{3(s)} + Na_2CO_{3(s)} + 2(NH_4)_2HPO_{4(s)}$ 53

2.3.10 Solid- State Reactions of $Dy_2O_{3(s)} + Li_2CO_{3(s)} + Na_2CO_{3(s)} +2(NH_4)_2HPO_{4(s)}$ 53

2.3.11 Solid- State Reactions of $Nd_2O_{3(s)}+6CaHPO_42H_2O_{(s)}+2CaCO_{3(s)}$.....54

2.3.12 Solid- State Reactions of $Gd_2O_{3(s)}+6CaHPO_42H_2O_{(s)}+ 2CaCO_{3(s)}$....54

2.3.13 Solid- State Reactions of $Dy_2O_{3(s)}+6CaHPO_42H_2O_{(s)}+2CaCO_{3(s)}$.....54

2.3.14 Solid-State Reactions of $2Nd_2O_3$ with B_2O_3 and $2(NH_4)_2HPO_4$ 55

2.3.15 Solid-State Reactions of $2Gd_2O_3$ with B_2O_3 and $2(NH_4)_2HPO_4$ 55

2.3.16 Solid-State Reactions of $2Dy_2O_3$ with B_2O_3 and $2(NH_4)_2HPO_4$ 56

3. RESULTS AND DISCUSSION 57

3.1 Solid-State Reactions of $2Ni(NO_3)_2 .6H_2O$ with MgO and $2H_3BO_3$.....57

3.1.1 X-Ray Powder Diffraction Study 57

3.1.2 IR Studies 59

3.2 Solid-State Reactions of $2Co(NO_3)_2.6H_2O$ with MgO and $2H_3BO_3$ 60

3.2.1 X-Ray Powder Diffraction Study 61

3.2.2 IR Results 62

3.3 SEM and EDX Analysis of $MgNi_2(BO_3)_2$ and $MgCo_2(BO_3)_2$ 63

3.4 Thermal Studies (DTA-TG) of $MgNi_2(BO_3)_2$ and $MgCo_2(BO_3)_2$.....66

3.5 Solid-State Reactions of $Ni(NO_3)_2.6H_2O$ with 2MgO and $2H_3BO_3$.....67

3.5.1 X-Ray Powder Diffraction Study 67

3.5.2 IR Studies 69

3.6 Solid-State Reactions of $Co(NO_3)_2.6H_2O$ with 2MgO and $2H_3BO_3$ 70

3.6.1 X-Ray Powder Diffraction Study.....71

3.6.2 IR Studies.....72

3.7 SEM and EDX Analysis of $Mg_2Ni(BO_3)_2$ and $Mg_2Co(BO_3)_2$ 73

3.8 Thermal Studies (DTA-TG) of $Mg_2Ni(BO_3)_2$ and $Mg_2Co(BO_3)_2$.....76

3.9 Solid- State Reactions of $Ln_2O_{3(s)} + 2Li_2CO_{3(s)} + 2(NH_4)_2HPO_{4(s)}$ (Nd, Gd, Dy).....77

3.9.1 X-Ray Powder Diffraction Studies for Nd, Gd and Dy Compounds 77

3.9.2 IR Studies for Nd, Gd and Dy Compounds.....87

3.10 SEM and EDX Analysis of Li_2LnOPO_4 (Ln: Nd,Gd,Dy) 92

3.11 Thermal Studies (DTA-TG) of Li_2NdOPO_4, Li_2GdOPO_4 and Li_2DyOPO_4 Compounds.....95

3.12 Solid- State Reactions of $Ln_2O_{3(s)} + Li_2CO_{3(s)} + Na_2CO_{3(s)} + 2(NH_4)_2HPO_{4(s)}$ (Nd, Gd, Dy).....97

3.12.1 X-Ray Powder Diffraction Studies for Nd, Gd and Dy Compounds.....98

3.12.2 IR Studies for $LiNaLnOPO_4$ (Ln: Nd, Gd, Dy) Compounds.....107

3.13 SEM and EDX Analysis of $LiNaLnOPO_4$ (Ln: Nd,Gd,Dy) Compounds.....112

3.14 Thermal Studies (DTA-TG) of $LiNaNdOPO_4$, $LiNaGdOPO_4$ and $LiNaDyOPO_4$ Compounds.....115

3.15 Solid- State Reactions of $Ln_2O_{3(s)} + 6CaHPO_4.2H_2O_{(s)} + 2CaCO_{3(s)}$ (Nd, Gd, Dy).....117

3.15.1 X-Ray Powder Diffraction Study of the Products.....117

3.15.2 IR Spectra of the Products.....124

3.16 Solid State Reactions of $2Nd_2O_3 + B_2O_3 + 2(NH_4)_2HPO_4$.....128

3.16.1 X-Ray Powder Diffraction Study of the Products.....128

3.16.2 IR Spectra of the Products at Different Temperatures.....130

3.17 Solid-State Reactions of $2Gd_2O_3 + B_2O_3 + 2(NH_4)_2HPO_4$.....133

3.17.1 X-Ray Powder Diffraction Study of the Products.....133

3.17.2 IR Spectra of the Products at Different Temperatures.....136

3.18. Solid State Reactions of $2Dy_2O_3 + B_2O_3 + 2(NH_4)_2HPO_4$ 138

3.18.1 X-Ray Powder Diffraction Study of the Products 138

3.18.2 IR Spectra of the Products at Different Temperatures..... 141

3.19 Thermal Studies of the Products 143

4. GENERAL REVIEW AND CONCLUSION..... 147

REFERENCES 152

CIRRICULUM VITAE..... 162

LIST OF TABLES

TABLE

1.1 Common Borate Minerals [2]..... 2

1.2 Distribution of Boron..... 3

1.3 Boron Reserves in the World (million tons, as B_2O_3) [3]..... 4

1.4 Boron Reserves in Turkey [3]..... 4

1.5 O:B ratio of different types of borates..... 12

1.6 IR frequencies for the calcite structure..... 20

1.7 IR frequencies for the aragonite structure..... 20

1.8 IR frequencies for the vaterite structure..... 20

1.9 The observed IR frequencies of $Co_2Ni(BO_3)_2$ and $CoNi_2(BO_3)_2$ 23

1.10 The cell parameters of the $M_3(BO_3)_2$ (M= Mg, Co and Ni) compounds having kotoite structure..... 24

1.11 Cell parameters, space group and z values of α and β $Sr_2Cu(BO_3)_2$..... 26

1.12 Crystallographic data for the Borates $A_2^{2+}B^{2+}(BO_3)_2$..... 27

1.13 The unit cell, space groups and z values of the $M_2M(BO_3)_2$ compounds having kotoite (orthorhombic) structure..... 30

1.14 Cell parameters and the Space Groups of $M_3[BPO_7]$ (M= Mg, Ba and Sr) reported by Gözel..... 32

1.15 The formula and structural types of known oxyphosphate..... 35

3.1 X-ray Powder Diffraction Data of Orthorhombic $MgNi_2(BO_3)_2$ 58

3.2 IR Absorption Bands and Assignments for the $MgNi_2(BO_3)_2$ 60

3.3 X-ray Powder Diffraction Data of Orthorhombic $MgCo_2(BO_3)_2$ 61

3.4 X-ray Powder Diffraction Data of Orthorhombic $Mg_2Ni(BO_3)_2$ 68

3.5 X-ray Powder Diffraction Data of Orthorhombic $Mg_2Co(BO_3)_2$ 71

3.6 X-ray Powder Diffraction Data of Orthorhombic Structure of Li_2NdOPO_4 (1000^oC 6h) 79

3.7 X-ray Powder Diffraction Data of Orthorhombic Structure of Li_2GdOPO_4 (1000^oC-18h) 82

3.8 X-ray Powder Diffraction Data of Orthorhombic Structure of Li_2DyOPO_4 (1000^oC-6h) 86

3.9 X-ray Powder Diffraction Data of Orthorhombic Structure of $LiNaNdOPO_4$ (1000^oC-12h) 100

3.10 X-ray Powder Diffraction Data of Orthorhombic Structure of $LiNaGdOPO_4$ (1000^oC-12h) 102

3.11 X-ray Powder Diffraction Data of Orthorhombic Structure of $LiNaDyOPO_4$ (1000^oC-6h) 106

3.12 The Assignments of IR Absorption Bands for the Compounds of $LiNaNdOPO_4$, $LiNaGdOPO_4$ and $LiNaDyOPO_4$, at 1000^oC 108

3.13 X-ray Powder Diffraction Pattern Indexed Tetragonal System of $DyPO_4$ and Unit Cell Parameters a= 6.912, c= 6.041Å 139

3.14 X-ray Powder Diffraction Pattern Indexed Hexagonal System of $DyBO_3$ and Unit Cell Parameters a= 3.793, c= 8.847 Å 139

LIST OF FIGURES

FIGURE

1.1 (a) β-rhombohedral boron, (b) α-rhombohedral boron, (c) tetragonal boron..... 5

1.2 The orthoborate BO_3^{3-} ion 9

1.3 The pyroborate $B_2O_5^{4-}$ ions 10

1.4 Some actual or hypothetical boron oxygen groupings in borates. (a) Isolated triangles, BO_3^{3-}, e.g. orthoborates. (b) Triangles sharing one oxygen atom, $B_2O_5^{4-}$, e.g. pyroborates. (c-e) Triangles sharing two oxygen atoms to form closed rings or an open chain, $[BO_2]_n^{n-}$, e.g. metaborates..... 11

1.5 The projection of the structure of $LaBO_3$ (Aragonite-Type) paralel to [010]..... 14

1.6 The coordination polyhedra of La-Atom in the structure of $LaBO_3$ (Aragonite-type) 14

1.7 Representation of the aragonite-type LT-$LaBO_3$ structure. LaO_9 groups are shown as hatched polyhedra and B atoms as black spheres. B-O bonds are indicated as solid black lines. 15

1.8 The structure of triclinic *(P-1)* $SmBO_3$ 16

1.9 The $[SmO_8]$ polyhedra in triclinic $SmBO_3$ structure 17

1.10 The structure of calcite type rare earth orthoborate (Abrahams et al.) 18

1.11 Sketches of the $Cu_2(BO_3)_4$ unit. Top: view [100]. Angles in ^{o}. Bottom:

view along direction orthogonal to mirror plane at y = ¼..... 27

1.12 Ba sites in (a) $Ba_2Mg(BO_3)_2$ and (b) $Ba_2Ca(BO_3)_2$. Filled circles = Ba; open circles = O. 28

1.13 (a) Hexagonal unit cell of $Ba_2Mg(BO_3)_2$ and (b) the pseudohexagonal cell of $Ba_2Ca(BO_3)_2$..... 29

1.14 The structure of $Li_{(1-2x)}Ni_xTiOPO_4$ represented by Ti-O-Ti-O- chains..... 40

1.15 A polyhedral view of framework as projected in the (b, c) plane..... 41

1.16 Chain of TiO_6 octahedra in oxyphosphate $Fe_{0.50}TiO(PO_4)$ linked to PO_4 tetrahedra, along c-axis..... 42

1.17 Crystal structure of apatite. Projection onto the (0001) plane..... 44

1.18 Types of calcium polyhedra in the structure of apatite.(a) Columns of ninefold coordinated Ca1 polyhedra, and (b) triangles of sevenfold coordinated Ca2 polyhedra. 45

3.1 X-ray Powder Diffraction Pattern of Orthorhombic $MgNi_2(BO_3)_2$ at 900^oC 58

3.2 IR Spectrum of $MgNi_2(BO_3)_2$..... 60

3.3 X-ray Powder Diffraction Pattern of Orthorhombic $MgCo_2(BO_3)_2$ at 900^oC 61

3.4 IR Spectrum of $MgCo_2(BO_3)_2$ 63

3.5 SEM image of the $MgNi_2(BO_3)_2$ at 900^oC 64

3.6 SEM image of the $MgCo_2(BO_3)_2$ at 900^oC..... 64

3.7 EDX Spectrum of the Products Obtained from the Reaction of $2Ni(NO_3)_2.6H_2O + MgO + 2H_3BO_3$ at 900^oC 65

3.8 EDX Spectrum of the Products Obtained from the Reaction of $2Co(NO_3)_2.6H_2O + MgO + 2H_3BO_3$ at 900^oC..... 65

3.9 DTA-TG of the Product Obtained at 900°C (48h) Through the Solid-State Reaction of $2Ni(NO_3)_2.6H_2O + MgO + 2H_3BO_3$ 66

3.10 DTA-TG of the Product Obtained at 900°C (48h) Through the Solid-State Reaction of $2Co(NO_3)_2.6H_2O + MgO + 2H_3BO_3$ 67

3.11 X-ray Powder Diffraction Pattern of Orthorhombic $Mg_2Ni(BO_3)_2$ at 900°C 68

3.12 IR Spectrum of $Mg_2Ni(BO_3)_2$ 70

3.13 X-ray Powder Diffraction Pattern of Orthorhombic $Mg_2Co(BO_3)_2$ at 900°C 71

3.14 IR Spectrum of $Mg_2Co(BO_3)_2$ 73

3.15 SEM image of the $Mg_2Ni(BO_3)_2$ at 900°C 74

3.16 SEM image of the $Mg_2Co(BO_3)_2$ at 900°C..... 74

3.17 EDX Spectrum of the Products Obtained from the Reaction of $Ni(NO_3)_2.6H_2O + 2MgO + 2H_3BO_3$ at 900°C 75

3.18 EDX Spectrum of the Products Obtained from the Reaction of $Co(NO_3)_2.6H_2O + 2MgO + 2H_3BO_3$ at 900°C..... 75

3.19 DTA-TG of the Product Obtained at 900°C (48h) Through the Solid State Reaction of $Ni(NO_3)_2.6H_2O + 2MgO + 2H_3BO_3$ 76

3.20 DTA-TG of the Product Obtained at 900°C (48h) Through the Solid State Reaction of $Co(NO_3)_2.6H_2O + 2MgO + 2H_3BO_3$ 77

3.21 X-ray Powder Diffraction Patterns of the Products Obtained of the Solid State Reaction of $Nd_2O_{3(s)} + 2Li_2CO_{3(s)} + 2(NH_4)_2HPO_4(s)$ at 900-1000°C 78

3.22 X-ray Powder Diffraction Patterns of the Products Obtained of the Solid State Reaction of $Gd_2O_{3(s)} + 2Li_2CO_{3(s)} + 2(NH_4)_2HPO_4(s)$

at 900-1100^{o}C 81

3.23 X-ray Powder Diffraction Patterns of the Products Obtained of the Solid State Reaction of $Dy_2O_{3(s)} + 2Li_2CO_{3(s)} + 2(NH_4)_2HPO_4(s)$ at 800-1100^{o}C 85

3.24 IR Spectra of the Products of the Solid State Reactions of $Nd_2O_{3(s)} + 2Li_2CO_{3(s)} + 2(NH_4)_2HPO_{4(s)}$ at 600-1000^{o}C 88

3.25 IR Spectra of the Products of the Solid State Reactions of $Gd_2O_{3(s)} + 2Li_2CO_{3(s)} + 2(NH_4)_2HPO_{4(s)}$ at 800 -1100^{o}C 90

3.26 IR Spectra of the Products of the Solid State Reactions of $Dy_2O_{3(s)} + 2Li_2CO_{3(s)} + 2(NH_4)_2HPO_{4(s)}$ at 800 -1100^{o}C 91

3.27 SEM image of the Li_2NdOPO_4 at 1000^{o}C (6h)..... 92

3.28 SEM image of the Li_2GdOPO_4 at 1000^{o}C (18h)..... 93

3.29 SEM image of the Li_2DyOPO_4 at 1000^{o}C (6h)..... 93

3.30 EDX Spectrum of the Products Obtained from the Reaction of $Nd_2O_{3(s)} + 2Li_2CO_{3(s)} + 2(NH_4)_2HPO_{4(s)}$ at 1000^{o}C (6h) 94

3.31 EDX Spectrum of the Products Obtained from the Reaction of $Gd_2O_{3(s)} + 2Li_2CO_{3(s)} + 2(NH_4)_2HPO_{4(s)}$ at 1000^{o}C (18h) 94

3.32 EDX Spectrum of the Products Obtained from the Reaction of $Dy_2O_{3(s)} + 2Li_2CO_{3(s)} + 2(NH_4)_2HPO_{4(s)}$ at 1000^{o}C (6h) 95

3.33 DTA-TG of the Product Obtained at 1000^{o}C (6h) Through the Solid State Reaction of $Nd_2O_{3(s)} + 2Li_2CO_{3(s)} + 2(NH_4)_2HPO_{4(s)}$ 96

3.34 DTA-TG of the Product Obtained at 1000^{o}C (18h) Through the Solid State Reaction of $Gd_2O_{3(s)} + 2Li_2CO_{3(s)} + 2(NH_4)_2HPO_{4(s)}$ 96

3.35 DTA-TG of the Product Obtained at 1000^{o}C (6h) Through the Solid State Reaction of $Dy_2O_{3(s)} + 2Li_2CO_{3(s)} + 2(NH_4)_2HPO_{4(s)}$ 97

3.36 X-ray Powder Diffraction Patterns of the Products Obtained of the Solid State Reaction of $Nd_2O_{3(s)} + Li_2CO_{3(s)} + Na_2CO_{3(s)} + 2(NH_4)_2HPO_{4(s)}$ at 800 -1100^oC 99

3.37 X-ray Powder Diffraction Pattern of Orthorhombic $LiNaGdOPO_4$ at 1000^oC (12h) 102

3.38 X-ray Powder Diffraction Patterns of the Products Obtained of the Solid State Reaction of $Dy_2O_{3(s)} + Li_2CO_{3(s)} + Na_2CO_{3(s)} + 2(NH_4)_2HPO_{4(s)}$ at 800 - 1100^oC 105

3.39 IR Spectra of the Products of the Solid State Reactions of $Nd_2O_{3(s)} + Li_2CO_{3(s)} + Na_2CO_{3(s)} + 2(NH_4)_2HPO_{4(s)}$ at 800 and 1100^oC 109

3.40 IR Spectra of the Products of the Solid State Reactions of $Gd_2O_{3(s)} + Li_2CO_{3(s)} + Na_2CO_{3(s)} + 2(NH_4)_2HPO_{4(s)}$ at 800 and 1000^oC 110

3.41 IR Spectra of the Products of the Solid-State Reactions of $Dy_2O_{3(s)} + Li_2CO_{3(s)} + Na_2CO_{3(s)} + 2(NH_4)_2HPO_{4(s)}$ at 800 and 1100^oC 111

3.42 SEM image of the $LiNaNdOPO_4$ at 1000^oC (12h) 112

3.43 SEM image of the $LiNaGdOPO_4$ at 1000^oC (12h) 113

3.44 SEM image of the $LiNaDyOPO_4$ at 1000^oC (6h) 113

3.45 EDX Spectrum of the Products Obtained from the Reaction of $Nd_2O_{3(s)} + Li_2CO_{3(s)} + Na_2CO_{3(s)} + 2(NH_4)_2HPO_{4(s)}$ at 1000^oC (12h) 114

3.46 EDX Spectrum of the Products Obtained from the Reaction of $Gd_2O_{3(s)} + Li_2CO_{3(s)} + Na_2CO_{3(s)} + 2(NH_4)_2HPO_{4(s)}$ at 1000^oC (12h) 114

3.47 EDX Spectrum of the Products Obtained from the Reaction of

$Dy_2O_{3(s)} + Li_2CO_{3(s)} + Na_2CO_{3(s)} + 2(NH_4)_2HPO_{4(s)}$ at 1000°C (6h)..... 115

3.48 DTA-TG of the Product Obtained at 1000°C (12h) Through the Solid State Reaction of$Nd_2O_{3(s)} + Li_2CO_{3(s)} + Na_2CO_{3(s)} + 2(NH_4)_2HPO_{4(s)}$ 116

3.49 DTA-TG of the Product Obtained at 1000°C (12h) Through the Solid State Reactions $Gd_2O_{3(s)} + Li_2CO_{3(s)} + Na_2CO_{3(s)} + 2(NH_4)_2HPO_{4(s)}$ 116

3.50 DTA-TG of the Product Obtained at 1000°C (6h) Through the Solid State Reaction of$Dy_2O_{3(s)} + Li_2CO_{3(s)} + Na_2CO_{3(s)} + 2(NH_4)_2HPO_{4(s)}$ 117

3.51 X-ray Powder Diffraction Patterns of the Products Obtained of the Solid State Reaction of $Nd_2O_{3(s)}+6CaHPO_4.2H_2O_{(s)}+ 2CaCO_{3(s)}$ at 700-1300°C ..... .119

3.52 X-ray Powder Diffraction Patterns of the Products Obtained of the Solid State Reaction of $Gd_2O_{3(s)}+6CaHPO_4.2H_2O_{(s)}+ 2CaCO_{3(s)}$ at 700-1300°C 121

3.53 X-ray Powder Diffraction Patterns of the Products Obtained of the Solid State Reaction of $Dy_2O_{3(s)}+6CaHPO_4.2H_2O_{(s)}+2CaCO_{3(s)}$ at 700-1300°C 123

3.54 IR Spectra of the Products of the Solid State Reactions of $Nd_2O_{3(s)}+6CaHPO_4.2H_2O_{(s)}+ 2CaCO_{3(s)}$ at 700 and 1300°C 125

3.55 IR Spectra of the Products of the Solid State Reactions of $Gd_2O_{3(s)}+6CaHPO_4.2H_2O_{(s)}+ 2CaCO_{3(s)}$ at 700 and 1300°C 126

3.56 IR Spectra of the Products of the Solid State Reactions of $Dy_2O_{3(s)}+6CaHPO_4.2H_2O_{(s)}+ 2CaCO_{3(s)}$ at 700 and 1300°C 127

3.57 The X-ray powder Diffraction Patterns of the Solid State Reactions of $2Nd_2O_3 + B_2O_3 + 2(NH_4)_2HPO_4$ at 500-1300°C 129

3.58 IR Spectra of the Products of the Solid State Reactions of

$2Nd_2O_3 + B_2O_3 + 2(NH_4)_2HPO_4$ at 500-1300^oC 132

3.59 The X-ray powder Diffraction Patterns of the Solid State Reactions of

$2Gd_2O_3 + B_2O_3 + 2(NH_4)_2HPO_4$ at 500-1300^oC 135

3.60 IR Spectra of the Products of the Solid State Reactions of

$2Gd_2O_3 + B_2O_3 + 2(NH_4)_2HPO_4$ at 500-1300^oC 137

3.61 The X-ray powder Diffraction Patterns of the Solid State Reactions of

$2Dy_2O_3 + B_2O_3 + 2(NH_4)_2HPO_4$ at 500-1300^oC 140

3.62 IR Spectra of the Products of the Solid State Reactions of

$2Dy_2O_3 + B_2O_3 + 2(NH_4)_2HPO_4$ at 500-1400^oC 142

3.63 DTA -TG (Thermal Analysis) Curve of the Solid State Reactions of

$2Nd_2O_3 + B_2O_3 + 2(NH_4)_2HPO_4$ at 1200^oC 144

3.64 DTA -TG (Thermal Analysis) Curve of the Solid State Reactions of

$2Gd_2O_3 + B_2O_3 + 2(NH_4)_2HPO_4$ at 1200^oC 145

3.65 DTA -TG (Thermal Analysis) Curve of the Solid State Reactions of

$2Gd_2O_3 + B_2O_3 + 2(NH_4)_2HPO_4$ at 1200^oC 146

CHAPTER I

INTRODUCTION

1.1 History of Boron

Boron compounds may have been known for about 6000 years, starting with the Babylonians. The Egyptians, Chinese, Tibetans and Arabians are reported to have used such materials. The Arabs used the expression baurach for a number of minerals including the now familiar borax.

Elemental boron was not known until the early nineteenth century when Sir Humphrey Davy, Gay-Lussac and Thenard prepared boron by reduction of boron trioxide with potassium and by electrolysis of moistened boric acid. The purity of their products was about 50%.

Fifty years later impure boron products resembling both diamond and graphite were produced. The diamond-hard material was found to be largely aluminum boride (AlB12), while the graphite variety was a complex boron-aluminum-carbon. Much later, a higher purity boron was made by reduction of boron trioxide with magnesium. Purities of about 90% can be achieved by this procedure. The product is light boron in color and is considered to be amorphous [1].

Boron did not become of interest until the twentieth century when it was found that it formed many unusual and complex compounds. It has been during the last forty years that the right physical and chemical properties have been determined. High purity boron produced by electrolysis and vapor deposition methods have made such determinations possible.

1.1.1 Occurrence and Concentration

The elemental boron (B) is widely distributed in nature. Because of its high affinity for oxygen, boron always occurs in nature bound to oxygen, in the form of inorganic borates (Table 1.1). Apart from their occurrence in a few commercially exploitable deposits (mainly as sodium or calcium borate minerals), borates are present everywhere at low concentrations, in rocks (15-300 mgB/kg), soils (<10-20 mgB/kg), fresh waters (<1 mgB/kg) and sea water (5 mgB/kg). The content of boron in the lithosphere by mass is about 1.10^{-3}. Table 1.2 gives data on the distribution of boron in various compounds of the earth's crust.

Igneous rocks generally have low borate content. Sedimentary rocks have a higher borate content, which is related to the salinity of the water at the time of deposit on. The borate content from such marine segments ranges between 15-300 mgB/kg. The weathering of rocks, rainfall and erosion from rivers, provides a continuous small source of borate into the soil and the aqueous environment. Soils of low borate content (<10 mgB/kg) are most common on earth.

Table 1.1 Common Borate Minerals [2]

Mineral	Empiricial Formula	B_2O_3 Content, Wt %
Tincal (Natural borax)	$Na_2B_4O_7.10H_2O$	36.5
Kernite (rasortie)	$Na_2B_4O_7.4H_2O$	51.0

Tincalconite	$Na_2 B_4O_7 .5H_2O$	48.8
Colemanite	$Ca_2B_6O_{11}.5H_2O$	50.8
Ulexite	$NaCaB_5O_9 .8H_2O$	43.0
Probertite (kramerite)	$NaCaB_5O_9 .5H_2O$	49.6
Hydroboracite	$CaMgB_6O_{11}.6H_2O$	50.5
Szaibelyite (ascharite)	$Mg_2B_2O_5.H_2O$	41.4
Boracite (stassfurite)	$Mg_3B_7O_{13}Cl$	62.2
Priceite (pandermite)	$Ca_4B_{10}O_{19}.7H_2O$	49.8
Sassolite	$B(OH)_3$ or $B_2O_3.3H_2O$	56.4
Inyoite	$Ca_2B_6O_{11}.13H_2O$	37.6
Meyerhofferite	$Ca_2B_6O_{11}.7H_2O$	46.7
Inderborite	$CaMgB_6O_{11}.11H_2O$	41.5
Kurnakovite	$Mg_2B_6O_{11}.15H_2O$	37.3
Inderite	$Mg_2B_6O_{11}.15H_2O$	37.3
Suanite	$Mg_2B_2O_5$	46.3
Kotoite	$Mg_3B_2O_6$	36.5
Pinnoite	$MgB_2O_4.3H_2O$	42.5
Datolite	$Ca_2B_2Si_2O_9. H_2O$	21.8
Cahnite	$Ca_2AsBO_6.2H_2O$	11.7
Danburite	$CaB_2Si_2O_8$	28.3
Howlite	$Ca_4Si_2B_{10}O_{23}.5H_2O$	44.5
Vonsenite	$(Fe,Mg)_2FeBO_5$	10.3
Ludwigite	$(Fe,Mg)_4Fe_2B_2O_7$	17.8
Tunellite	$SrB_6O_{10}.4H_2O$	52.9

Table 1.2 Distribution of Boron

Source	Weight %	Source	Weight %
Earth's Crust	$1x10^{-3}$	Iron ores(maritime)	$5x10^{-2}$
Inside rocks	$1x10^{-4}$	Iron oreos (nonmaritime)	$5x10^{-4}$
Acid rocks (granites)	$1.5x10^{-3}$	Lime stones	$5x10^{-4}$
Sedimentary rocks	$1.2x10^{-2}$	Meteorites	$3x10^{-4}$
Soils	$1x10^{-3}$	Sea water (dry residue)	$1.5x10^{-2}$
Granite pegmatites	$(1\text{-}10)x10^{-2}$	Salt Springs (dry residue)	$(3\text{-}20)x10^{-3}$
Marine clays	$5x10^{-2}$	Salt lakes (dry residue)	$(1\text{-}60)x10^{-2}$

Large deposite of borate minerals are rare. The only known massive deposites are located in the Mojave Desert of California, USA, and in western Turkey. The world reserve is 885 billion tons and Turkey has 64% of these boron reserves. The distribution of boron reserves in the world and in Turkey is given in Table 1.3 and Table 1.4, respectively.

Table 1.3 Boron Reserves in the World (million tons, as B_2O_3) [3]

Country	Proven Economic Reserve	Probable & Possible Reserve	Total Reserve	% in Total Reserve	Reserve Life-span (year)
Turkey	224,000	339,000	563,000	64	389
USA	40,000	40,000	80,000	9	55
Russia	40,000	60,000	100,000	11	69
China	27,000	9,000	36,000	4	25
Chile	8,000	33,000	41,000	5	28
Bolivia	4,000	15,000	19,000	2	13
Peru	4,000	18,000	22,000	2	15
Argentina	2,000	7,000	9,000	1	6
Kazakhistan	14,000	1,000	15,000	2	10
TOTAL	**363,000**	**522,000**	**885,000**	**100**	**610**

Table 1.4 Boron Reserves in Turkey [3]

Production Area	Mineral	Reserve Million Tons	Content of B_2O_3 %	Capacity (Ton/Year)	Production (Ton/Year)
Kırka Bor Plant	Tincal	605.5	25.8	200,000	558
Bigadiç Bor Plant	Ulexite	49.2	29.1	200,000	200
	Colemanite	576.4	29.4	200,000	90
Emet Bor Plant	Colemanite	835.6	27.5-	500,000	300
Kestelek Bor Plant	Colemanite	7.7	25-33.2	100,00	60
TOTAL		**2074.4**		**1.200.000**	**1208**

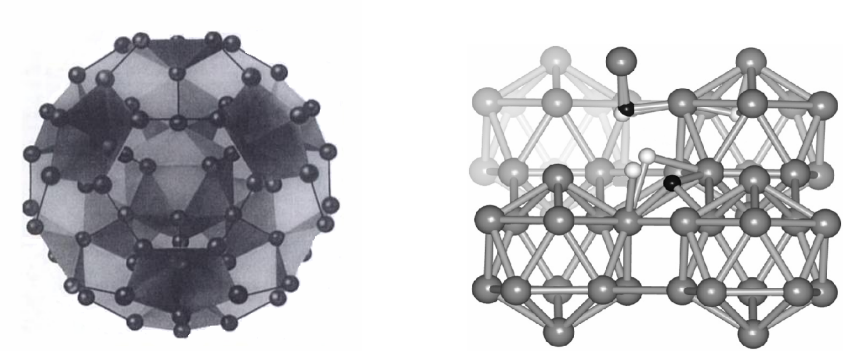
1.1.2. Structure and Polymorphism

There are several allotropic forms of boron. Boron compounds can be classified into two groups. These are amorphous boron and crystalline boron. Well established crystalline boron is α-rhombohedral boron, and β-rhombohedral boron. In

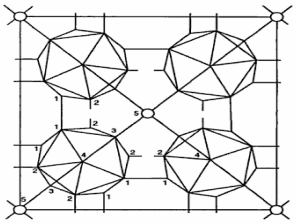
addition, four tetragonal forms have been described. However, these are probably stabilized by small amounts of nitrogen or carbon [4]

The β-rhombohedral form is the thermodynamically stable modification at all temperatures. Amorphous boron slowly converts to the β-rhombohedral form at ~ 1200^{o}C and to α-rhombohedral boron above 1500^{o}C. Any type of boron recrystallizes in β-rhombohedral structure when heated above the melting point and cooled. The unit cell of β-rhombohedral boron contains 105 boron atoms grouped 84B + 2x10B + 1B in complex arrangement. The structure of α-rhombohedral boron can be described as a slightly deformed cubic close packing of B12 icosahedra. The unit cell contains 12 B atoms at the vertices of the icosahedron [4].

Amorphous boron exhibits broad reflections in the X-ray diffraction pattern. It is believed to be a frozen-in intermediate between the α- and β-modifications or a microcrystalline deposit of β-rhombohedral boron. Amorphization can be achieved by intensive milling of β-rhombohedral samples [4].



(a) (b)



(c)

Figure 1.1 (a) β-rhombohedral boron, (b) α-rhombohedral boron, (c) tetragonal boron.

1.1.3 Application Areas

Boron compounds may be classified under two groups with respect to their production technologies and usage areas:

1) Compounds which are produced in large quantites: Boron mineral concentrates which are produced in large quantities with classic chemical engineering unit operations and find widespread application areas, i.e. agriculture, glass production and detergents, etc.

2) Specialty boron chemicals that are produced in limited amounts and have special application areas. Elemental boron, boron fiber, boron carbide and similar specialty boron compounds require special production technologies and generally are used in high technology areas.

Elemental boron is used in very diverse industries from metallurgy to electronics. Other areas of application include ceramic, propulsion, pyrotechnics, and nuclear chemistry. Boron is nontoxic. Workplace hygienic practices, however, include avoiding the breathing of boron dust or fine powder.

Boron is used in pyrotechnics and flares to produce a green color. It is used in some rockets as an ignition source. Boron is also used in air bags, placed in

automobiles as safety devices, for initiating the sodium azide which fills the bag with nitrogen. Boron-10, one of the naturally occurring isotopes of boron, is good absorber of neutron and is used in the control rods of nuclear reactors, as a radiation shield and as a neutron detector. Boron filaments are used in aerospace industry because of their high-strength and lightweight [5].

Dispersed mixture of boron and another metal as deoxidizing and degassing agents to harden steel, to increase the conductivity of copper in turbojet engines, and in making of brass and bronze. Two examples are alloys of ferroboron and magnese boron.

Cleaning and washing products use boron compounds. In North America, boron is mostly used as a washing aid and softener where ten percent of boron consumption is used in the cleaning industry. In Western Europe, sodium perborate is used as a bleaching agent in soap and detergent. Over 41% of their boron consumption is cleaning products.

Boron, an essential trace element for plant growth, is often added to crops as a fertilizer. In higher concentrations, it can also be used as a non-selective herbicide for weed control, insecticide, algaecide in water treatment and as a timber preservative. The United States uses approximately 5% of its boron consumption in the agrochemical field.

Boron compounds are widely employed in many branches of the national economy, for example in medicine for the preparation of disinfectants and drugs, in the glass industry for the production of optic and chemical stable glass (glass products use 53.6% of the boron consumption in the United States, and 32.7% in Western Europe . Boron compounds are also used in cosmetic, leather, textile, rubber

and paint industries. They also find application in the wood-processing industry as a protection against molds.

1.2 Crystal Chemistry of Anhydrous Borates

The main principles of anhydrous borate systemic are that

a) every boron atom is linked to three or four oxygen atoms;

b) a single structure mat contain either triangular or tetrahedral coordination or both;

c) polymerization or formation of chains, layers or framework is brought about by linking the tops of the triangles and tetrahedra;

d) in framework and layered polyanions the triangles and tetrahedra tend to form compact clusters with small negative charge of the type of diborate ($2\Delta + 2T$), triborate ($2\Delta + 1T$), pentaborate ($4\Delta + 1T$), boroxinic (3Δ), ditriborate ($1\Delta + 2T$), dipentaborate ($3\Delta + 2T$), and other single and double ring brn oxygen anions and radicals;

e) complex polyanions tent to “twinning”;

f) in the majority of complex polyanions each oxygen atom is bound to two boron atoms; for compounds with the general formula $mB_2O_3.nM_xO_y$ and $m> 1$, the relationship $n=n_\Delta/n_T= m-1$ is true;

g) a frequent exception for polyanions, including layered and framework structures, is a coordination number of one or three (in cubic boracites and hydrated complex higher polyborates even four) for some oxygen atoms;

h) no triangles and tetrahedra are encountered in anhydrous borates either in isolated forms nor in island polyanions;

i) an increase in the factor $N(B_2O_3)/N(M_xO_y)$ as well as in the cation size leads to a rise in the degree of polymerization of the anion and the number N, while an increased charge causes the opposite [6].

1.3 Borates

Borates are defined as "salts or esters of boric acid; a compound containing the radical B_2O_3. Borates are defined by industry as any compound that contains or supplies boric oxide [2]. The boron atom is normally trivalent, the bonds involved being sp^2 hybrids directed in a plane towards the corner of an equilateral triangle. The simplest oxy-anion is therefore BO_3^{3-}, which may be formulated it is, however, probable that the B-O bond also possesses some degree of ionic character [7].

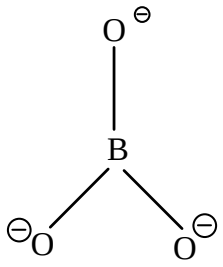


Figure 1.2 The orthoborate BO_3^{3-} ion

Since, however, the oxygen atom can form two bonds it is possible for two such groups to be linked together, by sharing a common oxygen atom, to give the polynuclear ion $B_2O_5^{4-}$:

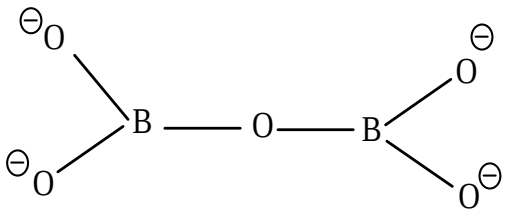


Figure 1.3 The pyroborate $B_2O_5^{4-}$ ions

This, however, is not the only way in which BO_3 triangles can be joined, for more than one of the oxygen atoms may be shared and more than two BO_3 groups may be united to give an indefinite number of polynuclear ions, some of which are shown in figure 1.4.

Figure 1.4 a represents the isolated BO_3^{3-} ion. The salts in which this ion occurs are the *orthoborates* with oxygen: boron ratio of 3:1, and structurally they are analogous to nitrates and carbonates. Thus $ScBO_3$, $InBO_3$ and $CaCO_3$ have the calcite structure, $SmBO_3$ have vaterite structure, YBO_3 and $LaBO_3$ has that of aragonite.

In (b) two BO_3 groups are linked by sharing a common oxygen atom to form the ion $B_2O_5^{4-}$, an ion which has been found in the pyroborates $Mg_2B_2O_5$ and $Co_2B_2O_5$.

If two of the three oxygen atoms of two BO_3 groups are shared the arrangement (c) results, but this is unknown in any crystal structure; nor indeed, is it a likely configuration for it involves an abnormally small angle between the two bonds of each of the shared oxygen atoms and a very close approach of the two boron atoms. It is not, however, necessary that the number of BO_3 groups in association should be limited to two, and once this point is accepted it becomes

possible for an indefinite number of these groups to be bonded together in the form of closed rings.

In (d) four groups are so bonded to give the ion $B_4O_8^{4-}$, but, whatever the number of the groups, the arrangement corresponds to oxygen: boron ratio of 2:1, as found in the *metaborates*. In potassium metaborates three BO_3 groups are linked in this way to give the ion $B_3O_6^{3-}$, and the formula should therefore be written $K_3B_3O_6$, rather than KBO_2, to emphasize this point.

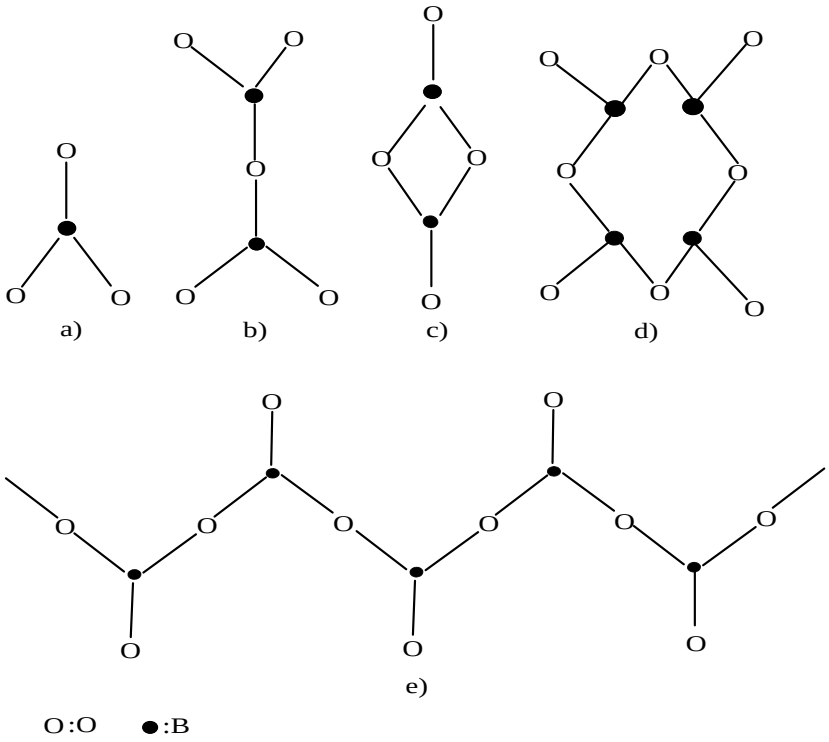


Figure 1.4 Some actual or hypothetical boron oxygen groupings in borates. (a) Isolated triangles, BO_3^{3-}, e.g. orthoborates. (b) Triangles sharing one oxygen atom, $B_2O_5^{4-}$, e.g. pyroborates. (c-e) Triangles sharing two oxygen atoms to form closed rings or an open chain, $[BO_2]_n^{n-}$, e.g. metaborates.

If the number of BO_3 groups in the ring is increased indefinitely we reach in the limit the infinitely extended open chain of composition $[BO_2]_n^{n-}$ shown in figure 1.4(e). Such an arrangement differ fundametally from all the other complex anions so far described in that it is no longer possible to point to any discrete radical. The repeat period in the crystal may extend over several units of the chain, at different points of which different atoms may be attached, so that in chemical terminology such a chain ion is indefinitely polybasic [7].

An infinite ion of this type (but somewhat distorted from the idealized form shown at (e)) is found in the crystal structure of calcium metaborate, CaB_2O_4. The ions extend parallel to one another through the structure and are linked together by ionic bonds between the calcium and the unshared oxygen atoms.

BO_3 coordination group containing borates has a simple relation between the O:B ration and the number of atoms shared by each BO_3 group, assuming these to be equivalent and each bonded to 2B atoms as given in table 1.5.

Table 1.5 O:B ratio of different types of borates

O:B ratio	**Borates types**	**# of atoms shared**
3:1	Orthoborate: discrete BO_3^{3-} ions	0
2:5	Pyroborate: discrete $B_2O_5^{4-}$ ions	1
2:1	Metaborates: discrete $B_3O_6^{3-}$ and $B_2O_4^{2-}$	2
3:2	Borontrioxide: B_2O_3	3

1.4. Rare Earth Orthoborates

Compounds equimolar in R_2O_3 and B_2O_3 are of the ABO_3 type. The classic study on the “Isomorphism of Borates and Carbonates” was made by Goldschmidt

and Hauptmann [8]. They studied the lanthanum, indium, scandium and yttrium borates.

In 1961, Levin et al. investigated their polymorphism and reported on the regions of stability of the different structures in relation with borates preparation temperature and the ionic radius of the rare earth [9]. The diagram they established showed that the structures of the rare earth borates are related to the three crystalline forms of $CaCO_3$, aragonite, vaterite, and calcite depending on the rare earth. The compound $LaBO_3$, $NdBO_3$ [9] and $CeBO_3$ [10] showed the aragonite type structure. The aragonite type structure is orthorombic, space group Pnam (No.62), Z=4. The unit cell dimensions determined for $LaBO_3$ a=5.104 Å, b=8.252 Å, c=5.872 Å; for $NdBO_3$ a=5.037 Å, b=8.076 Å, c=5.729Å. The crystal structure of aragonite type $LaBO_3$ were explained first time by Abdulaev et al. [11]. The aragonite and calcite type orthoborates contain triangular BO_3^{3-} groups confirmed by both X-ray diffraction and spectroscopic studies [9, 12].

A recent study at higher temperatures, two different forms have been found for $LaBO_3$ and $NdBO_3$. According to Bohlhoff et al., they crystallize in the monoclinic system [12].

The projection of the structure of $LaBO_3$ (aragonite-type) parallel to [010] and the coordination polyhedra of La- atom in the structure of $LaBO_3$ (aragonite-type) were well defined by Gornuyova and shown in figure 1.5 and figure 1.6, respectively [13]. In figure 1.5, it is obviously seen that trigonal planar [BO_3] surrounds nine coordinated La atoms. As shown in figure 1.5 the La atom is coordinated by nine O and the B atom is planar-triangularly coordinated by three O atoms. Each LaO_9 polyhedron shares edges with six other LaO_9 polyhedra and three BO_3 triangles, whereas each BO_3 triangle shares edges with three LaO_9 polyhedra.

The representation of the aragonite type LT-$LaBO_3$ structure with LaO_9 groups is given in figure 1.7 [14].

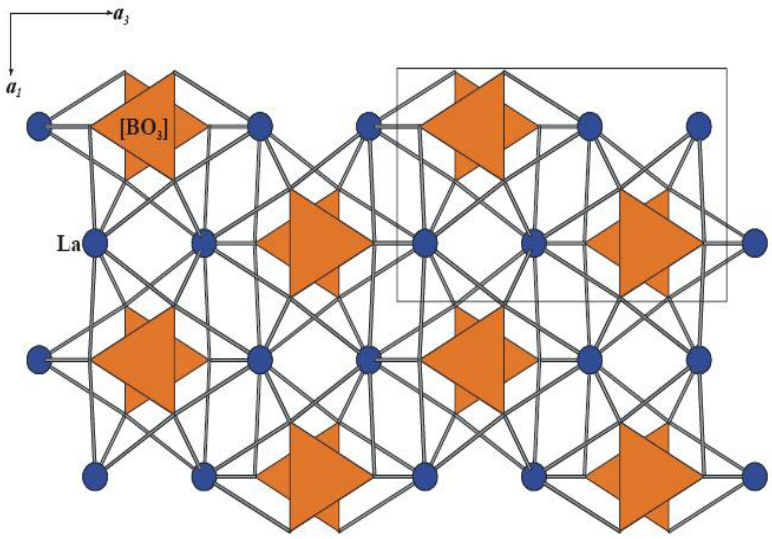


Figure 1.5 The projection of the structure of $LaBO_3$ (Aragonite-Type) parallel to [010]

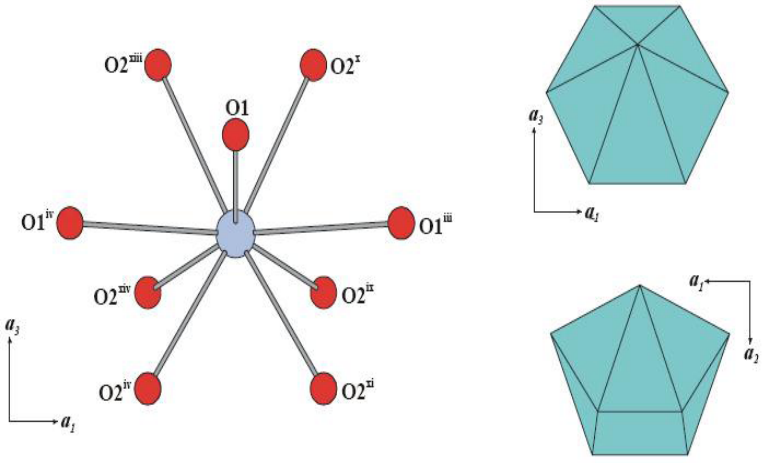


Figure 1.6 The coordination polyhedra of La-Atom in the structure of $LaBO_3$ (Aragonite-type)

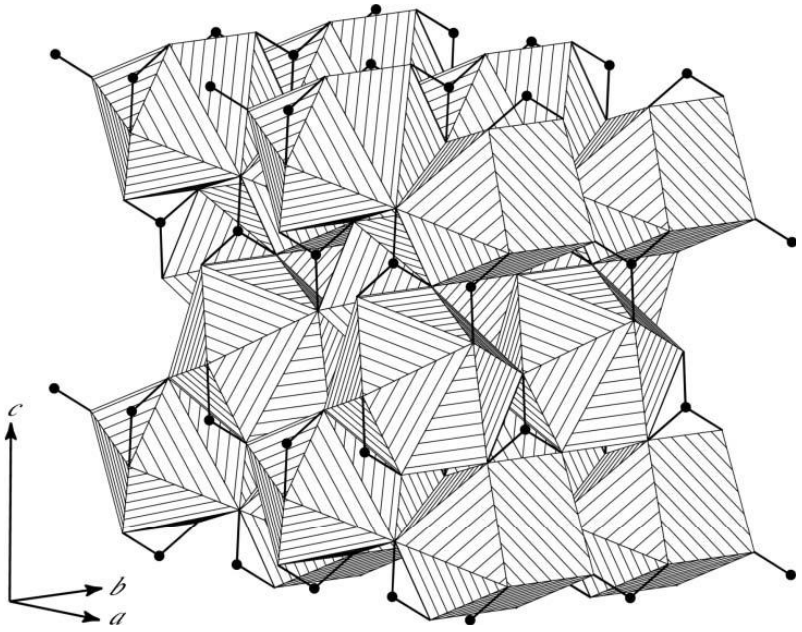


Figure 1.7 Representation of the aragonite-type LT-$LaBO_3$ structure. LaO_9 groups are shown as hatched polyhedra and B atoms as black spheres. B-O bonds are indicated as solid black lines.

For the smallest rare earth ions (Sm to Lu) the orthoborates possess the vaterite structure, which is consistent with a pseudo-hexagonal symmetry. In this series, $SmBO_3$ and $EuBO_3$ present both vaterite and H-forms.

Corbel et al. [15] have revised the crystal structure of $EuBO_3$ and assigned it to the space group *P-l*, similarly to the findings of Palkina et al. [16] for the case of low temperature $SmBO_3$. Triclinic $DyBO_3$ and $ErBO_3$ single crystals with *P-l* space group were obtained by Huppertz et al. [17] using high –pressure synthesis. Meyer obtained triclinic rare earth orthoborates $LnBO_3$ (Ln=Pr, Nd, Sm, Eu, Gd, Tb, Dy). Colorless single crystal rods of triclinic *(P-l)* $DyBO_3$ and triclinic *(P-l)* single crystals of $NdBO_3$ were synthesized by Emme and Huppertz [18] and Noirault et al. [19]

respectively. The structures of triclinic $SmBO_3$ were given by Gurnuyova in figure 1.8 [13]. In this figure, it is obvious that structure has $[BO_3]$ group around cationic polyhedra. In figure 1.8 the $[SmO_8]$ polyhedra in triclinic $SmBO_3$ structure.

In the structure of $SmBO_3$, the rare earth atoms occupy the centers of distorted SmO_8 triangulated dodecahedra (figure 1.9). Each dodecahedron shares edges with four others to build infinite double chains and also the isolated threefold coordination of boron is regular.

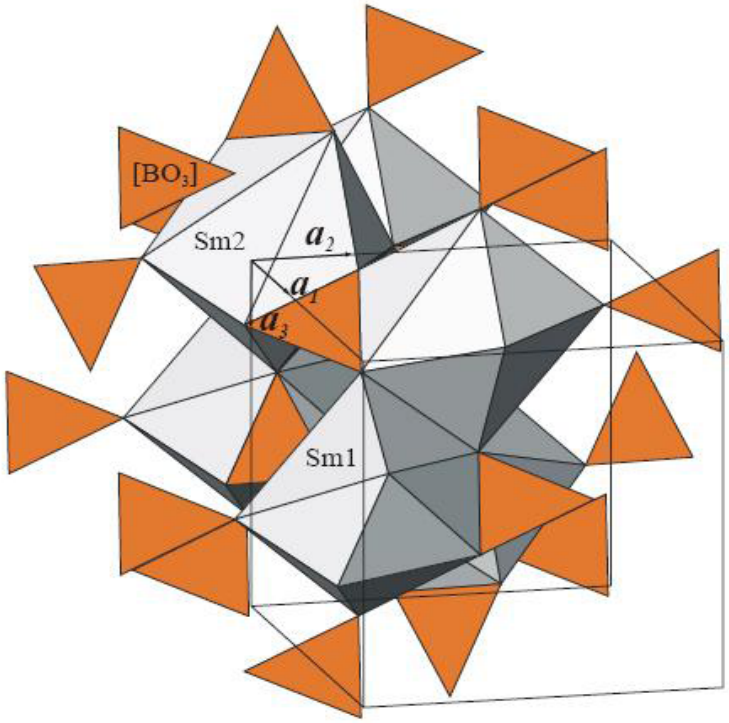


Figure 1.8 The structure of triclinic *(P-1)* $SmBO_3$

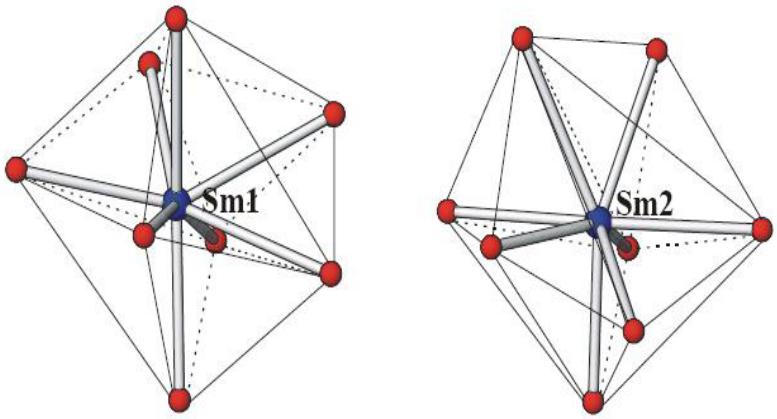


Figure 1.9 The [SmO_8] polyhedra in triclinic $SmBO_3$ structure

In the third series of borates, $InBO_3$, $LuBO_3$ and $ScBO_3$ are known to exhibit the calcite type [9, 20-22]. But $LuBO_3$ presents both a low temperature calcite form and a high temperature vaterite form. The calcite structure has a rhombohedral symmetry. The space group is $R\bar{3}c$ (z=6) with a single site for the rare earth having S_6 point symmetry.

In 1971, calcite structure of $YbBO_3$ has obtained by Meyer and Skohan [23]. The structural analysis of single crystal $LuBO_3$ and single crystal structural analysis of $YbBO_3$ were done by Abrahams et al. and Hupertz, respectively. The octahedral coordination of Lu-atoms and isolated trigonal [BO_3] groups were shown in figure 1.10.

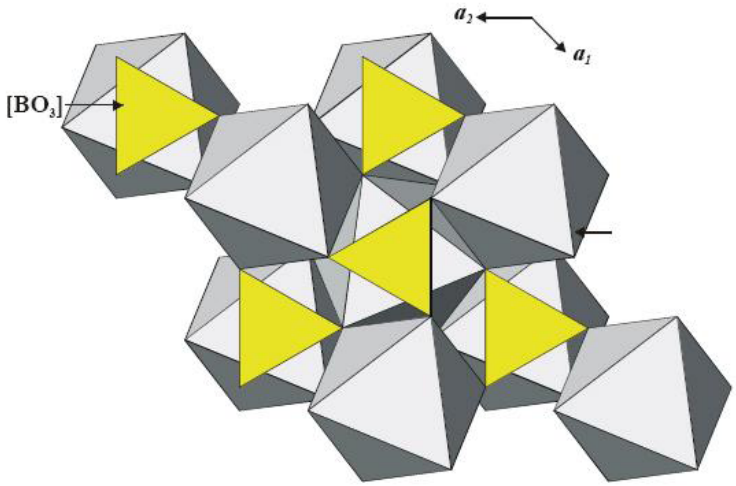


Figure 1.10 The structure of calcite type rare earth orthoborate (Abrahams et al.)

Many researchers have synthesized different vaterite type of $LnBO_3$ compounds using several techniques. In 2005, Tukia and coworkers have prepared vaterite type YBO_3 and $GdBO_3$ [24]. Felten prepared rare earth borates (Y, Sm, Eu, Gd, Dy, Ho, Er, Tm, Yb, Lu) of ABO_3 type by the reaction of the constituent oxides in equimolar rations between 1200 and 1400^oC in air and he observed that the borates of yttrium and smaller rare earth ions (samarium through lutetium) are isostructural with vaterite type $CaCO_3$ [25]. In Henkels and Schaak's work, $LnBO_3$ (Ln: Y, Nd, Sm, Eu, Gd, Ho) and YBO_3: Eu nanocrystallines were synthesized using a borohydride-based solution precursor route and they presented that they found vaterite structure for $LnBO_3$ orthoborates [26].

Recently, a new nonlinear optical (NLO) material $Ca_4YO(BO_3)_3$ has been found compounds of the borates family seem to be promising for NLO materials [27]. Consequently, in order to explore new NLO materials were studied several ternary system including La_2O_3-CaO-B_2O_3 [28], Y_2O_3-CaO-B_2O_3 [29], Li_2O-Al_2O_3-

B_2O_3 and MgO-Ga_2O_3-B_2O_3 [30] and found two new compounds $Ca_4LaO(BO_3)_3$, $LiAlB_2O_5$ [31] and the structure of the compounds $CaYBO_4$ and $MgGaBO_4$ was refined.

Zhang et al. investigated the Na_2O-O rich portion of the ternary diagram Ln_2O_3-Na_2O-B_2O_3 (Ln=Y, Gd). A new rare earth sodium borate with composition $Na_3Ln(BO_3)_2$ (Ln:Y,Gd) has been reported which was obtained by the solid state reaction of Na_2CO_3, H_3BO_3 with Ln_2O_3 (Ln:Y,Gd) for 24 hours of 900^oC [29]. These compounds crystallize in the monoclinic space group $P2_1/c$.

The cell parameters o these compounds are as follows [32]:

	a(Å)	b(Å)	c(Å)	β(^{o})
$Na_3Y(BO_3)_2$	6.499(8)	8.515(1)	12.020(2)	118.41(1)
$Na_3Nd(BO_3)_2$	6.618(5)	8.810(5)	12.113(5)	122.27

1.5. Infrared Studies of the Aragonite, Calcite and Vaterite Type Structures in Borates

For the isolated planar ion XO_3 having trigonal symmetry there are four fundamental modes of vibration; the symmetric stretching υ_1, the out of plane bending υ_2, the doubly degenerate antisymmetric stretching υ_3, the doubly degenerate planar bending υ_4. Of these fundamentals three are inherently active in the IR while the fourth, the symmetric stretching, is inactive in isolated ions.

In a crystalline solid containing more than one molecule per unit cell symmetry considerations indicate that all modes may even remove degeneracies [33]. In the calcite structure it is expected υ_2, υ_3, and υ_4 will be observed with υ_1 inactive and both υ_3 and υ_4 doubly degenerate. In the aragonite; six bands are expected since

in this structure υ_1 is active and the degeneracies are removed from υ_3, and υ_4. Vaterite is reported to have a hexagonal cell containing two or more molecules per unit cell.

Infrared frequencies for the calcite, aragonite and vaterite type structures in the borates are given in the table 1.6, 1.7 and 1.8 respectively [33].

Table 1.6 IR frequencies for the calcite structure

Compound	υ_1	υ_2	υ_3	υ_4	**(frequencies, cm^{-1})**
$InBO_3$	951	743 ,768	1288	676	
$LuBO_3$	951	748, 773	1275	630	

Table 1.7 IR frequencies for the aragonite structure

Compound	υ_1	υ_2	υ_3	υ_4	**(frequencies, cm^{-1})**
$LaBO_3$	944	725 ,790	1310	597, 613	
$NdBO_3$	951	720, 791	1307	598, 619	

Table 1.8 IR frequencies for the vaterite structure

Compound	**Distortion frequencies**	**Stretching frequencies cm^{-1}**
$LnBO_3$	578, 723	884, 952, 1093
$YbBO_3$	579, 722	881, 940, 1110
$TmBO_3$	576, 719	875, 940, 1080
$ErBO_3$	571, 716	876, 937, 1103
$HoBO_3$	569, 711	870, 931, 1096
$DyBO_3$	570, 708	872, 928, 1086
YBO_3	551, 714	874, 935, 1105
$GdBO_3$	567, 698	862, 922, 1082
$EuBO_3$	568, 693	860, 922, 1049
$SmBO_3$	568, 692	851, 910, 1035

1.6 Vibrational Spectra of Borates

There are three main groups for borates, e.g. the orthoborate BO_3^{3-}, the pyroborate $B_2O_5^{4-}$, the metaborate $(BO_2)_n^{n-}$.

The orthoborates are composed of isolated planar trigonal BO_3 group and they are expected D_{3h} symmetry with six fundamental modes of vibrations [33]. These modes are υ_1 (symmetric stretch, non-degenerate, 950 cm^{-1}), υ_2 (out plane bending, non degenerate, 750 cm^{-1}), υ_3 (antisymmetric stretch, doubly degenerate, around 1250 cm^{-1}) and υ_4 (in plane bending, doubly degenerate, 600cm^{-1}).

The IR spectra of the compounds of the type $M_x(B_2O_5)_y$ pyroborates (M: Mg, Ca, Sr, Ba, Cd) have been examined in literature [34]. Takeuchi [35] described the crystal structure of monoclinic mineral suanite, $Mg_2B_2O_5$, and also Mrose and Fleischer [36] studied and compared X-ray diffraction data of monoclinic and triclinic forms of $Mg_2B_2O_5$. The structure of the B_2O_5 group consists of two nonidentical BO_3 triangles with one common oxygen atom, so the spectrum of $Mg_2B_2O_5$ can be interpreted on the basis of these two, nonidentical joined triangles. It has been found that their strong characteristic absorption bands appeared in the region 600-800 cm^{-1} and 1100-1300 cm^{-1}.

The spectra of triclinic and monoclinic suanites are similar. But differ in the presence of two BO_3 deformation-vibration bands appearing at 612 and 630 cm^{-1} for the monoclinic form. In both natural and synthetic monoclinic suanite, the band at about 610 cm^{-1} splits to 613, 632 cm^{-1} and 612, 630 cm^{-1} respectively, whereas it appears as a single band in the spectrum of synthetic triclinic suanite [37].

There are data available about the vibrational spectra of the nine metaborate compounds in literature [34]. Metaborates are identified three types of borate ion with the overall formula $(BO_2)_n^{n-}$ and a fourth structure exists as a hydrated form. These structures are a chain structure, made up of $(-BO_2-)^-$ units, a ring structure, made from three of the same units, a three dimensional network, in which all the boron atoms are tetrahedral coordinated, and a double ring structure $B_5O_{10}^{5-}$, in

which the two rings are joined by a tetrahedral boron atom. The vibrational spectrum of these chain metaborates can be divided into four main spectral ranges [38]. υ_3 (1450 cm^{-1} for the $B\text{-}O_{ext,}$ 1150 cm^{-1} for the $B\text{-}O_{bridge}$), υ_2 (600-800cm^{-1} for deformation vibrations of the B-O group in $(BO_2)_n^{n-}$), υ_4 (~ 400 cm^{-1} bending vibrations).

In addition, tetrahedral BO_4 group gives nine fundamental modes of vibrations and are given by υ_1 (symmetric stretch, non-degenerate, 1000 cm^{-1}), υ_2 (bond bending, doubly degenerate, below 950 cm^{-1}), υ_3 (stretching mode, triply degenerate, near 600 cm^{-1}) and υ_4 (bending mode, triply degenerate, below 600 cm^{-1}) [39].

In the borates, the strong infrared band in the region 1250-1220 cm^{-1} is the characteristic of planar BO_3 group and this will be absent in borates having tetrahedral BO_4 groups.

The Infrared absorption spectra of natural and synthetic $Mg_3(BO_3)_2$ of the kotoite type were studied by Watanabe et al. [40]. The structure of $Mg_3(BO_3)_2$ is composed of flat triangles of BO_3^{3-} and divalent cations, which have an octahedral environment of oxygen atoms. The triangles have C_{2v} symmetry and are beveled toward the ab plane. Deformation in the symmetry of the triangle from D_{3h} to C_{2v} affects vibrations in the spectrum of kotoite that splitting of the twice degenerated υ_3 stretching vibration and the twice degenerated υ_4 deformation vibration are observed in the Infrared spectroscopy. These vibrations were given as υ_3: 1295, 1210 cm^{-1}; υ_2: 700 cm^{-1}; υ_4: 660, 613 cm^{-1} [41].

The IR spectrum of $Ni_3(BO_3)_2$ like kotoite structure were observed strong bands at 1200, 700, and 600 cm^{-1} [42].

IR absorption spectra of $Co_2Ni(BO_3)_2$ and $CoNi_2(BO_3)_2$, whose structure is the same with kotoite, binary metal borate compounds were studied by Güler [43-44] and the vibrational frequencies of (BO_3^{3-}) anion of $Co_2Ni(BO_3)_2$ and $CoNi_2(BO_3)_2$ were observed at 1255-450 cm^{-1} given in Table 1.9.

Table 1.9 The observed IR frequencies of $Co_2Ni(BO_3)_2$ and $CoNi_2(BO_3)_2$

Frequency (cm^{-1}) $Co_2Ni(BO_3)_2$	**Assignments**	**Frequency (cm^{-1}) $CoNi_2(BO_3)_2$**	**Assignments**
$\upsilon_3(BO_3)$	1255, 1170	$\upsilon_3(BO_3)$	1253, 1180
$\upsilon_2(BO_3)$	707, 668	$\upsilon_2(BO_3)$	712, 688
$\upsilon_4(BO_3)$	615, 485	$\upsilon_4(BO_3)$	622

1.7 Transition Metal Orthoborates

Different types of anhydrous transition metal orthoborates, M^xBO_3 and $M^aM^b(BO_3)_2$ where M are an element in the oxidation state x=1,2,3 and a=1,2,3 ; b=2,3,4,5 were reported in literature [6].

Orthoborates containing M^{3+}, MBO_3, such as $ScBO_3$, $InBO_3$, $GaBO_3$, $CrBO_3$, $TiBO_3$, and VBO_3 are the isostructural of the mineral calcite which studied by Waugh [45].

Another transition metal orthoborate which includes M^{2+}, $Ni_3(BO_3)_2$ was prepared preliminary with formula $3NiO.B_2O_3$[46]. Later, nickel orthoborate, $Ni_3(BO_3)_2$, had been reported by Götz [47] as isomorphous with the cobalt and magnesium orthoborates [48]. The crystal structure of $Ni_3(BO_3)_2$ were found in 1974 by Pardo et al.[42] and it crystallized in the orthorhombic system space group Pnnm. The synthesis of nickel orthoborate was carried out stoichiometry of three $NiO.B_2O_3$

at 1200^{o}C. The single crystal forms of the three compound $M_3(BO_3)_2$ (M=Mg, Co and Ni) and compared with crystal system of $Mn_3(BO_3)_2$ [49] were produced by Effenberger et al. [50]. They found that all of the synthesized metal orthoborates were crystallized in the kotoite form. The unit cell parameters of these kotoite type borates are shown in table 1.10.

Table 1.10 The cell parameters of the $M_3(BO_3)_2$ (M= Mg, Co and Ni) compounds having kotoite structure

Compounds and references	a (Å)	b (Å)	c (Å)
$Mg_3(BO_3)_2$ [48]	5.398(2)	8.416(2)	4.497(2)
$Co_3(BO_3)_2$ [48]	5.462(2)	8.436(2)	4.529(2)
$Ni_3(BO_3)_2$ [42]	5.396(1)	8.297(2)	4.459(1)

Searching for nickel borates, only one nickel borate with the composition $Ni_3(BO_3)_2$ could be found in the ternary system Ni-B-O, which shows trigonally coordinated boron atoms and Ni^{2+} ions in an octahedral coordination. Recently, Pompetzki et al. [51] found a new synthetic route to synthesize $Ni_3(BO_3)_2$ without impurities of NiO. Instead of a reaction between B_2O_3 and NiO [51] or $Ni(OH)_2$ [50], the authors favored the thermal decomposition of a mixture of $NiCO_3.2Ni(OH)_2.4H_2O$ and H_3BO_3 [51].

The synthesis of the isomorphous orthoborates of cobalt and magnesium were prepared by heating mixtures of $CoCl_2.6H_2O$ and $B(OH)_3$ at 900^{o}C in the ratio 3:2 [50] and from the starting material of $MgCl_2$ and B_2O_3 at 800^{o}C [52] in respectively.

The crystal structure of kotoite $Mg_3(BO_3)_2$ has also been analyzed by Berger [48] using synthetic crystals. The structure of a mineral jimbolite [40] (the jimbolite name was given to honor professor Kotora Jimbo the founder of the Mineralogical Institute, University of Tokyo, Japan), the manganese analogue of kotoite, has been

analyzed by Sadanaga et al. [53] and that of synthetic jimboite by Bandareva et al. [49] (The kotoite name was given to honor Professor Bundjiro Kato Japanese geologist, University of Tokyo, Japan who studied the ore deposits of Hoi Kol, North Korea).

$Mn_3(BO_3)_2$, such as jimbolite was formed in manganese carbonate ores by a boron trioxide at about 700^oC for 30 minutes, as shown in the following reaction:

$$3MnCO_3 + B_2O_3 \rightarrow Mn_3(BO_3)_2 + 3CO_{2(g)}$$

Rhodochrosite jimbolite

(Rhodochrosite is a crystalline mineral composed mainly of manganese carbonate $MnCO_3$). It has an orthorhombic structure (jimbolite) unit cell with parameters a= 5.658(1), b= 8.740(1), c= 4.646(2) Å.

In 1980, $Ca_3(BO_3)_2$ and $Sr_3(BO_3)_2$ have been reported as isostructural, trigonal, space group $R\bar{3}c$. The lattice parameters and the powder diffraction data were also reported [54].

Smith and Keszler synthesized two phases, a low-temperature α form and a high-temperature β form, $Sr_2Cu(BO_3)_2$ compound, by solid state reactions and published its single crystal X-ray data [55]. The α and β form $Sr_2Cu(BO_3)_2$ compounds have been crystallized monoclinic and orthorhombic structure respectively. Cell parameters, space group and z values of α and β $Sr_2Cu(BO_3)_2$ are given table 1.11

Table 1.11 Cell parameters, space group and z values of α and β $Sr_2Cu(BO_3)_2$

Compound	**Spacegroup / System**	**Unit cell parameters**	**z values**
α-$Sr_2Cu(BO_3)_2$	$P2_1/c$ monoclinic	a= 5.707(1) b=8.796(2) c= 6.027(1) β= 116.98(1)^o	2
β-$Sr_2Cu(BO_3)_2$	Pnma orthorhombic	a= 7.612(3) b=10.854(7) c= 13.503(4)	8

The high-temperature β form exhibits larger coordination numbers for the Sr atoms and a substantial rearrangement of the copper borate network relative to that of the low-temperature α form.

Later on, in 1991, the new orthoborate $SrCu_2(BO_3)_2$ has been reported to have tetragonal crystal structure with space group $I\overline{4}2m$ and unit cell parameters a= 8.995(1)Å c= 6.649(1)Å V=537.9(1)Å^3 with z=4 [56].

The BaO-CuO-B_2O_3 phase system [57] has also been studied by Keszler et al. At the 2:1 composition and preparation temperatures at 1173K for 18h, $Ba_2Cu(BO_3)_2$ is found to be isostructural with orthorhombic β-$Sr_2Cu(BO_3)_2$. The structure features discrete units of formula $Cu_2(BO_3)_4$ that are interconnected by three crystallographically independent Ba atoms as shown in figure 1.11. The copper borate unit is composed of two highly distorted O square planes occupied by the Cu atoms that are bridged by two triangular BO_3 groups.

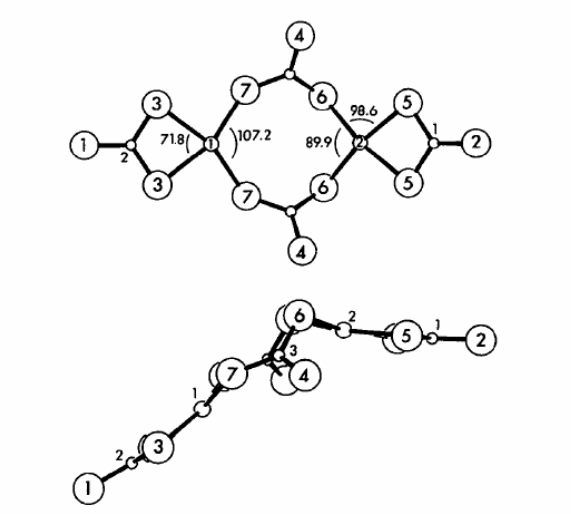


Figure 1.11 Sketches of the $Cu_2(BO_3)_4$ unit. Top: view [100]. Angles in °. Bottom: view along direction orthogonal to mirror plane at y = ¼.

Four other borates with a similar formula $A_2^{2+}B^{2+}(BO_3)_2$ A: Ba, Sr, Ca and B= Ca, Mg have been reported. The compound $Ba_2Mg(BO_3)_2$ is isomorphous to the trigonal mineral buetschliite, $K_2Ca(CO_3)_2$, [58] the compound $Ca_2Mg(BO_3)_2$ is tetragonal, and the compounds $Ba_2Ca(BO_3)_2$ and $Sr_2Mg(BO_3)_2$ are related to buetschliite [59].(Buetschliite was recognized as a mineral and named by Milton and Axelrod who found it in wood-ash stones from half a dozen localities in the Western United States [60])

In table 1.12 the crystal structures of $A_2^{2+}B^{2+}(BO_3)_2$ are given together with their space groups and unit cell parameters.

Table 1.12 Crystallographic data for the Borates $A_2^{2+}B^{2+}(BO_3)_2$

Compound	**Space group**	**a (Å)**	**b (Å)**	**c(Å)**	**β**
$Ba_2Mg(BO_3)_2$ [61]	$R\bar{3}m$	5.343	5.343	6.52	
$Ba_2Ca(BO_3)_2$ [62]	C2/m	9.635	5.432	6.635	119.38
$Sr_2Mg(BO_3)_2$ [63]	C2/m	9.035	5.146	6.099	118.59

$Ba_2Mg(BO_3)_2$ and $Ba_2Ca(BO_3)_2$ structures are represented in figure 1.12 and figure 1.13. In these structures, the hexagonal and monoclinic structures are related by a rotation of the small cation-centered (Mg or Ca) octahedra and a tilting of the BO_3 groups. This rotation and tilting move one of the three O atoms from the triangular, trigonal plane of the 6+3 coordination sphere about Ba in $Ba_2Mg(BO_3)_2$ to apposition outside the distorted hexagonal plane of the BaO_9 polyhedron in $Ba_2Ca(BO_3)_2$ [64].

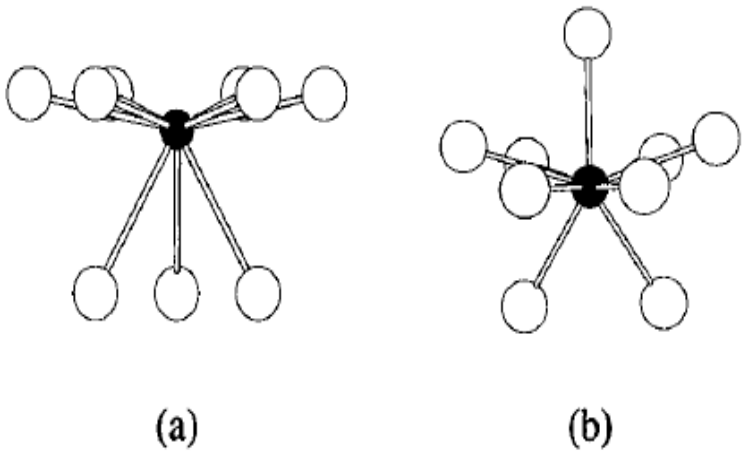


Figure 1.12 Ba sites in (a) $Ba_2Mg(BO_3)_2$ and (b) $Ba_2Ca(BO_3)_2$. Filled circles = Ba; open circles = O.

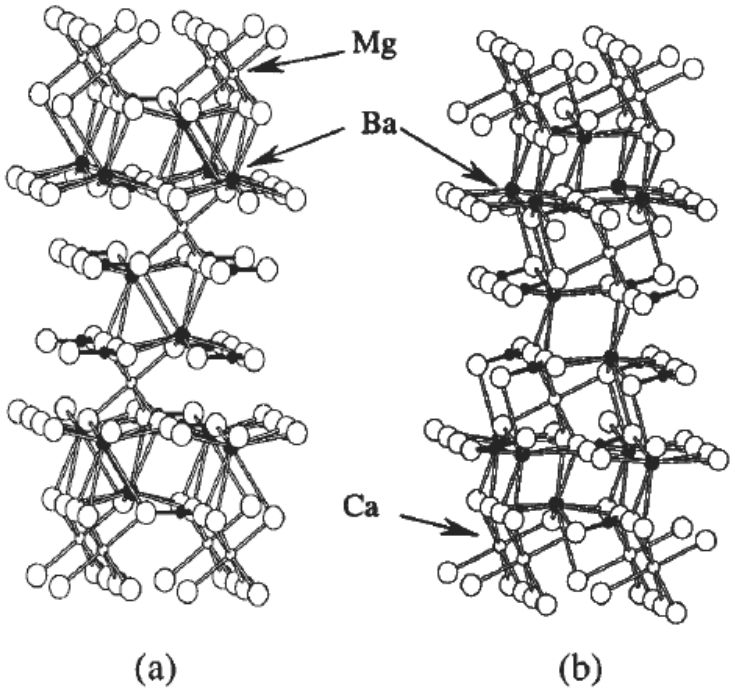


Figure 1.13 (a) Hexagonal unit cell of $Ba_2Mg(BO_3)_2$ and (b) the pseudohexagonal cell of $Ba_2Ca(BO_3)_2$.

Recently, a new binary metal orthoborate compounds, $Co_2Ni(BO_3)_2$ and $CoNi_2(BO_3)_2$, have been synthesized for the first time. Güler et al. [43, 44] prepared these compounds by heating mixtures of $Co(NO_3)_2.6H_2O$, $Ni(NO_3)_2.6H_2O$ and H_3BO_3 at 900°C in the ratios 2:1:2 and 1:2:2 by means of the following reactions.

$$2Co(NO_3)_2.6H_2O_{(s)} + Ni(NO_3)_2.6H_2O_{(s)} + 2H_3BO_{3(s)} \rightarrow \mathbf{Co_2Ni(BO_3)_{2(s)}} + 6NO_{2(g)} + 18H_2O_{(g)} + 3O_{2(g)}$$

$$Co(NO_3)_2.6H_2O_{(s)} + 2Ni(NO_3)_2.6H_2O_{(s)} + 2H_3BO_{3(s)} \rightarrow \mathbf{CoNi_2(BO_3)_{2(s)}} + 6NO_{2(g)} + 18H_2O_{(g)} + 3O_{2(g)}$$

The compounds were examined by X-ray powder diffraction technique, it was concluded that both compounds [$Co_2Ni(BO_3)_2$ and $CoNi_2(BO_3)_2$] have kotoite type, orthorhombic crystal system, and isostructural with the compounds having the formula $M_3(BO_3)_2$ where M= Mg, Co and Ni. The unit cell parameters, space groups and z values are shown in Table 1.13.

Table 1.13 The unit cell, space groups and z values of the $M_2M(BO_3)_2$ compounds having kotoite (orthorhombic) structure.

Compound	**a(Å)**	**b(Å)**	**c(Å)**	**Space group**	**Z**
$Co_2Ni(BO_3)_2$	5.444(8)	8.404(0)	4.504(1)	Pnmn	2
$CoNi_2(BO_3)_2$	5.419(9)	8.352(0)	4.478(8)	Pnmn	2

1.8 Borophosphates

The structural complexity of borophosphate compounds is influenced by localized bonding arrangements of the principal components, B_2O_3 and P_2O_5. In the structure of borate, boron atoms can form planar or pyramidal BO_3 group with 3-oxygen atoms by trigonal sp^2 bonds, or tetrahedral BO_4 group with 4-oxygen atoms by tetrahedral sp^3 bonds. Besides, borate can contain not only the above two simple groups, but also many complex groups, such as the more elaborate symmetrical B_3O_6 boroxol ring, unsymmetrical B_3O_7 ring which containing interconnected BO_3 and BO_4, and infinite chain $(BO_2)_n$ containing only threefold coordinated borons [65].

In the structure of phosphate there are mainly two kinds of groups: the relatively simple PO_4 tetrahedral group, and the complex P_2O_7 group consisting of two distorted tetrahedra PO_4 with nonlinear P-O-P bond. For the borophosphate Levesseur et al. [66] reported the existence of "BPO_7 group" which is the basic constituent of a silica-like network where B and P are four-fold coordinated and all

oxygens are bridging ones. In addition, the introduction of alkaline earth oxide may create new structural units. Therefore, the considerable variety in crystal structure of borophosphate compounds provides a great deal object for the study aiming at exploring new functional materials, especially for the nonlinear optical materials.

Ramamoorthy et al. [67] was first prepared $CaBPO_5$ from phase equilibria studies on the system $CaO\text{-}B_2O_3\text{-}P_2O_5$ at 900°C.

M^I_2O / $M^{II}O\text{-}B_2O_3\text{–}P_2O_5\text{-}(\text{-}H_2O)$ systems (M^I: alkali metal, M^{II}: alkaline earth metal) have been reported which were obtained by the solid state reaction using the following reactions and X ray diffraction pattern of the isostructural (hexagonal) phases $M^{II}[BPO_5]$ (M^{II}: Ca, Sr, Ba) by Bauer [68,69].

$$CaHPO_4.\ 2H_2O + H_3BO_3 \rightarrow CaBPO_5 + 4H_2O$$

$$SrCO_3 + H_3BO_3 + (NH_4)_2HPO_4 \rightarrow SrBPO_5 + 3H_2O + CO_2 + 2NH_3$$

$$BaCO_3 + H_3BO_3 + (NH_4)_2HPO_4 \rightarrow BaBPO_5 + 3H_2O + CO_2 + 2NH_3$$

These borophosphates were found to have hexagonal structure and, respectively, unit cell parameters were a=6.688, c=13.234; a=6.857, c=13.657; a=7.111, c=13.977 Å.

Kniep et al. [70] and Gözel [71] solved the structure of $CaBPO_5$ and $SrBPO_5$ by Rietveld method. $CaBPO_5$ and $SrBPO_5$ are hexagonal and, respectively, unit cell parameters are a= 6.6799 c= 6.6121; and a= 6.8488 c= 6.8159 Å. It was observed that the ‘c’ parameter is about the half of the ‘c’ given by Bauer.

Synthesis of $CaBPO_5$ [72] and $SrBPO_5$ [73] were also prepared by Baykal et al. In recent years, $BaBPO_5$ was prepared by using three different methods [65, 74, 75].

In 1982, Mg_3BPO_7 and Zn_3BPO_7 have been reported to have α (low temperature form) and β (high temperature form) structure. Liebertz and Stähr reported that there were two different crystal structures [76]. Later on, Bluhm et al. [77] were able to synthesize single crystals of α-$Zn_3(BO_3)(PO_4)$ at 1050^oC by the reaction of B_2O_3, P_2O_5 and $ZnCO_3$ as starting materials. The structure is monoclinic, space group Cm, and cell parameters a=9.725(2), b=12.723(3), c=4.874(3), β= 119.30^o(4) and Z=4. In 2002, Wang and coworkers [78] growth the single crystal of this compound from melt in hexagonal systems. In recent years, Yılmaz et al. were able to prepare Co_3BPO_7 by the boron flux method [79].

$M_3[BPO_7]$ (M: Mg, Ba and Sr) was obtained by the solid state reactions given below in the temperature range of 700-1500^oC and indexed all of them in the orthorhombic crystal system as reported by Gözel [71]. The cell parameters and the space groups are given in Table 1.14.

$$MgHPO_4.3H_2O + 2MgCO_3 + H_3BO_3 \rightarrow Mg_3[BPO_7] + 2CO_2 + 5H_2O$$

$$3SrCO_3 + H_3BO_3 + (NH_4)_2HPO_4 \rightarrow Sr_3[BPO_7] + 2NH_3 + 3CO_2 + 3H_2O$$

$$3BaCO_3 + H_3BO_3 + (NH_4)_2HPO_4 \rightarrow Ba_3[BPO_7] + 2NH_3 + 3CO_2 + 3H_2O$$

Table 1.14 Cell Parameters and the Space Groups of $M_3[BPO_7]$ (M=Mg, Ba and Sr) reported by Gözel.

Compound	**a (Å)**	**b (Å)**	**c (Å)**	**Space group**
α $Mg_3[BPO_7]$	8.49	4.88	12.55	Pmmm
α $Sr_3[BPO_7]$	9.0561	9.7984	13.9531	P2/m
α $Ba_3[BPO_7]$	11.7947	9.6135	12.9548	P2/m

Besides these, many other borophosphate compound with the anion groups $[B_2P_3O_{13}]^{5-}$ [80], $[BP_3O_{14}]^{10-}$= ($[(BPO_6)(PO_4)_2]$) [81], $[BP_3O_{12}]^{6-}$ =($[(PO_4)_2BPO_4]$)

[70, 82] and $[BP_2O_8]^{3-}$ [83] were synthesized and characterized by many research groups.

The crystal structure of the isomorphical rare-earth borophosphate compound $Ln_7O_6(BO_3)(PO_4)_2$ Ln= La, Nd, Gd and Dy) has been synthesized from H_3BO_3, Ln_2O_3 and $NH_4H_2PO_4$ through solid state reactions at 1300^oC. Then, these isomorphical borophosphate compounds were indexed in monoclinic system [84].

Later on, a new series of borophosphates A_3BPO_7 (A=Ca, Sr, Ba) have been obtained and characterized. Polycrystalline Ba_3BPO_7 was prepared from the mixtures of $BaCO_3$, H_3BO_3 and $NH_4H_2PO_4$ by solid state reaction at 1200^oC in Pt crucible for 48h. The crystal structure of new compound Ba_3BPO_7 was determined by ab inito method from high resolution conventional X-ray powder diffraction data [85].

1.9 Phosphorus and Phosphates

It is generally accepted that elemental phosphorous was for the first time isolated by Brand in 1669. A huge amount of data has been accumulated on the phosphorous since the Brand's discovery. Three forms of phosphorous exist, white, black and red. White phosphorous is the most reactive of the three phosphorous forms and reacts with most of the elements. Although red phosphorous was discovered in 1847 by Von Schrotter, our knowledge about red phosphorous is fragmentary and still confuse. To the difference with the white form, red phosphorous does not ignite when in contact with oxygen. Black phosphorous discovered by Bridgeman in 1994 can be considered as a high pressure form of the white phosphorous. It is not soluble in the classical of the white form suggesting and it is not molecular but polymeric arrangement [86].

Phosphates are the salts of P_2O_5 with metal oxide or simple and complex oxides obtained from phosphoric acid. Phosphates materials can be presently classified in three families: Monophosphates, condensed phosphates and heteropolyphosphates.

Monophosphates, previously known as orthophosphates, is given to compounds whose anionic entity, $[PO_4]^{3-}$ is composed by an almost regular tetrahedral arrangement of for oxygen atoms centered by a phosphorous atom. The term "condensed phosphates" is applied to salts containing condensed phosphoric anions. There are three types of condensations for the phosphoric anion: Polyphosphates ($[P_nO_{3n+1}]^{(n+2)-}$), cyclophosphates ($[P_nO_{3n}]^{n-}$) and ultraphosphates ($[P_{n+2}O_{3n+5}]^{n-}$) [86].

1.10 Oxyphosphates

Oxyphosphates with the general formula $M(PO_4)_nO_m$ where m or n= 1,2,… can be considered in five groups based on the valance electrons of central metal ion, M. M can be pentavalent $MoPO_5$, monovalent and quadrovalent $KTiPO_5$, trivalent $Gd_3(PO_4)O_3$, trivalent and divalent $CaBPO_5$ and divalent $Ca_4(PO_4)_2O$ [86].

For several reasons related to potential applications such as, laser properties, nonlinear optical properties, ferroelectricity, magnetism, ionic conductivity or superconductivity catalytic activity, etc., metal oxide phosphate compounds are still currently being investigated.

Until now, the known oxyphosphates type of $MOPO_4$ (M: V, Nb, Mo, Ta, W, Sb) and $MM'OPO_4$ (M: K, Rb, Tl; M:Ti) , (M: Na; M': La, Nd, Gd and Dy) orthorhombic, monoclinic and tetragonal structures have been reported using

different solid-state reactions [86]. The formula and structural types of these oxyphosphates are given in table 1.15.

Table 1.15 The formula and structural types of known oxyphosphate

Formula Type	Compound	Space Group	Unit cell parameters (Å)	Structural type	Refs.
$MOPO_4$	α $VOPO_4$ β $VOPO_4$		a= 6.20, c=7.41	Tetragonal Orthorhombic	[87], [88]
	$NbOPO_4$	P_{nma}	a=11.304(2), b=5.316(2), c=6,640(2)	Orthorhombic	[89]
	$MoOPO_4$			Tetragonal	[90]
	$TaOPO_4$	$P2_1/c$	a=11.272 b=5.281 c=6.621	Monoclinic	[91]
	$WOPO_4$		a=11.1721(8) b=5.217(1) c=6.543(2)	Monoclinic	[92]
	$WOPO_4$		a=6.250(1) c=4.066(1)	Tetragonal	[92]
	$SbOPO_4$	C2/c	a=6.791 b=8.033 c=7.046	Monoclinic	[93]

$MM'OPO_4$ M: alkali metal M': transition metal	$KTiOPO_4$ (KTP)	Pnma or $Pn2_1a$	a=12.814 b=10.616 c=6.404	Orthorhombic	[94]
	$RbTiOPO_4$ (RTP)	Pnma or $Pn2_1a$	a=12.971 b=10.577 c=6.942	Orthorhombic	[94]
	$TlTiOPO_4$ (TTP)	Pnma or $Pn2_1a$	a=12.893 b=10.573 c=6.490	Orthorhombic	[94]
	$LiTiOPO_4$	Pnma	a=7.394(2) b=6.371(2) c=7.228(1)	Orthorhombic	[95]
	$KSnOPO_4$	$Pn2_1a$	a=13.145(3) b=6.526(2) c=10.738	Orthorhombic	[96]
	$NaVOPO_4$	$P2_1/c$	a=6.5296(4) b=8.4643(7) c=7.1228(6)	Monoclinic	[97] [98]
$MM'OPO_4$ M: alkali metal M':rare-earth metal	Na_2GdOPO_4	Pmm2	a=13.074(6) b=10.637(5) c=6.469(3)	Orthorhombic	[99]
	Na_2GdOPO_4	Pmm2	a=14.709(6) b=10.661(4) c=13.081(6)	Orthorhombic	[100]

	Na_2GdOPO_4	Pmm2	a=14.719(5) b=10.669(3) c=13.091(5)	Monoclinic	[100]
	Na_2LaOPO_4	Pmm2	a=13.657(5) b=11.076(5) c=6.730(3)	Orthorhombic	[100]
	Na_2NdOPO_4	Pmm2	a=15.924 b=10.734 c=13.171	Orthorhombic	[86]
	Na_2DyOPO_4	Pmm2	a=12.856 b=10.621 c=6.403	Orthorhombic	[86]
$MM'OPO_4$ M: alkali metal M':rare-earth metal	Na_2DyOPO_4	Pmm2	a=14.676 b=10.623 c=13.042	Orthorhombic	[86]
	Na_2LaOPO_4	Pmm2	a=13.60(1) b=12.71(1) c=6.96(1)	Orthorhombic	[101]
	Na_2NdOPO_4	Pmm2	a=13.466(5) b=12.547(6) c=6.932(5)	Orthorhombic	[101]
	Na_2SmOPO_4	Pmm2	a=13.54(1) b=12.577(8) c=7.047(5)	Orthorhombic	[101]

MM'OPO_4 M: alkali metal M':rare-earth metal	Na_2GdOPO_4	Pmm2	a=13.37(1) b=12.775(9) c=6.910(9)	Orthorhombic	[101]
	Na_2DyOPO_4	Pmm2	a=13.66(2) b=12.609(9) c=6.611(6)	Orthorhombic	[101]
	Na_2HoOPO_4	Pmm2	a=13.148(4) b=12.577(2) c=6.967(1)	Orthorhombic	[101]
	Na_2ErOPO_4	Pmm2	a=13.563(5) b=12.604(4) c=7.003(3)	Orthorhombic	[101]
	Na_2YbOPO_4	Pmm2	a=13.501(7) b=17.579(9) c=6.729(4)	Orthorhombic	[101]

Recently, it has been shown that the same type of structure can be obtained by substitution of the K^+ by Li^+, Rb^+, Tl^+ [102,103] and substitution of the Ti^{IV}, Sn^{IV}, Ge^{IV}, Zr^{IV} [104, 105]. In our group, we conceived the idea of preparing new oxyphosphates analogues of KTP by subtitution of the K^+ by Na^+ and substitution of titanium by a rare earth metal such as, Nd, Gd and Dy. The initially study in this field was performed by Uztetik and Kızılyallı [99]. They prepared sodium gadolinium oxyphosphate, Na_2GdOPO_4, analogue of KTP through the solid-state route. Later on,

a different orthorhombic form of this compound are also reported [100]. In our previous study [86], sodium neodymium oxyphosphate, Na_2NdOPO_4, and sodium dysprosium oxyphosphate, Na_2DyOPO_4, are synthesized by using different solid-state reaction and characterized by XRPD, IR and Thermal methods. In 2008, Seyyidoglu and coworkers investigated Na_2LnOPO_4 (Ln: La, Nd, Sm, Gd, Dy, Ho, Er and Yb) through the solid-state reaction by using Ln_2O_3, Na_2CO_3 and $NH_4H_2PO_4$ which were mixed with the mol ratio of 1:2:2 respectively and studied its XRD, IR, Raman data and SEM micrographs [101]

In the literature survey given above the rare earth oxyphosphate were synthesized using only Na alkali metal. However no attempt for the syntheses of other lithium lanthanide oxide phosphates has yet been reported in the literature. In this theses are synthesized and investigated lithium rare earth (mainly Nd, Gd and Dy) oxyphoshates and structural information for known sodium gadolinium oxyphosphates.

In recent years inorganic oxyphosphates with the general formula $AMOPO_4$ with either A monovalent (K^+, Na^+, Li^+, Rb^+) and M tetravalent (Ti^{4+}, Zr^{4+}) or A divalent (Ni^{2+}, Co^{2+}, Fe^{2+}, Cu^{2+}, Sn^{2+}) and M trivalent (Bi^{3+}, Cr^{3+}, Fe^{3+}, V^{3+}, Gd^{3+}, La^{3+}) have been exhaustively investigated [106]. Among these compounds, titantium phosphates both in glass and crystalline forms have been extensively studied for the interest in their properties as ionic conductors or non linear optical materials. The most known is potassium titantium oxide phosphate ($KTiOPO_4$), or KTP, which is an excellent nonlinear optical properties in the visible range, because of their high nonlinear coefficients and wide acceptance of temperature and angular fluctuations. The qualities and the potential applications of KTP arose great interest in analogue which has partial or complete substitution on K, Ti and P sites.

Chaminade and Manoun et al. [107] were found on the existence of $LiTiOPO_4$, $Ni_{0.50}TiOPO_4$, $Li_{(1-2x)}M_xTiOPO_4$ (M: Ni,Co) oxyphosphates. The structure of $Ni_{0.50}TiOPO_4$ ($P2_1/c$ space group), $Li_{0.50}Ni_{0.25}TiOPO_4$ ($P2_1c/c$ space group) and $LiTiOPO_4$ (Pnma space group) have been determined from powder for these compounds and single crystal for $LiTiOPO_4$ from X-ray diffraction data.

The structure of $Li_{(1-2x)}Ni_xTiOPO_4$ was resolved by Manoun et al. and the structure of the composition $0 \leq x \leq 0.25$ is based on a three-dimensional anionic framework constructed of chains of alternating TiO_6 octahedra and PO_4 tetrahedra, with the lithium and nickel atoms in the cativies in the framework as shown in the figure 1.14. KTP has an orthorhombic structure and belongs to the acentric point group mm2 (space group $Pna2_1$). Its structure consists of PO_4 and TiO_6 octahedra with potassium in larger voids. Ti-O bonds are short which are believed to be the prime cause of the nonlinear properties of $KTiOPO_4$.

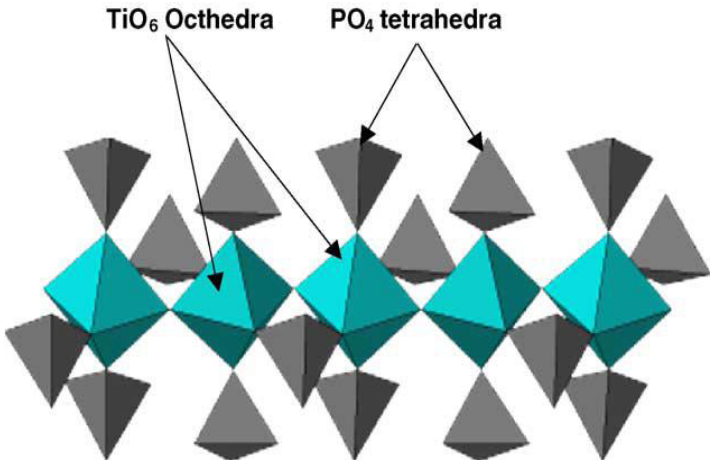


Figure 1.14 The structure of $Li_{(1-2x)}Ni_xTiOPO_4$ represented by Ti-O-Ti-O- chains

In another study Benmokhtar et al. synthesized a new iron titanyl oxyphosphate $Fe_{0.50}TiOPO_4$ by both solid state reaction and by exchange reaction [108]. A new oxyphosphate compound crystallizes in the monoclinic system $P2_1/c$ space group. The structure of the new oxyphosphate is represented in figure 1.15 and figure 1.16. The structure has been described from $[TiO_6]$ octahedra and $[PO_4]$ tetrahedra. $[TiO_6]$ octahedra are linked together by corners and form infinite chains along the c-axis. Ti atoms are displaced from the center of octahedral units showing an alternating short distance (1.73Å) and a long one (2.22Å).

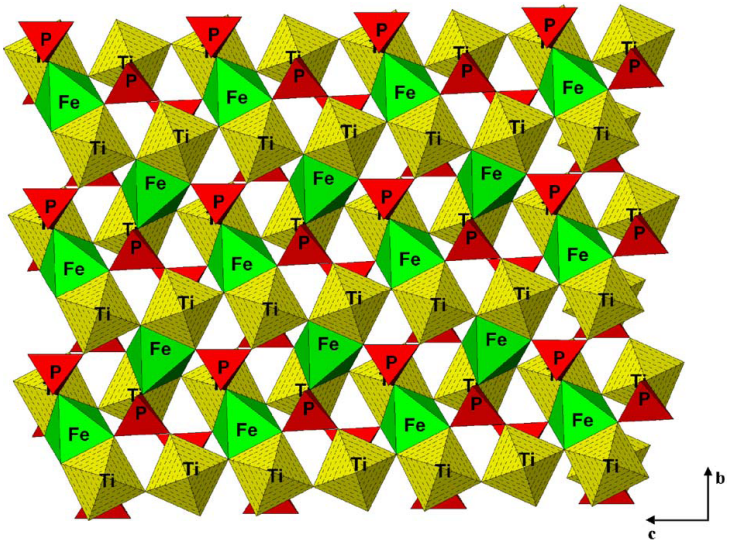


Figure 1.15 A polyhedral view of framework as projected in the (b, c) plane.

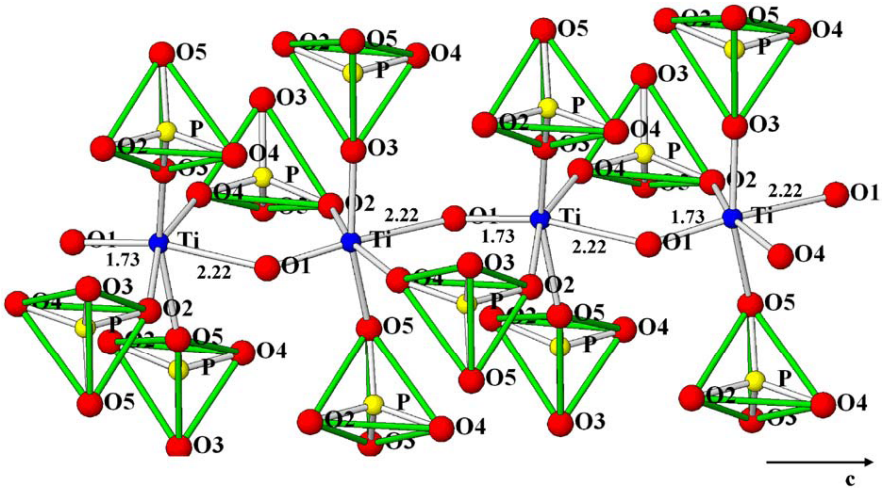


Figure 1.16 Chain of TiO_6 octahedra in oxyphosphate $Fe_{0.50}TiO(PO_4)$ linked to PO_4 tetrahedra, along c-axis

These chains are linked together by $[PO_4]$ tetrahedra Fe^{2+}cations occupy a triangle-based antiprism sharing two faces with two $[TiO_6]$ octahedra.

The most recent studies, a new family of titano-oxyphosphate of formulation $M^{II}_{0.50}TiO(PO_4)$ for M^{II}: Mg, Co, Cu, Zn was synthesized [109,111]. Among these compounds syntheses of copper II oxyphosphate $Cu_{0.50}TiO(PO_4)$ was found mixtures of two allotropic phases α and β. Single crystal of the β phase were not obtained. Despite of the relatively strong difference between their cell parameters, α and β varies have similar structure types and the same space group $P2_1/c$ [110].

1.11 Apatite

Apatite is a mineral composed primarily of calcium and phosphate. It is the most stable and abundant form of phosphorus on Earth. Apatites are widely distributed as accessory minerals in igneous rocks and in small quantities in most metamorphic rocks. This wide-spread occurence is an important factor in their

extensive use in fission-track chronothermometry for the study of geological thermal history. Rock phosphates (microcrystalline apatites), mostly of biological origin, are the starting material for phosphate fertilizer manufacture and a source of phosphorus for the chemical industry [112].

Apatites have the general chemical formula $Ca_{10}(PO_4)_6X_2$ where X is typically OH (hydroxyapatite, OHAp), F (flourapatite, FAp) or Cl (chlorapatite, ClAp). The lattice is very tolerant of substitutions, vacancies and solid solutions, for example, X can be replaced by ½ CO_3 or ½ O; Ca by Sr, Ba, Pb, Na or vacancies; and PO_4 by HPO_4, AsO_4, VO_4, SiO_4 or CO_3 [113]. They most frequently crystallize in a hexagonal system $P6_3/m$.

The basic apatite structure $Ca_5(PO_4)_3$(OH, F, Cl) was determined by Naray-Szabo [114] and Mehmel [115] in 1930. It can be described (Figure 1.17) as the three- dimensional network of PO_4 tetrahedra, which are linked together by the columns of ninefold coordinated Ca_1 atoms (Figure 1.18 a).

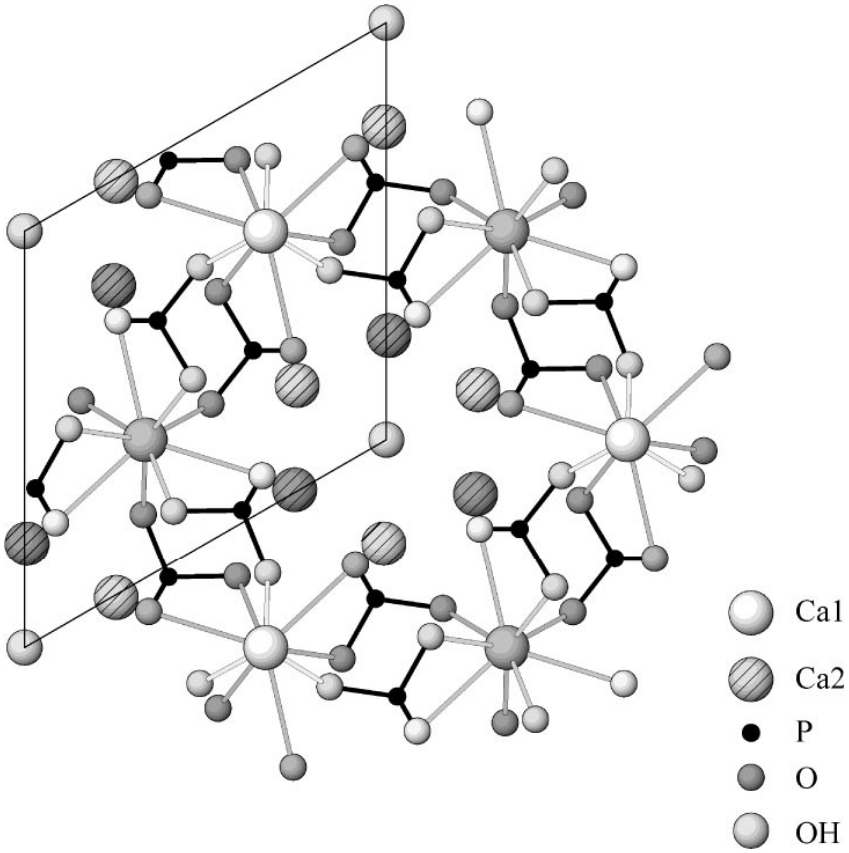


Figure1.17 Crystal structure of apatite. Projection onto the (0001) plane

The channels passing through the network have the axes coinciding with the sixfold screw axes and contain the triangles of sevenfold coordinated Ca2 atoms (Figure 1.18 b) and OH^-, F^- or Cl^- ions.

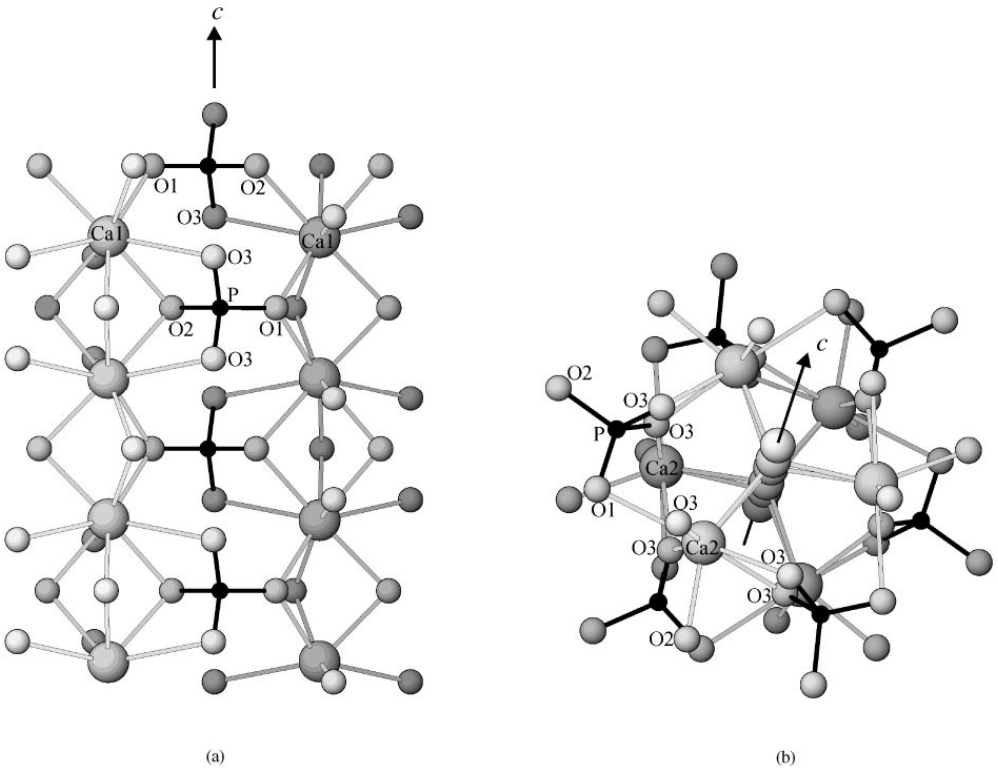


Figure 1.18 Types of calcium polyhedra in the structure of apatite.(a) Columns of ninefold coordinated Ca1 polyhedra, and (b) triangles of sevenfold coordinated Ca2 polyhedra.

Hydroxyapatite (HAP: $Ca_{10}(PO_4)_6(OH)_2$) is the main mineral constituent of teeth and bones. HAP ceramics does not exhibit any cytoxic effects. It shows excellent biocompatibility with hard tissues and also with skin and muscle tissues. Moreover, HAP can directly bond to the bone. Unfortunately, due to reliability, especially in wet environments, the HAP cannot presently be used for heavy load-bearing application, like artificial teeth or bones [116].

Morgan and coworkers [117] were synthesized $Ca_{10}(PO_4)_6(OH)_2$, hydroxyapatite, (HAP or OHAP) by heating an aqueous slurry mixture of $CaCO_3$ and $CaHPO_4$ by means of the following reaction,

$4CaCO_3 + 6CaHPO_4 \rightarrow Ca_{10}(PO_4)_6(OH)_2 + 4CO_2 + 2H_2O$

In addition, there are many different techniques for OHAP synthesis, like chemical precipitate in water, hydrolysis, hydrothermal synthesis, solid state reaction and sol-gel…etc in literature [118].

There are two studies which presents the oxyapatites of general formula $Ca_8Ln_2(PO_4)_6O_2$, calcium lanthanide oxide phosphates, in the literature. In the first study Escobar and coworkers [119] were prepared by the reaction $CaCO_3$, Ln_2O_3 and $(NH_4)_2HPO_4$ (Ln: La, Pr,Nd, Sm, Eu, Gd, Tb, Dy, Ho) and results of X-ray powder diffraction and vibrational spectra were reported in 1982. In second one, Mikou et al. were synthesized $Ca_8Ln_2(PO_4)_6O_2$ (Ln: Sm, Tb) by a different reaction which was the heating of the mixture of β-$Ca_2P_2O_7$, $CaCO_3$ and Ln_2O_3 in 1985 [120].

Furthermore, H. Benmoussa et al. prepared rare earth containing vanadocalcic oxyapatities, $Ca_8Ln_2(VO_4)_6O_2$, (Ln: La, Pr) which were obtained via a solid-state reaction in air of $CaCO_3$, V_2O_5 with rare earth oxide for heating rate of 100^oC followed by intermediary grinding until 1100^oC [121].

In other study, the apatite structure $M_2^{II}Ln_8(SiO_4)_6O_2$ (M^{II}= Ca, Sr, Pb; Ln=La, Pr, Nd, Gd, Er,Yb) orthosilicates were synthesized by a sol-gel process from tetraethyl orthosilicate ($Si(OEt)_4$, TEOS) and metal alkoxides and nitrates at an M^{II}: Ln: Si atomic ratio of 2:8:6 by Teterskii and coworkers [122].

CHAPTER 2

EXPERIMENTAL TECHNIQUES

2.1. Chemical Substances

The following chemicals are used in the synthesis of the products:

Gd_2O_3: Merck (pure 99.9%), Nd_2O_3: Fluka (pure 99.9%), Dy_2O_3: Merck (pure 99.9%), $Ni(NO_3)_2$.$6H_2O$: Aldrich, $Co(NO_3)_2$.$6H_2O$: Aldrich, $(NH_4)_2HPO_4$: Merck, $Cu(NO_3)_2$.$3H_2O$: Merck, $Mn(NO_3)_2$.$4H_2O$: Lachema, B_2O_3: Fluka (97 %), H_3BO_3: Fluka, MgO: Merck, $SrCO_3$: Merck, Li_2CO_3: Merck, Na_2CO_3: Aksım, $CaHPO_4.2H_2O$: Merck, $CaCO_3$: Merck

Spectroscopic grade of KBr was used for making IR pellets. It was dried at 180^oC for two hours before using.

2.2 Instrumentation

2.2.1. X-ray Powder Diffractometer (XRD)

X-ray powder diffraction patterns (XRD) were taken by using Rigaku DMAX 2000/PC and Rigaku Multiflex diffractometer using CuK_α (λ=1.5406) radiation. (36 kV / 26 mA, Goniometer: Multiflex + goniometer (with a shutter), Div Slit: ½ deg.,

Sct Slit: ½ deg., Rec Slit: 0.15 mm, Scan Speed: 3 deg/min., Attachment: Standart sample holder)

2.2.2 Infrared Spectrophotometer

Shimadzu Fourier Transform Infrared (FTIR) Spectrometer was used in the range of 4000-400 cm^{-1}. For taking solid IR spectra by means of pellets composed of 0.0050 g of KBr and 0.0003 g of sample were employed.

2.2.3. Thermogravimetric-Differential Thermal Analyser (TG / DTA)

TG/ DTA 6300, SII EXSTAR 6000 Differential Thermal Analyser was used to investigate the thermal properties of the products in the range of $20^{o}C$ to $1400^{o}C$.

2.2.4. Scanning Electron Microscope (SEM)- Energy Dispersive X-ray (EDX)

SEM-EDX photographs were taken using Jeol JSM 6390LV. The samples used for SEM were coated with carbon.

2.2.5. Camera Furnace

All the reactions have been carried out in air with the aid of Nüve MF 1400, Nuve 1200 and Alser 1600 furnaces. Heating were done in the range of 500^{o}-$1300^{o}C$.

2.3. Experimental Procedure

For the rare earth borate phosphate and oxyphosphate reactions, the amounts of Nd_2O_3, Gd_2O_3 and Dy_2O_3 were taken as 0.5 g and the amounts of other reactants are stoichiometrically calculated

For the transition metal borates, the amount of H_3BO_3 was taken as 0.5g and the amounts of other reactants are stoichiometrically calculated.

For the apatite reactions, the amounts of Nd_2O_3, Gd_2O_3 and Dy_2O_3 were taken as 0.25 g and the amounts of other reactants are stoichiometrically calculated.

2.3.1 Solid-State Reactions of $2Ni(NO_3)_2.6H_2O$ with MgO and $2H_3BO_3$

The reaction mixture was prepared by weighing the stoichiometric amounts of reactants separately and grinding together in an agate mortar. Then the mixture was transferred into a platinum crucible and placed into the furnace. The title compound was obtained with four steps.

Firstly, the temperature was raised up to 450^{o}C with an increase of 15^{o}C/min. After being held for 4 hours at 450^{o}C the sample was taken out from the furnace and cooled down and placed to the oven back again after crushing and blending well.

Secondly, the temperature was raised up to 600^{o}C with an increase of 1^{o}C/min and the sample was held for 3 h at 600^{o}C. In the third stage, the specimen was heated to 900^{o}C with an increase of 1^{o}C/min and was held for 48 h at 900^{o}C.

Finally, the product was cooled down to the room temperature with a decrease of 1^{o}C/min. The final product was washed with hot distilled water and dried at 60^{o}C for 4 hours to get rid of unreacted reagents. The expected reaction is:

$$2Ni(NO_3)_2 .6H_2O_{(s)} + MgO_{(s)} + 2H_3BO_{3(s)} \rightarrow MgNi_2(BO_3)_{2(s)} + 4NO_{2(g)} + 15H_2O_{(g)} + O_{2(g)}$$

2.3.2 Solid-State Reactions of $2Co(NO_3)_2 .6H_2O$ with MgO and $2H_3BO_3$

2.3513g $Co(NO_3)_2 .6H_2O$, 0.1638g MgO and 0.5041g H_3BO_3 were weighed and ground together in an agate mortar, then the mixture was weighed again, and transferred into a porcelain crucible for heating. The reaction was heated at 450°C for 4 hours, 600°C for 3 hours, and 900°C for 48 hours. The final product was washed with hot distilled water and dried at 60°C for the 4 hours to get rid of unreacted reagents. The following reaction is expected:

$$2Co(NO_3)_2 .6H_2O_{(s)} + MgO_{(s)} + 2H_3BO_{3(s)} \rightarrow MgCo_2(BO_3)_{2(s)} + 4NO_{2(g)} + 15H_2O_{(g)} + O_{2(g)}$$

2.3.3 Solid-State Reactions of $Ni(NO_3)_2 .6H_2O$ with 2MgO and $2H_3BO_3$

In this reaction also stoichiometric quantities of the reactants were used and the same procedure was followed in weighing and grinding and heating as mentioned in section 2.3.4. The following reaction is expected:

$$Ni(NO_3)_2 .6H_2O_{(s)} + 2MgO_{(s)} + 2H_3BO_{3(s)} \rightarrow Mg_2Ni(BO_3)_{2(s)} + 2NO_{2(g)} + 9H_2O_{(g)} + 1/2O_{2(g)}$$

2.3.4 Solid-State Reactions of $Co(NO_3)_2.6H_2O$ with $2MgO$ and $2H_3BO_3$

The solid state reactions were prepared from mixtures of $Co(NO_3)_2.6H_2O$, MgO and H_3BO_3 in 1:2:2 molar rations. Heating the mixture at 450°C for 4h, and then cooled down and the placed to the oven back again after crushing. Then, heated at 600 and 900°C as mentioned in section 2.3.4. The desired reaction is:

$$Co(NO_3)_2.6H_2O_{(s)} + 2MgO_{(s)} + 2H_3BO_{3(s)} \rightarrow Mg_2Co(BO_3)_{2(s)} + 2NO_{2(g)} + 9H_2O_{(g)} + 1/2O_{2(g)}$$

2.3.5 Solid- State Reactions of $Nd_2O_{3(s)} + 2Li_2CO_{3(s)} + 2(NH_4)_2HPO_{4(s)}$

Nd_2O_3, Li_2CO_3, and $(NH_4)_2HPO_4$ in the molar ratio 1:2:2 was heated at different temperatures in the range of 600 to 1000°C in a porcelain crucible for 6 hours. At the end of each heating period and crucible was weighed, the mixture was ground and the samples were taken from this mixture for X-ray and IR analysis. The following reaction is predicted:

$$Nd_2O_{3(s)} + 2Li_2CO_{3(s)} + 2(NH_4)_2HPO_{4(s)} \rightarrow 2Li_2NdOPO_{4(s)} + 4NH_{3(g)} + 2CO_{2(g)} + 3H_2O_{(g)}$$

2.3.6 Solid- State Reactions of $Gd_2O_{3(s)} + 2Li_2CO_{3(s)} + 2(NH_4)_2HPO_{4(s)}$

The reactants were weighed separately and ground together in an agate mortar. Then the mixture was transferred into a porcelain crucible, weighed again and put into a furnace for heating. The mixture was heated at 600, 700, 800, 900°C

for 6 hours and 1000°C for 24 hours. The crucible with the sample was cooled and weighed. The expected reaction is:

$$Gd_2O_{3(s)} + 2Li_2CO_{3(s)} + 2(NH_4)_2HPO_{4(s)} \rightarrow 2Li_2GdOPO_{4(s)} + 4NH_{3(g)} + 2CO_{2(g)} + 3H_2O_{(g)}$$

2.3.7 Solid- State Reactions of $Dy_2O_{3(s)} + 2Li_2CO_{3(s)} + 2(NH_4)_2HPO_{4(s)}$

Stoichometrical amounts of Dy_2O_3, Li_2CO_3 and $(NH_4)_2HPO_4$ were used. The some procedure was followed in weighing and grinding as mentioned above in section 2.3.10. The mixture was heated at 800°C for 12 hours, 900°C for 6 hours, 1000°C for 6 hours, and 1100°C for 6 hours. The sample was transferred to a desiccator to cool and weighed again. The following reaction is expected:

$$Dy_2O_{3(s)} + 2Li_2CO_{3(s)} + 2(NH_4)_2HPO_{4(s)} \rightarrow 2Li_2DyOPO_{4(s)} + 4NH_{3(g)} + 2CO_{2(g)} + 3H_2O_{(g)}$$

2.3.8 Solid- State Reactions of $Nd_2O_{3(s)} + Li_2CO_{3(s)} + Na_2CO_{3(s)} + 2(NH_4)_2HPO_{4(s)}$

The reaction mixture was prepared by weighing the stoichiometric amounts of reactants separately and grinding together in an agate mortar, then heating at 800°C for 12 hours, 900°C for 6 hours, 1000°C for 12 hours and 1100°C for 6 hours. The expected reaction is:

$$Nd_2O_{3(s)} + Li_2CO_{3(s)} + Na_2CO_{3(s)} + 2(NH_4)_2HPO_{4(s)} \rightarrow 2NaLiGdOPO_{4(s)} + 2CO_{2(g)} + 4NH_{3(g)} + 3H_2O_{(g)}$$

2.3.9 Solid- State Reactions of $Gd_2O_{3(s)} + Li_2CO_{3(s)} + Na_2CO_{3(s)} + 2(NH_4)_2HPO_{4(s)}$

$NaLiGdOPO_4$ was prepared from 1:1.1:2 molar mixture of gadolinium oxide, lithium carbonate, sodium carbonate and diamonium hydrogen phosphate according to the reaction:

$$Gd_2O_{3(s)} + Li_2CO_{3(s)} + Na_2CO_{3(s)} + 2(NH_4)_2HPO_{4(s)} \rightarrow 2NaLiGdOPO_{4(s)} + 2CO_{2(g)} + 4NH_{3(g)} + 3H_2O_{(g)}$$

This mixture was heated slowly in porcelain crucible at 800^{o}C for 12 hours, 900^{o}C for 6 hours, 1000^{o}C for 12 hours and 1100^{o}C for 6 hours. After each heating, grinding was done.

2.3.10 Solid- State Reactions of $Dy_2O_{3(s)} + Li_2CO_{3(s)} + Na_2CO_{3(s)} + 2(NH_4)_2HPO_{4(s)}$

The reactants were mixed in the required proportions and crushed well in an agate mortar the mixture was heated at 800^{o}C for 12 hours, 900^{o}C for 6 hours, 1000^{o}C for 12 hours and 1100^{o}C for 6 hours. The following reaction is expected:

$$Dy_2O_{3(s)} + Li_2CO_{3(s)} + Na_2CO_{3(s)} + 2(NH_4)_2HPO_{4(s)} \rightarrow 2NaLiDyOPO_{4(s)} + 2CO_{2(g)} + 4NH_{3(g)} + 3H_2O_{(g)}$$

2.3.11 Solid- State Reactions of $Nd_2O_{3(s)} + 6CaHPO_4.2H_2O_{(s)} + 2CaCO_{3(s)}$

Nd_2O_3, $CaHPO_4.2H_2O$ and $CaCO_3$ in the molar ratio 1:6:2 was heated at different temperatures in the range of 700 to 1300^oC in a porcelain crucible for 8 hours to 24 hours. At the end of each heating period and crucible was weighed, the mixture was ground and the samples were taken from this mixture for X-ray and IR analysis. The following reaction is predicted:

$$Nd_2O_{3(s)} + 6CaHPO_4 2H_2O_{(s)} + 2CaCO_{3(s)} \rightarrow Ca_8Nd_2(PO_4)_6O_2 + CO_{2(g)} + H_2O_{(g)}$$

2.3.12 Solid- State Reactions of $Gd_2O_{3(s)} + 6CaHPO_4.2H_2O_{(s)} + 2CaCO_{3(s)}$

The reactants were weighed separately and ground together in an agate mortar. Then the mixture was transferred into a porcelain crucible, weighed again and put into a furnace for heating. The mixture was heated at 700, 800, 900, 1000^oC for 8 hours, 1100, 1200^oC for 24 hours and 1300^oC for 12 hours. The crucible with the sample was cooled and weighed.

The expected reaction is:

$$Gd_2O_{3(s)} + 6CaHPO_4 2H_2O_{(s)} + 2CaCO_{3(s)} \rightarrow Ca_8Gd_2(PO_4)_6O_2 + 2CO_{2(g)} + 15H_2O_{(g)}$$

2.3.13 Solid- State Reactions of $Dy_2O_{3(s)} + 6CaHPO_4.2H_2O_{(s)} + 2CaCO_{3(s)}$

The reaction mixture was prepared by weighing the stoichiometric amounts of reactants separately and grinding together in an agate mortar, then heating at

700°C for 8 hours, 800°C for 8 hours, 900°C for 8 hours, 1000°C for 8 hours, 1100°C for 24 hours, 1200°C for 12 hours and 1300°C for 12 hours. The expected reaction is:

$$Dy_2O_{3(s)} + 6CaHPO_4 2H_2O_{(s)} + 2CaCO_{3(s)} \rightarrow Ca_8Dy_2(PO_4)_6O_2 + 2CO_{2(g)} + 15H_2O_{(g)}$$

2.3.14 Solid-State Reactions of $2Nd_2O_3$ with B_2O_3 and $2(NH_4)_2HPO_4$

The reactants were weighed separately and ground together in an agate mortar. Then, the mixture was transferred into a porcelain crucible, weighed again and put into a furnace for heating. The mixture was heated at 500°C, 600°C, 800°C, 900°C, 1000°C, 1100°C, 1200°C and 1300°C for 6 hours. The crucible with the sample was cooled and weighed. The weight losses of the reacting mixtures for every process were detected. The expected reaction is:

$$2Nd_2O_3 + B_2O_3 + 2(NH_4)_2HPO_4 \longrightarrow 2Nd_2(BO_3)(PO_4) + 4NH_3 + 3H_2O$$

2.3.15 Solid-State Reactions of $2Gd_2O_3$ with B_2O_3 and $2(NH_4)_2HPO_4$

The reaction mixture was prepared by weighing the stoichiometric amounts of reactants separately and grinding together in an agate mortar. Then, the mixture was heated at 500-1300°C temperature ranges. The desired reaction is:

$$2Gd_2O_3 + B_2O_3 + 2(NH_4)_2HPO_4 \longrightarrow 2Gd_2(BO_3)(PO_4) + 4NH_3 + 3H_2O$$

2.3.16 Solid-State Reactions of $2Dy_2O_3$ with B_2O_3 and $2(NH_4)_2HPO_4$

Stoichiometric amounts of the reactants were taken separately, then combined together and ground in an agate mortar. The mixture was heated in porcelain crucible at 500-1300^oC temperature ranges. The following reaction is expected:

$$2Dy_2O_3 + B_2O_3 + 2(NH_4)_2HPO_4 \longrightarrow 2Dy_2(BO_3)(PO_4) + 4NH_3 + 3H_2O$$

CHAPTER 3

RESULTS AND DISCUSSION

3.1 Solid-State Reactions of $2Ni(NO_3)_2.6H_2O$ with MgO and $2H_3BO_3$

In this work, the following solid state reaction was proposed to synthesize the compound $MgNi_2(BO_3)_2$, which is not reported in the literature.

$$2Ni(NO_3)_2.6H_2O_{(s)} + MgO_{(s)} + 2H_3BO_{3(s)} \rightarrow \mathbf{MgNi_2(BO_3)_{2(s)}} + 4NO_{2(g)} + 15H_2O_{(g)} + O_{2(g)}$$

3.1.1 X-ray Powder Diffraction Study

In the X-ray powder diffraction patterns of the products obtained at 450 and 600^{o}C, unreacted reactants were observed indicating no appreciable amount of reaction took place. At 900^{o}C, the X-ray powder diffraction pattern was different from the data of the products obtained at low temperatures. This product seems to be a new compound colored with peanut green. Figure 3.1 shows the XRD pattern of $MgNi_2(BO_3)_2$. The X-ray diffraction data of this product was successfully indexed in the orthorhombic system with the refined unit cell parameters of a= 5.393(9), b=

8.350(2), c= 4.462(3) Å [123]. It was found to be a single phase table 3.1 shows the indexing and the d-spacings of this compound. Examination of table 3.1 revealed that there are common d-spacings with the, $M_3(BO_3)_2$, kotoite type of orthorhombic compounds (M: Mg, Co, Ni) [42].

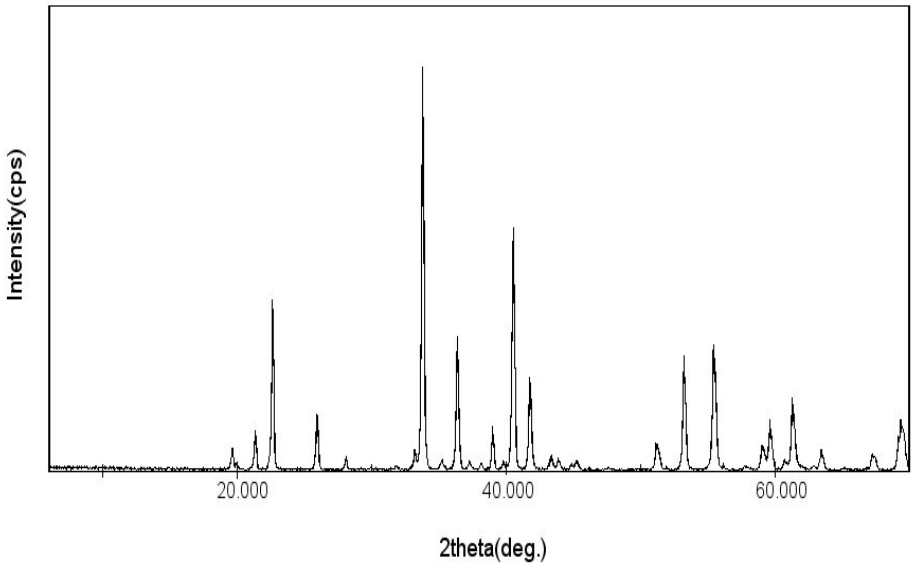


Figure 3.1 X-ray Powder Diffraction Pattern of Orthorhombic $MgNi_2(BO_3)_2$ at 900^{o}C

Table 3.1 X-ray Powder Diffraction Data of Orthorhombic $MgNi_2(BO_3)_2$

I/I_o	h k l	d_{obs}(Å)	d_{calc}(Å)
6	1 1 0	4.5255	4.5308
11	0 2 0	4.1641	4.1751
43	0 1 1	3.9277	3.9356
15	1 0 1	3.4320	3.4382
4	1 1 1	3.1707	3.1793
6	2 0 0	2.6946	2.6969
100	1 2 1	2.6512	2.6541

4	2 1 0	2.5419	2.5664
34	1 3 0	2.4688	2.4735
2	-	2.4087	-
2	0 3 1	2.3612	2.3616
12	2 0 1	2.3087	2.3081
3	2 2 0	2.2641	2.2654
61	2 1 1	2.2234	2.2247
24	1 3 1	2.1612	2.1634
5	0 4 0	2.0851	2.0875
4	1 0 2	2.0625	2.0617
3	1 1 2	2.0052	2.0016
8	1 4 1	1.7840	1.7844
29	2 0 2	1.7191	1.7191
32	1 3 2	1.6560	1.6567
7	0 5 1	1.5638	1.5641
14	3 2 1	1.5495	1.5487
4	0 4 2	1.5236	1.5244
19	3 3 0	1.5105	1.5103
6	0 1 3	1.4655	1.4644
5	0 6 0	1.3905	1.3917
13	2 5 1	1.3538	1.3530

3.1.2 IR Studies

By analyzing the IR spectrum of the products obtained at 900^{o}C (Figure 3.2 and Table 3.2), it was shown that the presence of $MgNi_2(BO_3)_2$ was confirmed from the assigning of the vibrational bands of the planar, triangular BO_3^{3-} group in the region υ_3= 1000-1300cm^{-1} (asymmetric stretch B-O, broad and strong), υ_1= 900-1000 cm^{-1} (symmetric stretch B-O, weak), υ_2= 650-800 cm^{-1} (out of plane bend, sharp and strong) and υ_4= 450-650 cm^{-1}(in plane bend, medium) [67].

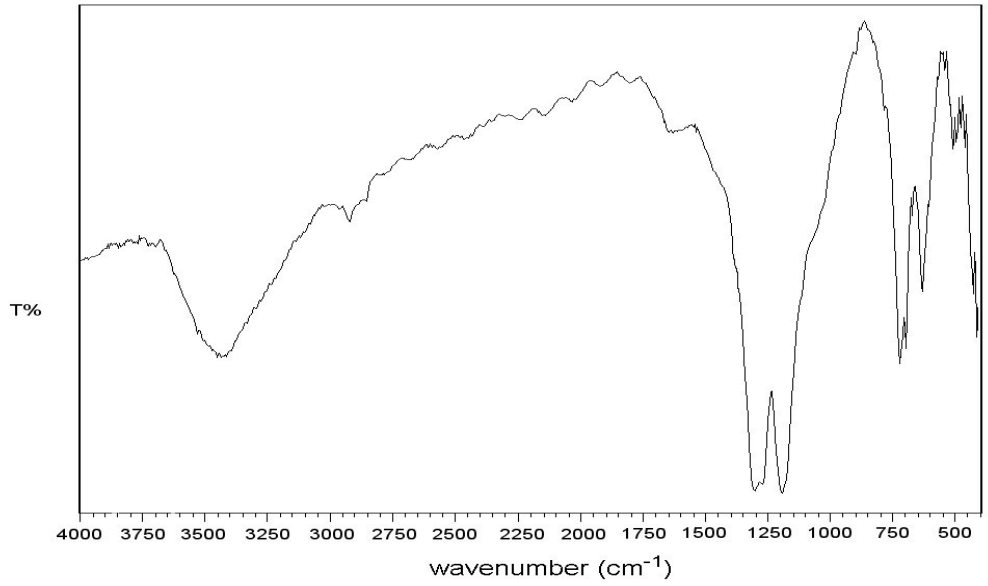


Figure 3.2 IR Spectrum of $MgNi_2(BO_3)_2$

Table 3.2 IR Absorption Bands and Assignments for the $MgNi_2(BO_3)_2$

Assignment	**Frequency, cm^{-1}**
υ_3 (BO_3)	1302, 1273, 1193
υ_2 (BO_3)	725,714, 694
υ_4 (BO_3)	632, 603, 506

3.2 Solid-State Reactions of $2Co(NO_3)_2 .6H_2O$ with MgO and $2H_3BO_3$

In this part of the study, the solid state reactions were performed at 450°C for 4 hours, 600°C for 3 hours, and 900°C for 48 hours.

The expected equation is:

$$2Co(NO_3)_2 .6H_2O_{(s)} + MgO_{(s)} + 2H_3BO_{3(s)} \rightarrow \mathbf{MgCo_2(BO_3)_{2(s)}} + 4NO_{2(g)} + 15H_2O_{(g)} + O_{2(g)}$$

3.2.1 X-ray Powder Diffraction Study

No appreciable amount of reaction took place at 450°C and 600°C according to XRD patterns. At 900°C, the kotoite type of borate, $MgCo_2(BO_3)_2$ (with a color of purple) was found in the X-ray diffraction data. The XRD pattern and details of XRD data of the $MgCo_2(BO_3)_2$ have been given in Figure 3.3 in Table 3.3 respectively. All peaks in the XRD pattern of the $MgCo_2(BO_3)_2$ are indexed in the orthorhombic crystal system (kotoite type) with the refined unit cell parameters of a= 5.442(2), b= 8.428(0), c= 4.517(4) Å [123]**.** It is also clearly seen that the XRD pattern is very similar to that of orthorhombic form of the $Co_2Ni(BO_3)_2$[43].

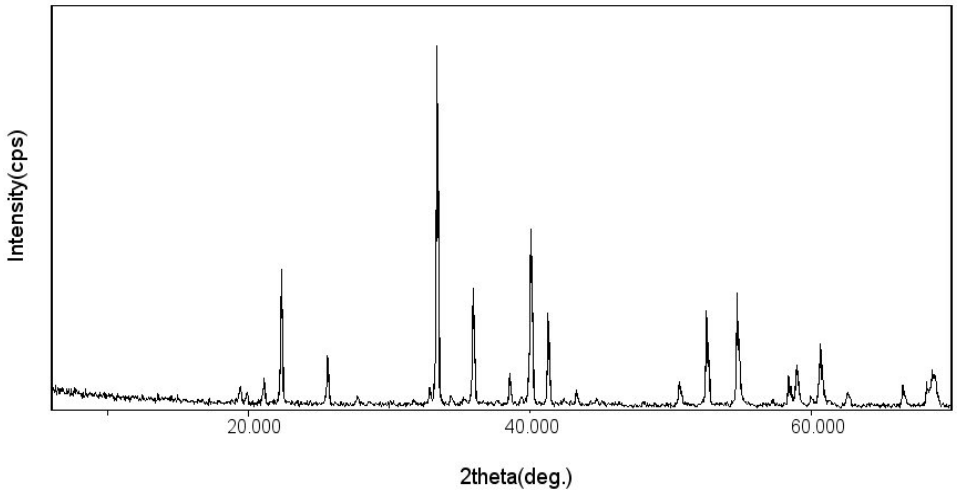


Figure 3.3 X-ray Powder Diffraction Pattern of Orthorhombic $MgCo_2(BO_3)_2$ at 900°C

Table 3.3 X-ray Powder Diffraction Data of Orthorhombic $MgCo_2(BO_3)_2$

I/I_o	h k l	d_{obs}(Å)	d_{calc}(Å)
7	1 1 0	4.5670	4.5719
5	0 0 1	4.4579	4.5174
9	0 2 0	4.2110	4.2140
39	0 1 1	3.9762	3.9815

16	1 0 1	3.4741	3.4759
4	1 1 1	3.2110	3.2134
6	2 0 0	2.7217	2.7211
100	1 2 1	2.6805	2.6814
4	2 1 0	2.6049	2.5895
33	1 3 0	2.4954	2.4963
10	2 0 1	2.3329	2.3309
4	2 2 0	2.2839	2.2859
51	2 1 1	2.2478	2.2466
27	1 3 1	2.1842	2.1849
6	1 0 2	2.0869	2.0862
8	1 4 1	1.8011	1.8018
28	2 0 2	1.7391	1.7380
32	1 3 2	1.6749	1.6749
10	0 5 1	1.5789	1.5792
13	3 2 1	1.5643	1.5633
4	0 4 2	1.5406	1.5407
18	3 3 0	1.5249	1.5240
5	1 4 2	1.4835	1.4824
6	0 6 0	1.4041	1.4047
8	1 2 3	1.3729	1.3722
11	2 5 1	1.3658	1.3659

3.2.2 IR Results

Figure 3.4 presents the IR spectrum of the magnesium cobalt(II) borate compound. When we analyzed the IR spectrum of $MgCo_2(BO_3)_2$, the characteristic bands of kotoite structure observed at 1300 and 1100 cm^{-1} were seen at 1260 and 1183 cm^{-1} as strong absorption bands. The vibrational bands obtained in the region between 710 and 450 cm^{-1} are ascribed to the splitting of the degenerate υ_4 and υ_2

BO_3 modes [41] which were observed at 709, 686, 628, 597 and 480 cm^{-1} in this work.

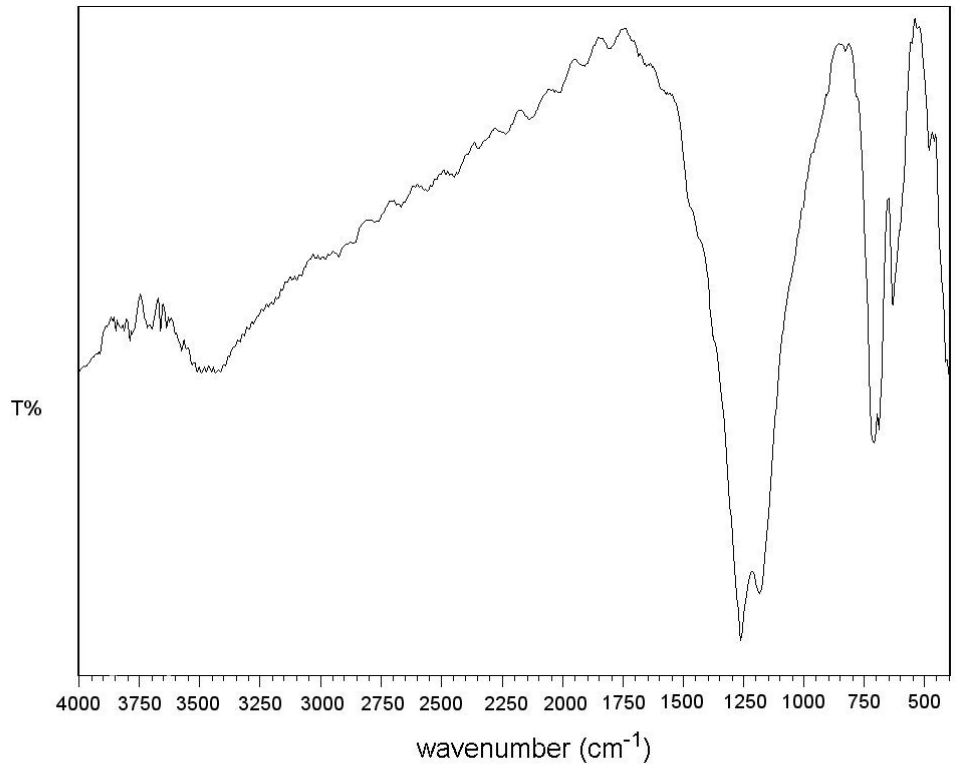


Figure 3.4 IR Spectrum of $MgCo_2(BO_3)_2$

3.3 SEM and EDX Analysis of $MgNi_2(BO_3)_2$ and $MgCo_2(BO_3)_2$

The particle size and the morphology of $MgNi_2(BO_3)_2$ and $MgCo_2(BO_3)_2$ were investigated using SEM, as given in Figure 3.5 and 3.6 respectively. SEM image of $MgNi_2(BO_3)_2$ showed that uniformity exists between the specimens of sample shape and particle size and have a regularly grained powder. SEM image of $MgCo_2(BO_3)_2$ indicates that the grains of $MgCo_2(BO_3)_2$ sample have irregular shape and flaky.

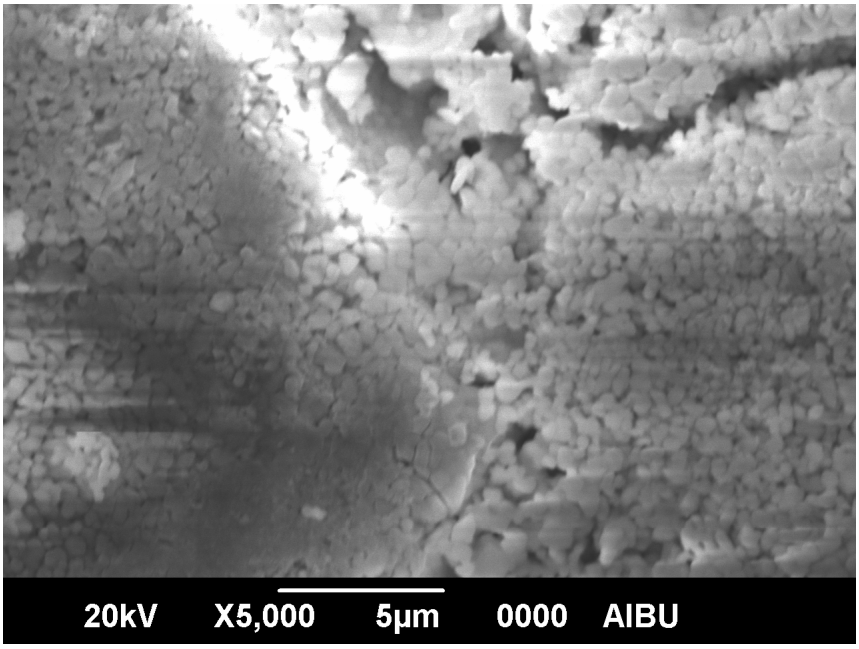


Figure 3.5 SEM image of the $MgNi_2(BO_3)_2$ at 900^oC

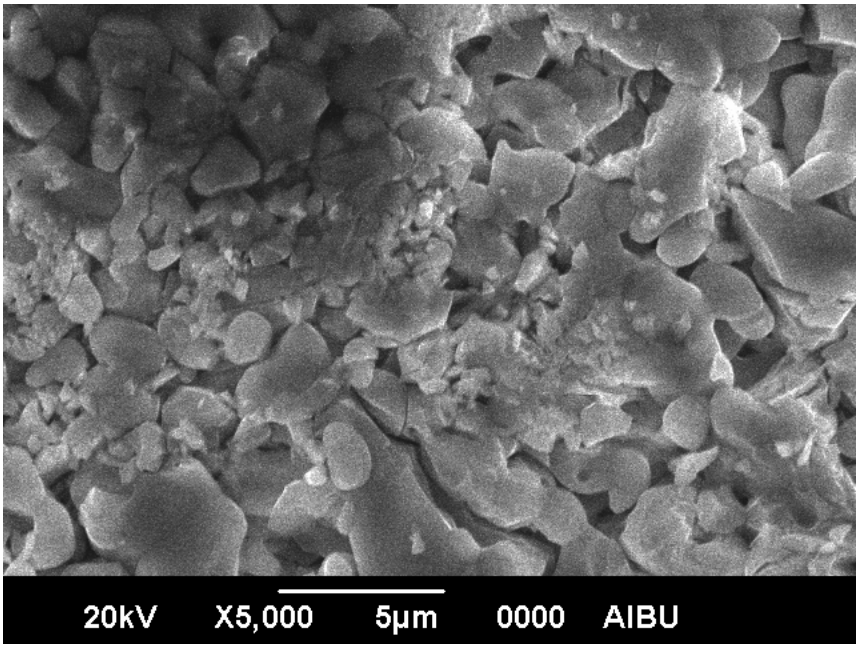


Figure 3.6 SEM image of the $MgCo_2(BO_3)_2$ at 900^oC

The EDX analysis of the products obtained from the reactions of $2Ni(NO_3)_2 .6H_2O$ + $MgO+ 2H_3BO_3$ and $2Co(NO_3)_2 .6H_2O$ + $MgO+ 2H_3BO_3$ showed the presence of Mg, Co, Ni, O and B elements as shown in Figure 3.7 and 3.8 respectively.

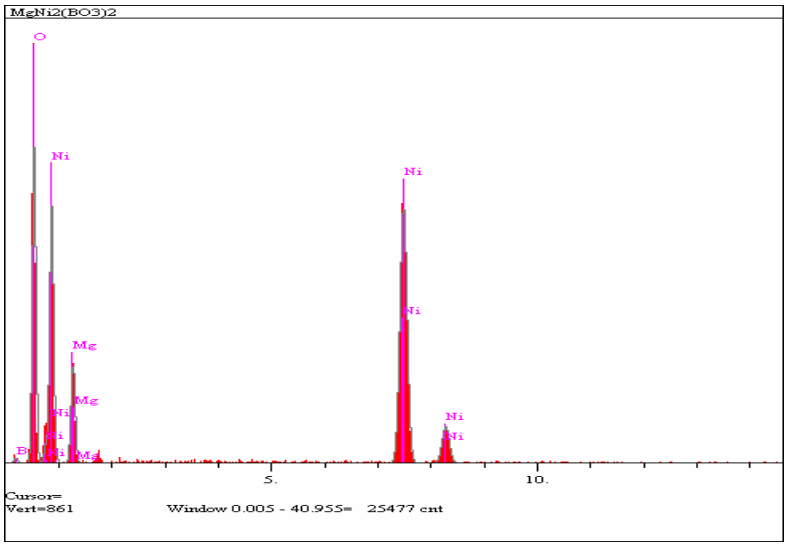


Figure 3.7 EDX Spectrum of the Products Obtained from the Reaction of $2Ni(NO_3)_2 .6H_2O$ + $MgO+ 2H_3BO_3$ at 900^oC

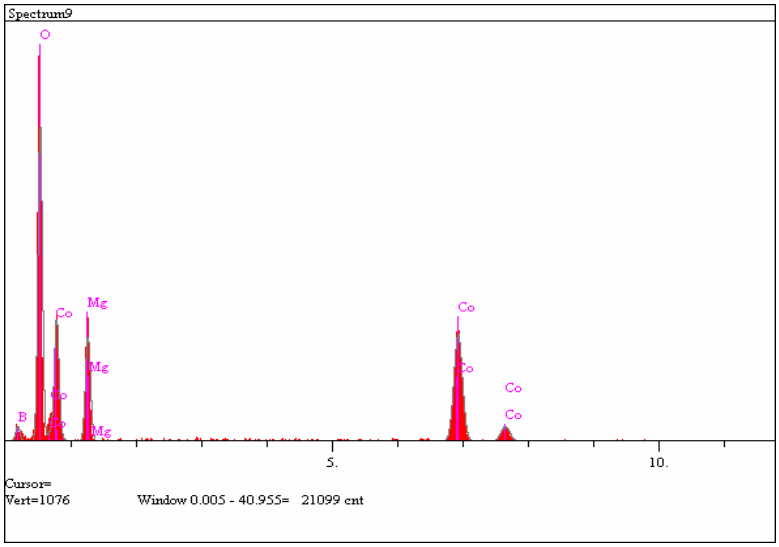


Figure 3.8 EDX Spectrum of the Products Obtained from the Reaction of $2Co(NO_3)_2 .6H_2O$ + $MgO+ 2H_3BO_3$ at 900^oC

3.4 Thermal Studies (DTA-TG) of $MgNi_2(BO_3)_2$ and $MgCo_2(BO_3)_2$

The simultaneous DTA/TG curves of the magnesium nickel orthoborate, $MgNi_2(BO_3)_2$, and magnesium cobalt(II) orthoborate, $MgCo_2(BO_3)_2$, are given in figure 3.9 and figure 3.10 respectively. The curves indicate that there is no weight loss and endothermic or exothermic peak from 20 to 1000°C. Therefore, it could be said that these compounds are thermodynamically stable within these temperatures ranges.

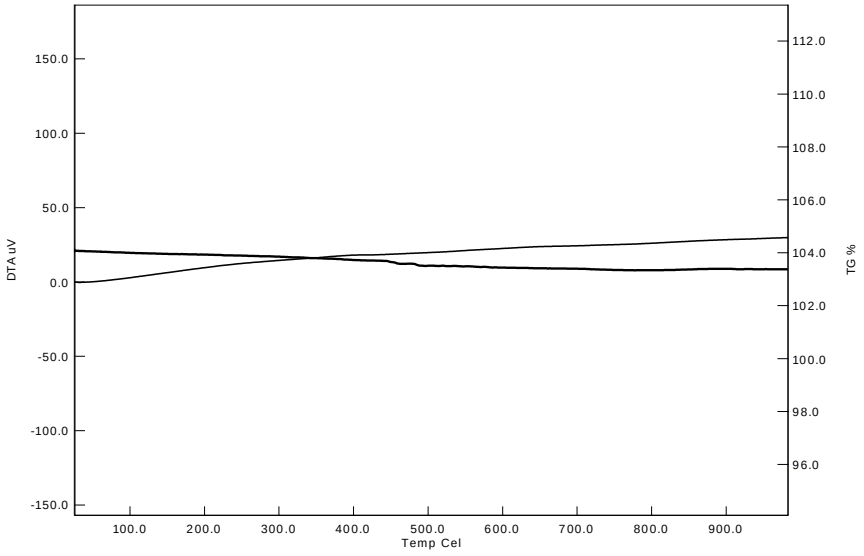


Figure 3.9 DTA-TG of the Products Obtained at 900°C Through the Solid-State Reaction of $2Ni(NO_3)_2.6H_2O + MgO + 2H_3BO_3$

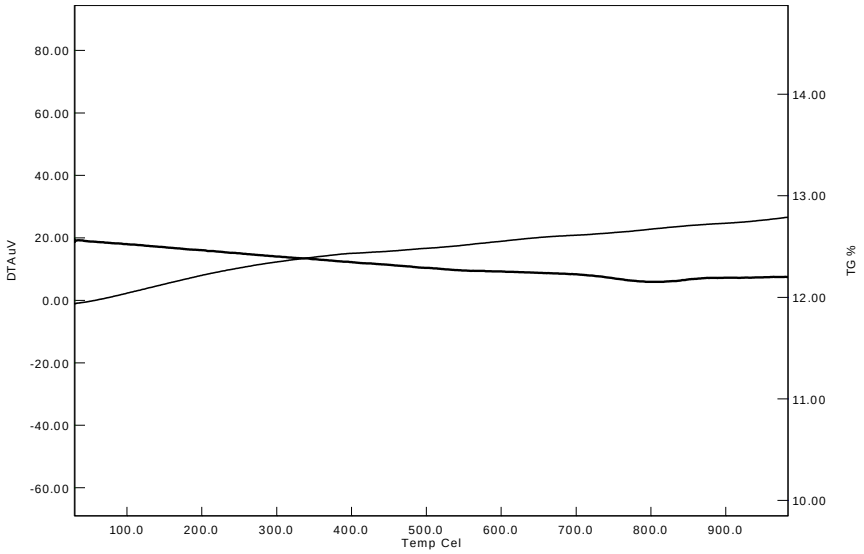


Figure 3.10 DTA-TG of the Products Obtained at 900°C Through the Solid-State Reaction of $2Co(NO_3)_2 .6H_2O + MgO + 2H_3BO_3$

3.5 Solid-State Reactions of $Ni(NO_3)_2 .6H_2O$ with 2MgO and $2H_3BO_3$

The reactions were performed by mixing $Ni(NO_3)_2 .6H_2O$, MgO and H_3BO_3 in 1:2:2 ratio at 450°C for 4 hours, 600°C for 3 hours, and 900°C for 48 hours. The following solid state reaction is expected:

$$Ni(NO_3)_2 .6H_2O_{(s)} + 2MgO_{(s)} + 2H_3BO_{3(s)} \rightarrow \mathbf{Mg_2Ni(BO_3)_{2(s)}} + 2NO_{2(g)} + 9H_2O_{(g)} + 1/2O_{2(g)}$$

3.5.1 X-ray Powder Diffraction Study

Figure 3.11 shows the XRD pattern of the products prepared at 900°C (48h) through the reaction of $Ni(NO_3)_2 .6H_2O_{(s)} + 2MgO_{(s)} + 2H_3BO_{3(s)}$. It is found that the XRD pattern is very similar to that of orthorhombic form of the $M_3(BO_3)_2$ (M= Mg,

Co, Ni) compounds having kotoite type of structure [50]. The product, $Mg_2Ni(BO_3)_2$, (with a color of peanut green) is indexed in the orthorhombic crystal system (kotoite structure) with the refined unit cell parameters of a= 5.398(9), b= 8.400(4), c= 4.490(7) Å [123]. It is clearly seen that the refined cell parameters of $Mg_2Ni(BO_3)_2$ are slightly smaller than that of $Mg_3(BO_3)_2$ [48]. The details of XRD data have been given in Table 3.4.

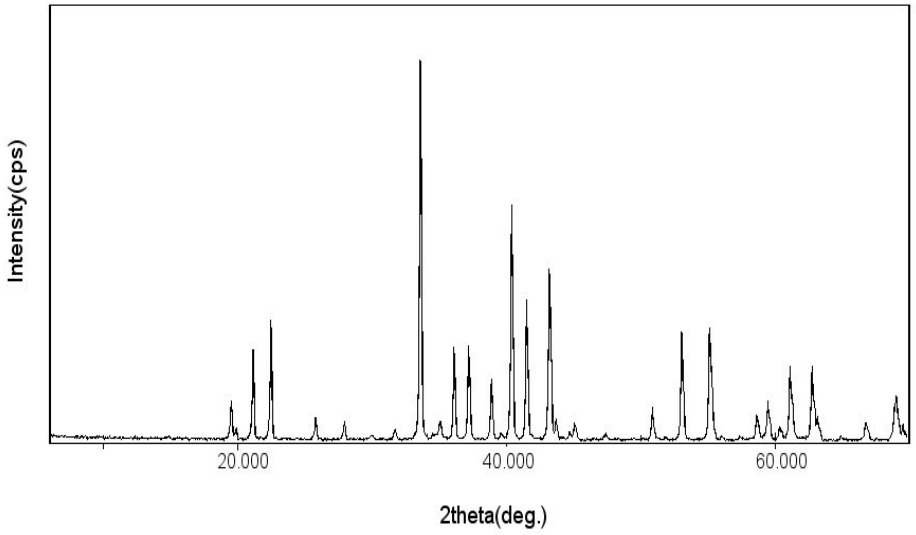


Figure 3.11 X-ray Powder Diffraction Pattern of Orthorhombic $Mg_2Ni(BO_3)_2$ at 900^oC

Table 3.4 X-ray Powder Diffraction Data of Orthorhombic $Mg_2Ni(BO_3)_2$

I/I_o	h k l	d_{obs}(Å)	d_{calc}(Å)
11	1 1 0	4.5458	4.5418
4	0 0 1	4.4624	4.4907
25	0 2 0	4.2031	4.2002
32	0 1 1	3.9553	3.9603
7	1 0 1	3.4503	3.4525
6	1 1 1	3.1907	3.1933
4	0 3 0	2.8273	2.8000
100	1 2 1	2.6666	2.6671

6	2 1 0	2.5545	2.5700
25	1 3 0	2.4860	2.4857
26	0 3 1	2.4162	2.3761
17	2 0 1	2.3144	2.3136
62	2 1 1	2.2308	2.2306
38	1 3 1	2.1741	2.1748
46	0 4 0	2.0924	2.1001
6	1 0 2	2.0688	2.0732
3	2 2 1	2.0257	2.0265
6	1 1 2	2.0103	2.0128
3	0 4 1	1.9156	1.9024
10	1 4 1	1.7932	1.7942
29	2 0 2	1.7245	1.7262
30	1 3 2	1.6643	1.6662
8	0 5 1	1.5730	1.5736
11	3 2 1	1.5528	1.5522
5	0 4 2	1.5327	1.5338
20	3 3 0	1.5150	1.5139
20	1 4 2	1.4793	1.4754
6	0 6 0	1.4008	1.4001
12	2 5 1	1.3589	1.3595
5	4 0 0	1.3510	1.3497

3.5.2 IR Studies

Figure 3.12 shows the infrared spectrum of kotoite-type of structure of magnesium nickel cobalt, $Mg_2Ni(BO_3)_2$, compound at 900^oC. The FT-IR spectrum of $Mg_2Ni(BO_3)_2$ exhibited the infrared absorption bands due to the planar, triangular borates [43,44]. These are the asymmetric stretching, out-of plane and in-plane

bending modes of B-O at 1283, 1194; 725, 697 and 642, 497, 420 cm^{-1} respectively. It was in agreement with the X-ray data given previously.

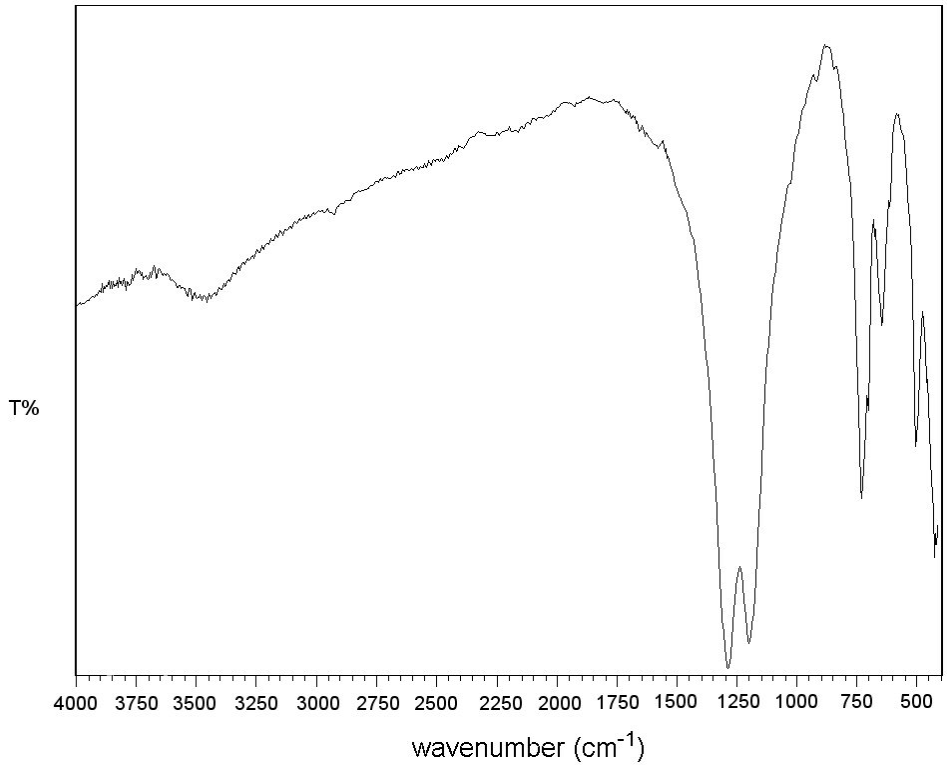


Figure 3.12 IR Spectrum of $Mg_2Ni(BO_3)_2$

3.6 Solid-State Reactions of $Co(NO_3)_2 .6H_2O$ with $2MgO$ and $2H_3BO_3$

The 1:2:2 mixture of the reactants $Co(NO_3)_2 .6H_2O$, MgO and H_3BO_3 was crushed well and heated at 450°C for 4 hours, 600°C for 3 hours, and 900°C for 48 hours. The following solid state reaction is expected:

$$Co(NO_3)_2 .6H_2O_{(s)} + 2MgO_{(s)} + 2H_3BO_{3(s)} \rightarrow \mathbf{Mg_2Co(BO_3)_{2(s)}} + 2NO_{2(g)} + 9H_2O_{(g)} + 1/2O_{2(g)}$$

3.6.1 X-ray Powder Diffraction Study

Figure 3.13 and Table 3.5 show the XRD pattern and data of the products obtained from the solid state reactions of $Co(NO_3)_2.6H_2O$, MgO and H_3BO_3 at 900°C. At this temperature, a new compound was identified in the powder data. By comparing the present data with the XRD data of $Co_3(BO_3)_2$ (ICDD No: 75-1808), it was found to be $Mg_2Co(BO_3)_2$ (with a color of dark purple). The X-ray data of the product, $Mg_2Co(BO_3)_2$, was indexed in the orthorhombic crystal system (kotoite structure) with the refined unit cell parameters of a= 5.423(2), b= 8.425(9), c= 4.509(4)Å [123].

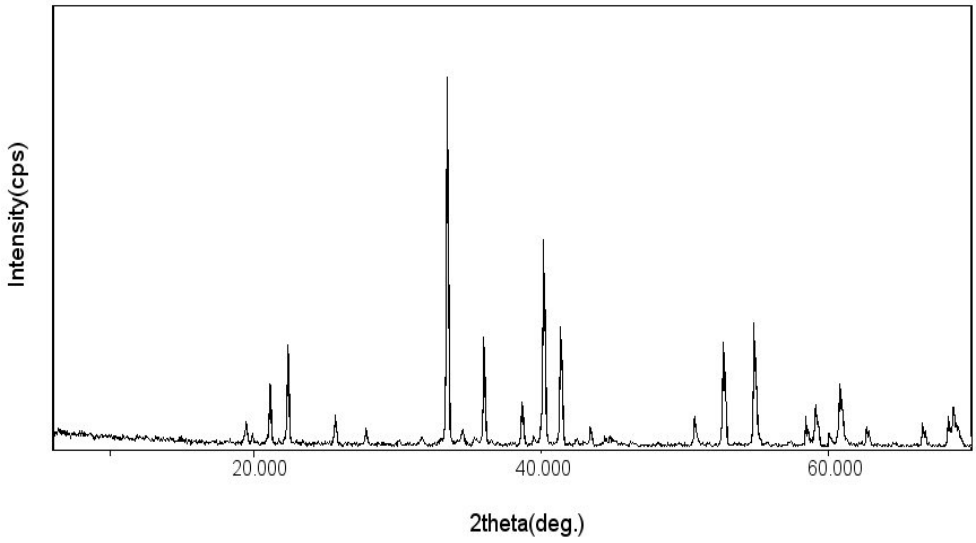


Figure 3.13 X-ray Powder Diffraction Pattern of Orthorhombic $Mg_2Co(BO_3)_2$ at 900°C

Table 3.5 X-ray Powder Diffraction Data of Orthorhombic $Mg_2Co(BO_3)_2$

I/I_o	h k l	d_{obs}(Å)	d_{calc}(Å)
8	1 1 0	4.5670	4.5602

5	0 0 1	4.4624	4.5094
18	0 2 0	4.2031	4.2129
29	0 1 1	3.9727	3.9758
10	1 0 1	3.4688	3.4673
6	1 1 1	3.2042	3.2064
4	0 3 0	2.8220	2.8086
100	1 2 1	2.6759	2.6772
5	2 1 0	2.5903	2.5812
31	1 3 0	2.4913	2.4940
13	2 0 1	2.3259	2.3238
4	2 2 0	2.2828	2.2801
57	2 1 1	2.2425	2.2402
34	1 3 1	2.1812	2.1825
6	1 0 2	2.0833	2.0819
9	1 4 1	1.7991	1.8003
29	2 0 2	1.7348	1.7337
35	1 3 2	1.6727	1.6725
9	0 5 1	1.5779	1.5785
12	2 4 1	1.5609	1.5607
5	0 4 2	1.5387	1.5392
18	3 3 0	1.5217	1.5201
7	1 4 2	1.4806	1.4807
6	2 3 2	1.4772	1.4752
8	0 6 0	1.4030	1.4043
9	1 2 3	1.3704	1.3698
12	2 5 1	1.3648	1.3642

3.6.2 IR Studies

The IR absorption spectrum of $[BO_3]^{3-}$ anion has been reported in literature [67] and it has been found that their strong characteristic absorption bands appeared in the region of 1000-1300 cm^{-1} and 650-800 cm^{-1}. Figure 3.14 shows the infrared

spectrum of the compound titled. It is clearly seen that the bands with the frequencies of 1269-1180 cm^{-1} may be assigned to the BO_3 asymmetric stretching vibrations whereas the bands at 707, 695 and 632 cm^{-1} is assigned to the out-of- plane bending modes of B-O bond.

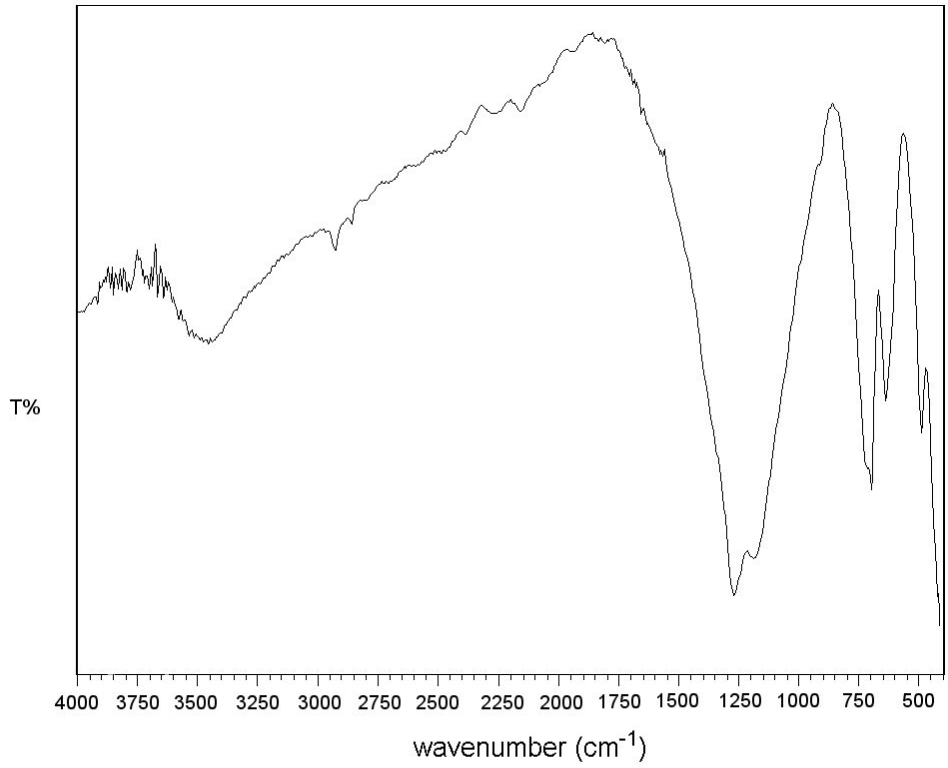


Figure 3.14 IR Spectrum of $Mg_2Co(BO_3)_2$

3.7 SEM and EDX Analysis of $Mg_2Ni(BO_3)_2$ and $Mg_2Co(BO_3)_2$

The particle size and the morphology of $Mg_2Ni(BO_3)_2$ and $Mg_2Co(BO_3)_2$ are illustrated in Figure 3.15-3.16 respectively. SEM images showed that the uniformity exists between the specimens of sample shape and particle size and have a regularly grained powder.

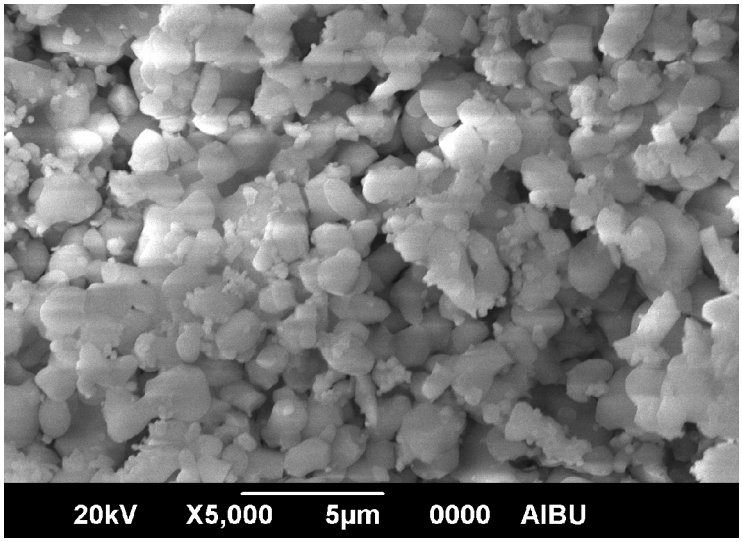


Figure 3.15 SEM image of the $Mg_2Ni(BO_3)_2$ at 900^oC

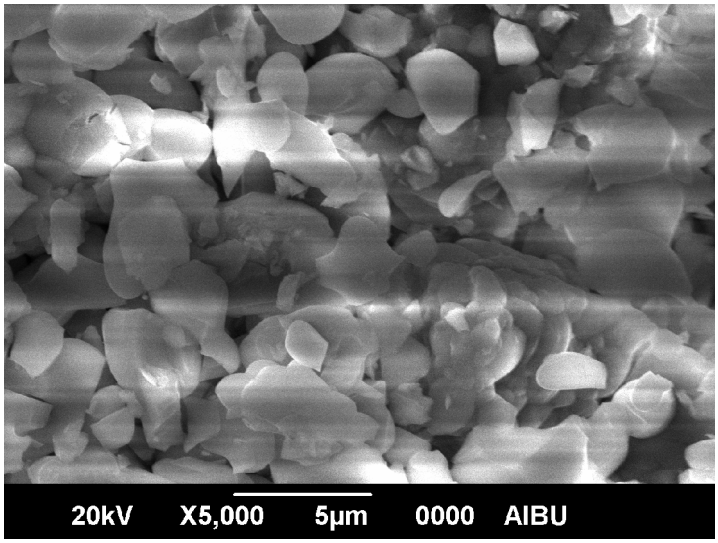


Figure 3.16 SEM image of the $Mg_2Co(BO_3)_2$ at 900^oC

From the EDX analysis of the products obtained, it was confirmed the presence of Mg, Co, Ni, O and B elements as shown in Figure 3.17 and 3.18.

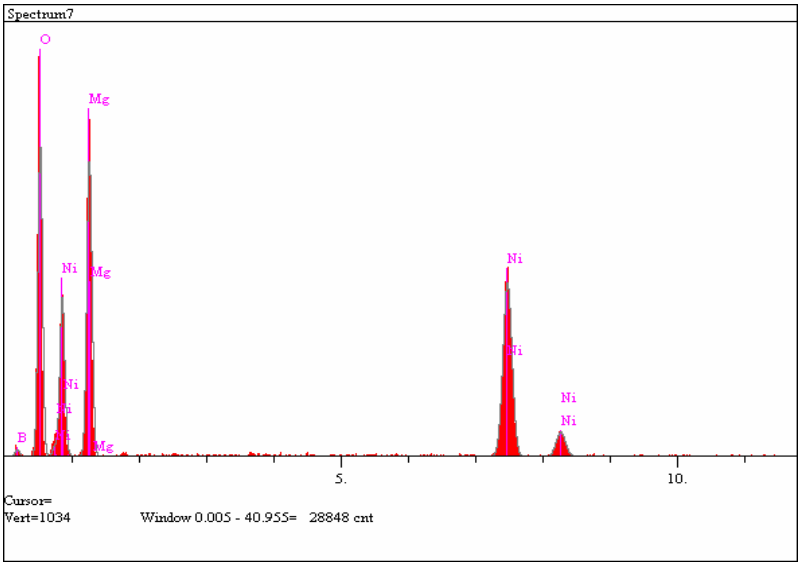


Figure 3.17 EDX Spectrum of the Products Obtained from the Reaction of $Ni(NO_3)_2 .6H_2O + 2MgO + 2H_3BO_3$ at 900°C

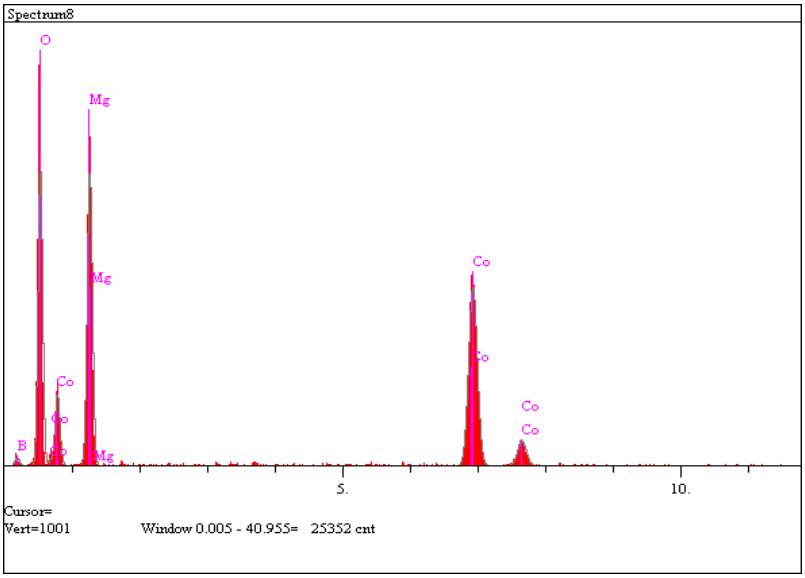


Figure 3.18 EDX Spectrum of the Products Obtained from the Reaction of $Co(NO_3)_2 .6H_2O + 2MgO + 2H_3BO_3$ at 900°C

3.8 Thermal Studies (DTA-TG) of $Mg_2Ni(BO_3)_2$ and $Mg_2Co(BO_3)_2$

The DTA-TG study of $Mg_2Ni(BO_3)_2$ and $Mg_2Co(BO_3)_2$ indicates that these compounds are thermodynamically stable up to 1000^oC as shown in Figure 3.19-3.20.

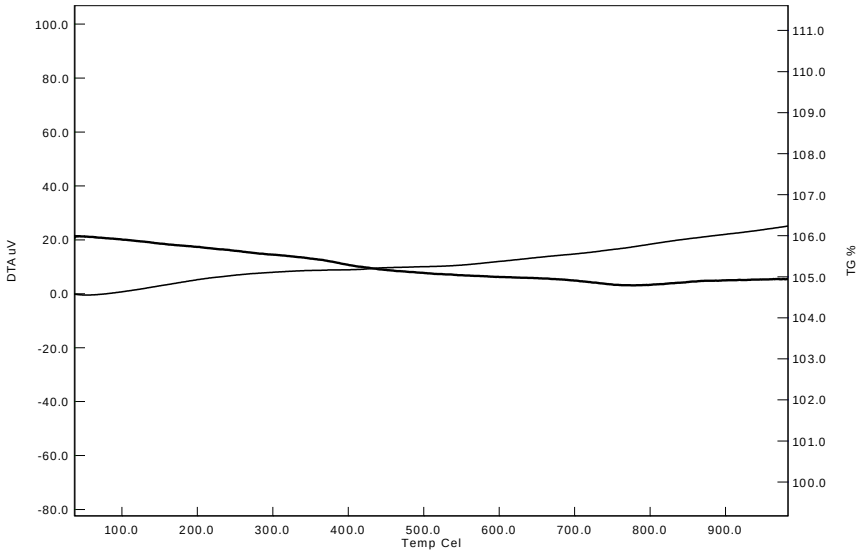


Figure 3.19 DTA-TG of the Products Obtained at 900^oC Through the Solid-State Reaction of $Ni(NO_3)_2.6H_2O$ +2MgO+ $2H_3BO_3$

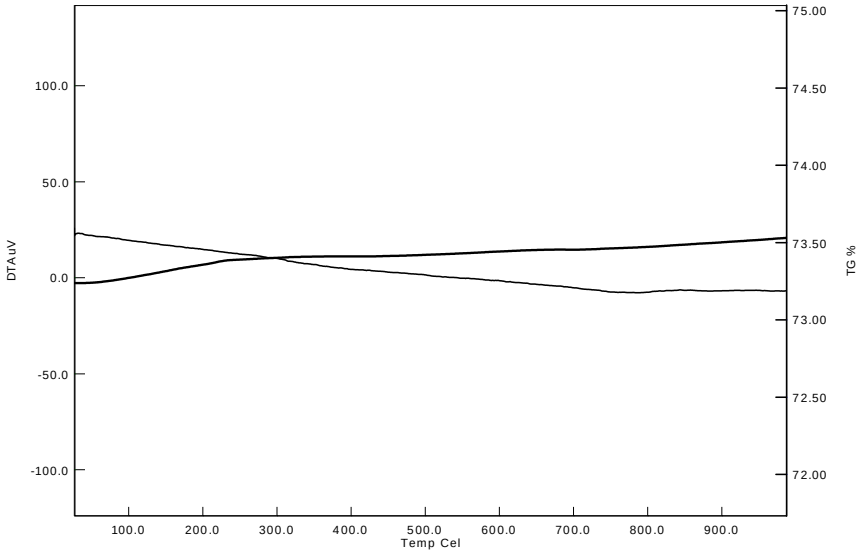


Figure 3.20 DTA-TG of the Products Obtained at 900°C Through the Solid-State Reaction of $Co(NO_3)_2 .6H_2O + 2MgO + 2H_3BO_3$

3.9 Solid- State Reactions of $Ln_2O_{3(s)} + 2Li_2CO_{3(s)} + 2(NH_4)_2HPO_{4(s)}$ (Nd, Gd, Dy)

In this part of the thesis, the solid state reactions of three different rare earths were proposed to synthesize the compounds, Li_2LnOPO_4, (Ln: Nd, Gd, Dy), which were not reported in the literature. The general equation for these reactions is given below. The reactions were performed at 800-1100°C for 6 hours.

$$Ln_2O_{3(s)} + 2Li_2CO_{3(s)} + 2(NH_4)_2HPO_4(s) \rightarrow 2Li_2LnOPO_{4(s)} + 4NH_{3(g)} + 2CO_{2(g)} + 3H_2O_{(g)}$$

3.9.1 X-ray Powder Diffraction Studies for Nd, Gd and Dy Compounds

The products obtained at different temperatures were subjected to X-ray powder diffraction analysis after each heating process. The X-ray diffraction patterns

observed for Nd compound are given in Figure 3.21. In the X-ray powder diffraction data of the reaction products at 900°C, Nd_3PO_7 (ICDD No: 33-0938), $NdPO_4$ (ICDD No: 78-1026), Li_3PO_4 (ICDD No: 84-0046) and Li_2O (ICDD No: 77-2144) lines are appeared. At 1000°C, a new oxyphosphate, Li_2NdOPO_4 (with a color of lilac) was found in the X-ray diffraction data. Table 3.6 shows the X-ray powder data of the product obtained from the reactions of $Nd_2O_{3(s)} + 2Li_2CO_{3(s)} + 2(NH_4)_2HPO_4(s)$ at 1000°C. The product, Li_2NdOPO_4 was indexed in the orthorhombic crystal system with the refined unit cell parameters of a= 14.865(1), b= 10.734(2), c= 13.231(1) Å [123].

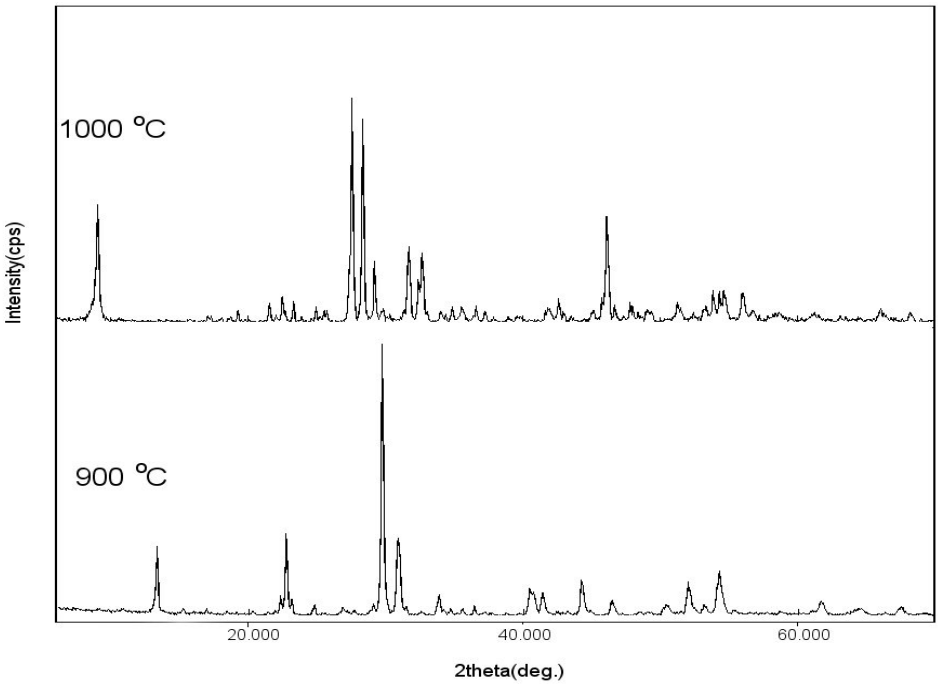


Figure 3.21 X-ray Powder Diffraction Patterns of the Products Obtained of the Solid State Reaction of $Nd_2O_{3(s)} + 2Li_2CO_{3(s)} + 2(NH_4)_2HPO_4(s)$ at 900-1000°C

Table 3.6 X-ray Powder Diffraction Data of Orthorhombic Structure of Li_2NdOPO_4 (1000^oC 6h)

I/I_o	h k l	d_{obs}	d_{calc}
53	1 0 1	9.7959	9.8832
6	3 0 1	4.6093	4.6403
11	2 2 1	4.1145	4.1334
12	3 0 2	3.9518	3.9659
12	2 0 3	3.8113	3.7929
9	2 1 3	3.5673	3.5762
6	1 3 0	3.4848	3.4787
100	1 0 4	3.2315	3.2288
88	0 3 2	3.1466	3.1472
30	4 2 0	3.0579	3.0553
29	3 3 1	2.8290	2.8335
38	0 2 4	2.8203	2.8159
21	1 2 4	2.7610	2.7667
33	1 3 3	2.7379	2 73 13
6	0 4 1	2.6316	2 6300
5	1 0 5	2.6063	2.6053
9	0 1 5	2.5701	2.5693
8	2 4 0	2.5239	2.5241
8	1 4 2	2.4532	2.4527
6	6 1 0	2.4125	2.4141
4	6 1 1	2.3768	2.3748
12	0 5 1	2.1196	2.1191
46	2 2 6	1.9673	1.9670
8	5 1 5	1.9442	1.9440
11	4 0 6	1.8990	1.8964
9	7 2 2	1.8931	1.8921
6	4 5 0	1.8589	1.8589
9	0 2 7	1.7814	1.7828
8	0 6 1	1.7737	1.7729

6	3 1 7	1.7446	1.7426
8	1 6 2	1.7149	1.7155
15	0 4 6	1.7014	1.7037
10	8 2 2	1.6967	1.6971
14	7 3 3	1.6869	1.6873
11	5 5 2	1.6834	1.6832
17	3 2 7	1.6778	1.6775
13	1 0 8	1.6418	1.6437
13	7 1 5	1.6370	1.6369
5	2 4 7	1.5128	1.5130
9	1 5 7	1.4124	1.4122
6	10 3 0	1.3729	1.3728

The X-ray diffraction patterns of the products obtained for the Gd compound are given in figure 3.22. In the analysis of XRD patterns of the products obtained at 800^{o}C and 900^{o}C, Gd_3PO_7 (ICDD No: 34-1066), $GdPO_4$ (ICDD No: 32-0386), Li_3PO_4 (ICDD No: 84-0046) and Li_2O (ICDD No: 77-2144) lines were appeared. At 1000^{o}C (6h and 12h), together with Gd_3PO_7 (ICDD No: 34-1066) and Li_3PO_4 (ICDD No: 84-0046) lines were observed. Prolonged heating of the products at 1000^{o}C (18h) resulted in a new compound, Li_2GdOPO_4 (with a color of cream). It was found that this new compound resembled to orthorhombic Na_2GdOPO_4 reported previously by Uztetik et al [99]. The indexing of the powder pattern of this product (Table 3.7) showed that Li_2GdOPO_4 is crystallized in orthorhombic system with the refined unit cell parameters a= 14.686(3), b= 10.634(5) c= 13.047(9) Å [123]. At 1100^{o}C, the decomposition of lithium gadolinium oxyphosphate to gadolinium orthophosphate and some condensed phosphates was observed.

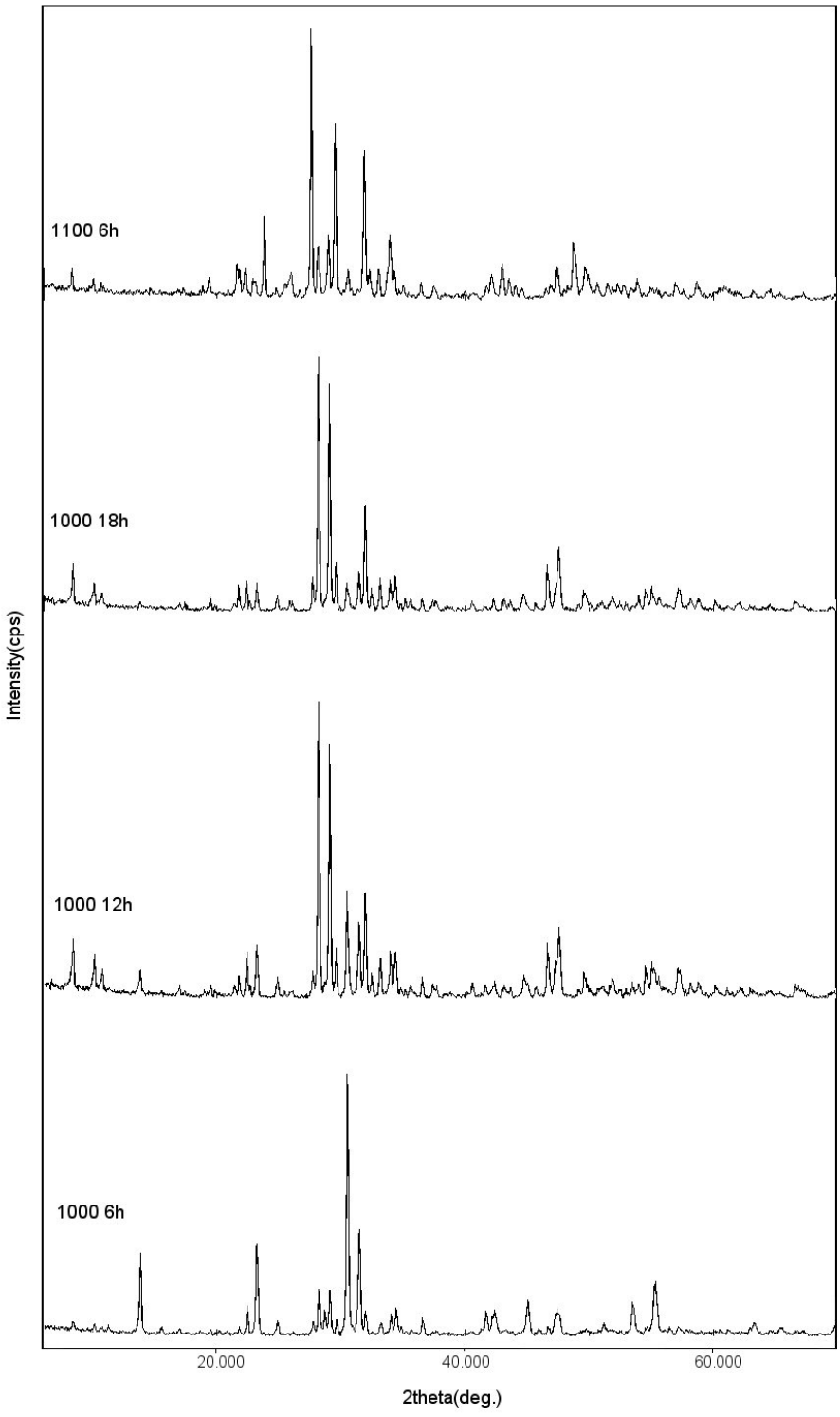


Figure 3.22 X-ray Powder Diffraction Patterns of the Products Obtained of the Solid State Reaction of $Gd_2O_{3(s)} + 2Li_2CO_{3(s)} + 2(NH_4)_2HPO_{4(s)}$ at 900-1100^oC

Table 3.7 X-ray Powder Diffraction Data of Orthorhombic Structure of Li_2GdOPO_4 (1000^oC-18h)

I/I_o	h k l	d_{obs}	d_{calc}
20	0 1 0	10.5425	10.6345
12	1 1 0	8.7680	8.6134
9	0 0 1	8.2459	8.2434
7	3 0 1	4.5670	4.5835
4	3 1 0	4.4802	4.4469
12	2 2 1	4.0809	4.0897
13	1 2 2	3.9727	3.9684
12	1 1 3	3.8275	3.8824
7	2 2 2	3.5758	3.5942
15	4 0 2	3.2178	3.1997
100	3 2 2	3.1663	3.1530
90	4 1 2	3.0702	3.0640
20	4 2 0	3.0174	3.0213
13	5 0 0	2.9304	2.9373
17	5 1 0	2.8430	2.8313
43	3 3 1	2.7997	2.8041
10	0 3 3	2.7560	2.7478
15	1 3 3	2.7010	2.7009
13	3 1 4	2.6391	2.6302
15	0 0 5	2.6093	2.6096
6	4 3 0	2.5503	2.5502
6	5 2 1	2.5184	2.5226
6	2 0 5	2.4571	2.4589
5	6 0 1	2.4038	2.4058
5	6 2 0	2.2213	2.2234
6	5 3 2	2.1368	2.1369
6	7 0 0	2.0961	2.0980
6	7 0 1	2.0733	2.0714
8	0 5 2	2.0257	2.0221
5	2 4 4	1.9853	1.9842
20	5 4 1	1.9466	1.9490
27	0 5 3	1.9133	1.9107

10	6 2 4	1.8378	1.8372
5	7 3 1	1.7879	1.7885
7	6 1 5	1.7616	1.7606
5	3 0 7	1.7422	1.7420
5	2 5 4	1.7287	1.7314
7	4 5 3	1.6967	1.6949
10	0 4 6	1.6800	1.6833
11	7 3 3	1.6671	1.6675
7	0 3 7	1.6500	1.6498
10	2 5 5	1.6091	1.6086
6	4 6 1	1.5848	1.5844
6	5 3 6	1.5686	1.5676
6	7 4 3	1.5378	1.5402
5	4 0 8	1.4913	1.4905
4	1 3 8	1.4746	1.4742
4	3 7 1	1.4419	1.4421
5	8 0 6	1.4026	1.4028

The X-ray diffraction patterns observed for Dy compound are given in Figure 3.23. At 800^{o}C (12h), Dy_2O_3 (ICDD No: 22-0612), $DyPO_4$ (ICDD No: 74-0774) and Li_3PO_4 (ICDD No: 84-0046) lines were observed in the X-ray diffraction patterns. As the reaction proceeded at 900^{o}C, Dy_2O_3, $DyPO_4$ and Li_3PO_4 were still present but additional lines due to Dy_3PO_7 were also observed. According to these lines, the following reaction was suggested;

$$DyPO_4 + Dy_2O_3 \rightarrow Dy_3PO_7$$

By combining these results, the following reaction could be written:

$$3Dy_2O_{3(s)} + 6Li_2CO_{3(s)} + 6(NH_4)_2HPO_{4(s)} \rightarrow Dy_3PO_{7(s)} + DyPO_{4(s)} + Dy_2O_{3(s)} + 4Li_3PO_{4(s)} + 12NH_{3(g)} + 6CO_{2(g)} + 9H_2O_{(g)}$$

At 1000^{o}C, examination of the XRD pattern showed that a new compound was identified in the powder data as shown in table 3.8. By comparing the X-ray pattern of this new product with Na_2GdOPO_4 [99,100], it was found to be Li_2DyOPO_4 (with a color of dark cream). The X-ray data of Li_2DyOPO_4 was indexed in the orthorhombic system with the refined unit cell parameters of a= 14.554(1), b= 10.589(8), c= 12.926(2) Å [123] which agreed with Na_2GdOPO_4. It was observed that Li_2DyOPO_4 decomposed to $DyPO_4$ and some condense phosphates at 1100^{o}C.

.

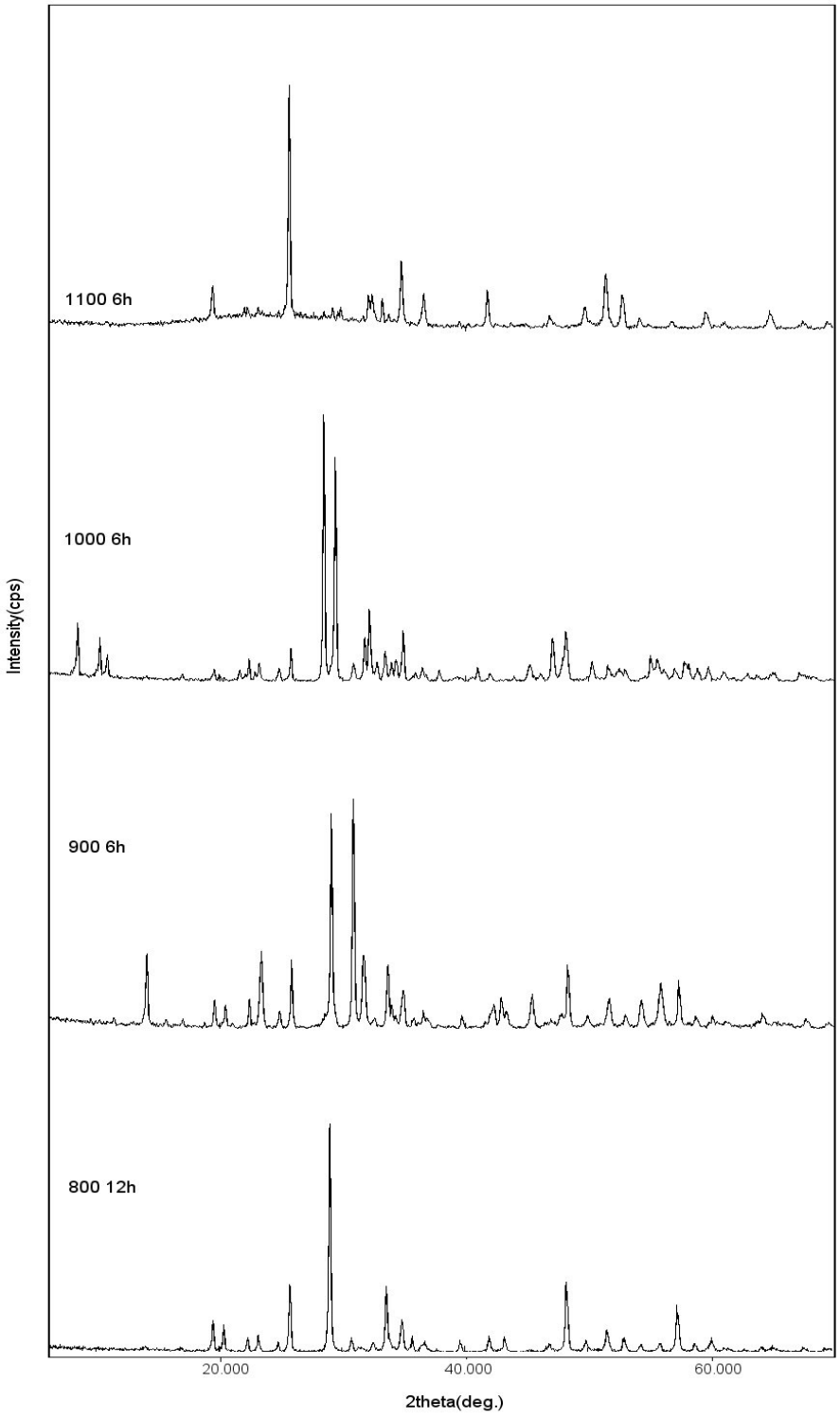


Figure 3.23 X-ray Powder Diffraction Patterns of the Products Obtained of the Solid State Reaction of $Dy_2O_{3(s)} + 2Li_2CO_{3(s)} + 2(NH_4)_2HPO_{4(s)}$ at 800-1100^oC

Table 3.8 X-ray Powder Diffraction Data of Orthorhombic Structure of Li_2DyOPO_4 (1000^oC-6h)

I/I_o	h k l	d_{obs}	d_{calc}
23	0 1 0	10.443	10.5898
19	1 1 0	8.6482	8.5630
11	0 1 1	8.170	8.1918
7	3 0 1	4.5347	4.5420
5	3 1 0	4.3114	4.4106
7	1 0 3	4.1258	4.1315
10	0 1 3	3.9692	3.9910
8	1 1 3	3.8372	3.8489
6	3 2 0	3.5814	3.5770
14	3 2 1	3.4503	3.4474
100	3 2 2	3.1336	3.1296
89	4 1 2	3.0375	3.0374
9	5 0 0	2.9101	2.9108
19	5 1 0	2.8117	2.8067
29	4 0 3	2.7827	2.7799
9	0 3 3	2.7314	2.7306
13	1 3 1	2.6743	2.6838
9	0 4 0	2.6368	2.6475
10	3 3 2	2.6093	2.6110
23	5 1 2	2.5687	2.5744
6	4 2 3	2.4597	2.4613
6	2 1 5	2.3756	2.3741
7	4 2 4	2.2005	2.1981
8	5 2 4	2.0019	2.0022
18	2 2 6	1.9171	1.9245
22	3 4 4	1.8886	1.8867
9	4 5 1	1.8125	1.8124
9	3 5 3	1.7705	1.7698
13	3 5 4	1.6671	1.6640
10	6 4 3	1.6510	1.6518

7	0 0 8	1.6143	1.6158
9	4 5 4	1.5928	1.5927
8	7 3 4	1.5667	1.5668
7	0 2 8	1.5457	1.5454
6	7 5 1	1.4742	1.4740

3.9.2 IR Studies for Nd, Gd and Dy Compounds

As shown in Figures 3.24, 3.25 and 3.26, the infrared spectra of the products were obtained by the reactions of $Ln_2O_{3(s)}$ (Nd, Gd, Dy) + $2Li_2CO_{3(s)}$ $+2(NH_4)_2HPO_{4(s)}$ (for neodymium; at 600-1000^oC, for gadolinium and dysprosium; at 800-1100^oC).

The stretching and bending modes of free CO_3^{2-} anion with D_{3h} symmetry have four internal modes of vibrations; these are assigned as υ_1: 1063cm^{-1}, υ_2: 879 cm^{-1}, υ_3: 1415 cm^{-1}, and υ_4: 680 cm^{-1}, where the υ_3 and υ_4 modes are degenerate [39].

The vibration bands of CO_3^{2-} ion were observed at 854 and 1467 cm^{-1} in the IR spectra of the products containing neodymium (Figure 3.24) prepared at 600-800^oC. As the temperature increased (at 900^oC), the bands of CO_3 disappeared and the additional IR absorption frequencies were assigned to Nd_3PO_7, $NdPO_4$ and Li_3PO_4. However, these bands disappeared at 1000^oC, and the new bands (υ_3: 1151, 1097, 1036, 999, 960 cm^{-1}; υ_1: 922 cm^{-1}; υ_4: 623, 580, 539, 521cm^{-1}; $\upsilon_{2:}$ 460, 423 cm^{-1}) were assigned to Li_2NdOPO_4 which agreed to by the IR data given in the literature [99, 100].

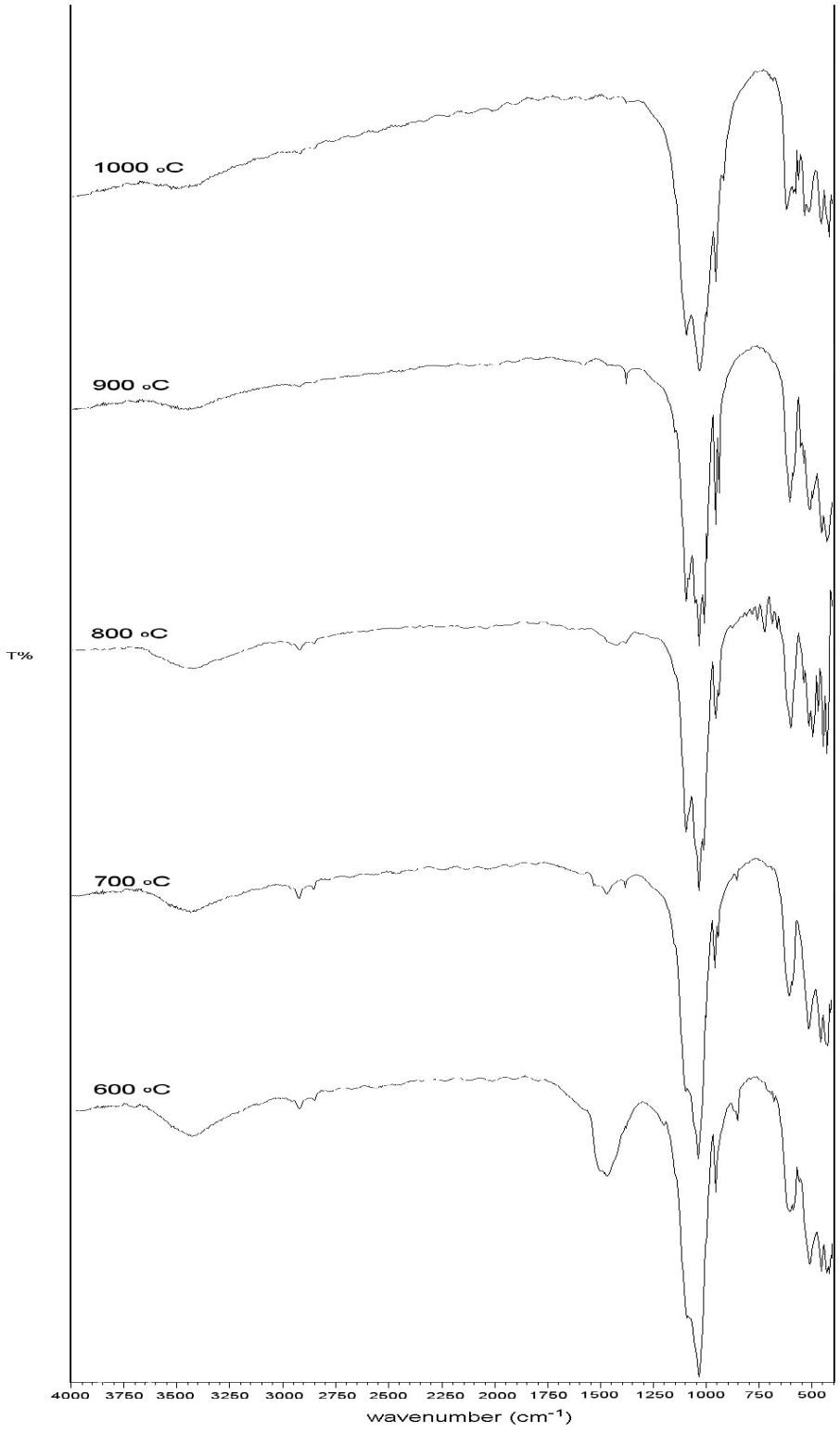


Figure 3.24 IR Spectra of the Products of the Solid State Reactions of $Nd_2O_{3(s)}$ + $2Li_2CO_{3(s)}$ +$2(NH_4)_2HPO_{4(s)}$ Solid-State Reactions at 600 - 1000^oC

In the infrared spectra of the products observed for gadolinium compound, the vibrational frequencies due to Gd_2O_3 and Li_3PO_4 at 800-900^oC (6h), and Gd_3PO_7 and Li_3PO_4 at 1000^oC (6h) were observed as shown in Figure 3.25. The bands of Gd_3PO_7 and Li_3PO_4 were disappeared at 1000^oC (18h) and the remaining bands in the infrared spectra of the products were assigned to Li_2GdOPO_4 which agreed with the literature [99,100]. At 1100^oC, the vibrational bands (1099, 1034, 963) were assigned to the modes of $GdPO_4$ and the broad bands observed at 706 cm^{-1} were attributed to condense phosphates in the IR spectrum as shown in Figure 3.25. It was observed that Li_2GdOPO_4 decomposed to $GdPO_4$ and some condense phosphates at 1100^oC.

The IR spectra of the solid state reaction of $Dy_2O_{3(s)}$ + $2Li_2CO_{3(s)}$ $+2(NH_4)_2HPO_{4(s)}$ were given in figure 3.26. It was observed that the IR spectrum of the products indicated the formation of $DyPO_4$, Dy_2O_3 and Li_3PO_4 at 800^oC (12h). Besides these products, Dy_3PO_7 was observed in the IR spectrum with the increasing temperature up to 900^oC.

At 1000^oC in the IR data, the absorption bands due to the compound of Li_2DyOPO_4 (lithium dysprosium oxyphosphate) was obtained. However, it was observed that Li_2DyOPO_4 decomposed to $DyPO_4$ and some unidentified condense phosphates at 1100^oC.

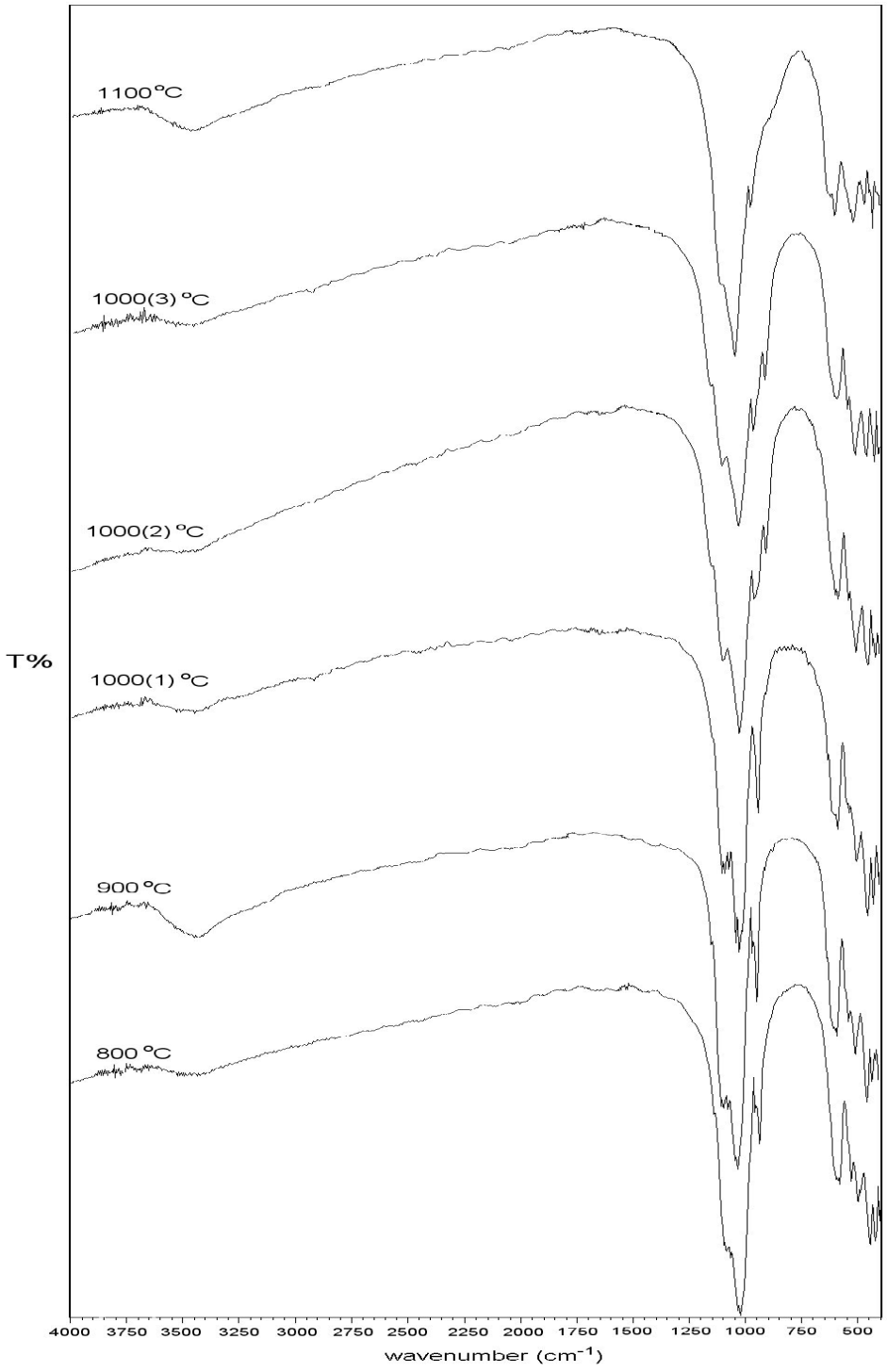


Figure 3.25 IR Spectra of the Products of the Solid-State Reactions of $Gd_2O_{3(s)}$ + $2Li_2CO_{3(s)}$ +$2(NH_4)_2HPO_{4(s)}$ at 800 - 1100^oC

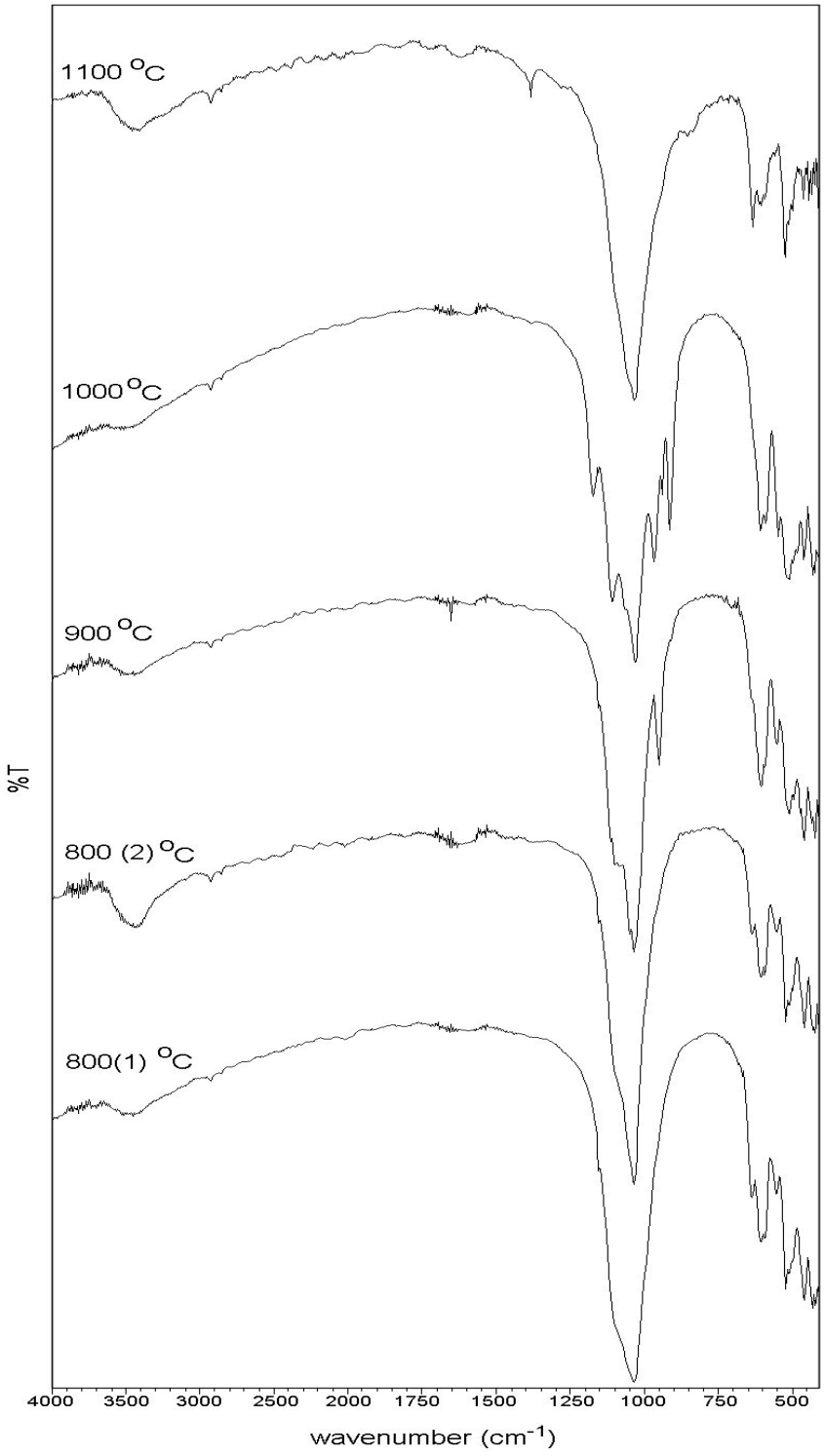


Figure 3.26 IR Spectra of the Products of the Solid-State Reactions of $Dy_2O_{3(s)}$ + $2Li_2CO_{3(s)}$ +$2(NH_4)_2HPO_{4(s)}$ at 800 - 1100°C

3.10 SEM and EDX Analysis of Li_2LnOPO_4 (Ln: Nd,Gd,Dy)

The particle size and the morphology of Li_2LnOPO_4 (Ln: Nd, Gd, Dy) samples were investigated using SEM, as given in Figure 3.27, 3.28, 3.29 respectively. SEM images showed that the uniformity exists between the specimens of sample shape and particle size and have an irregularly grained powder.

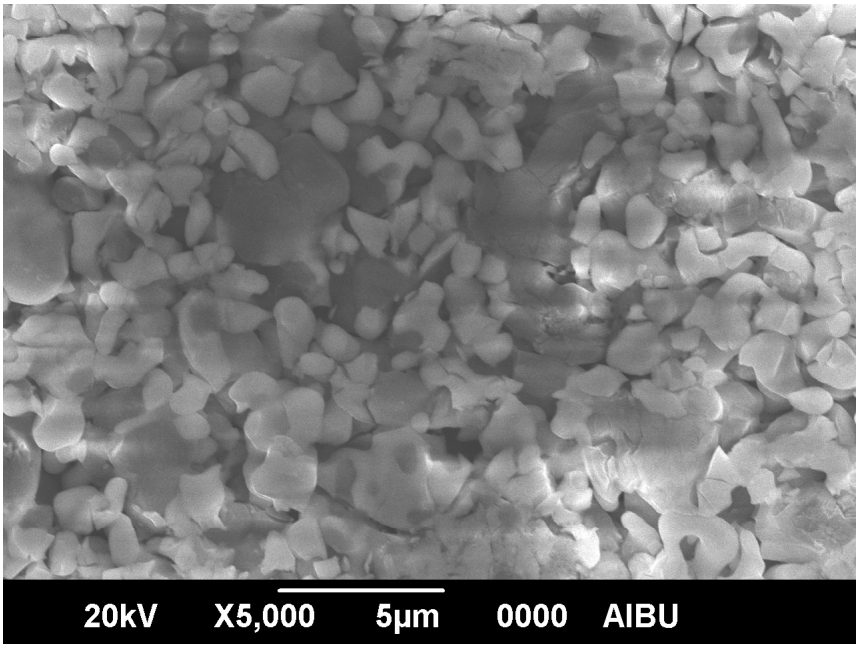


Figure 3.27 SEM image of the Li_2NdOPO_4 at 1000^oC (6h)

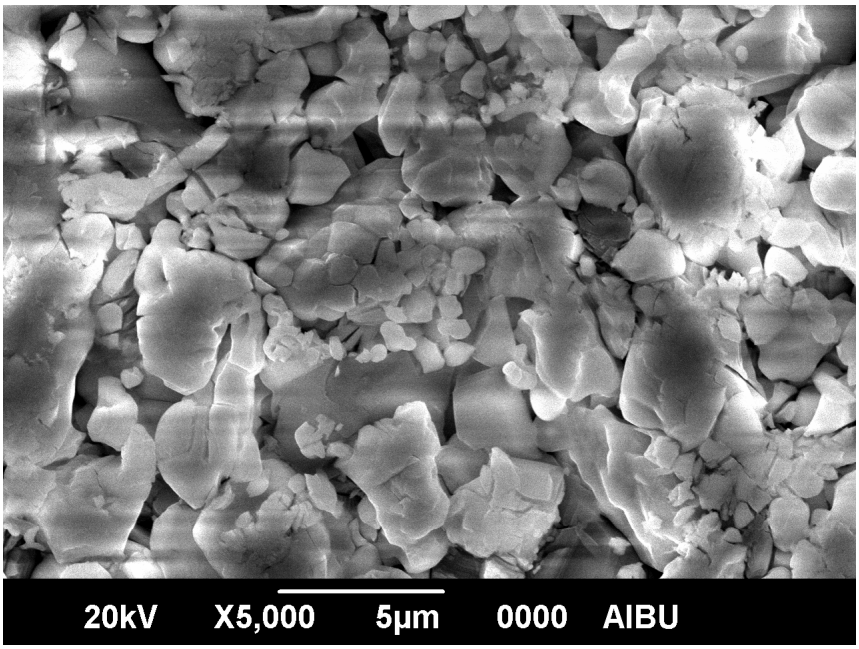


Figure 3.28: SEM image of the Li_2GdOPO_4 at 1000^oC (18h)

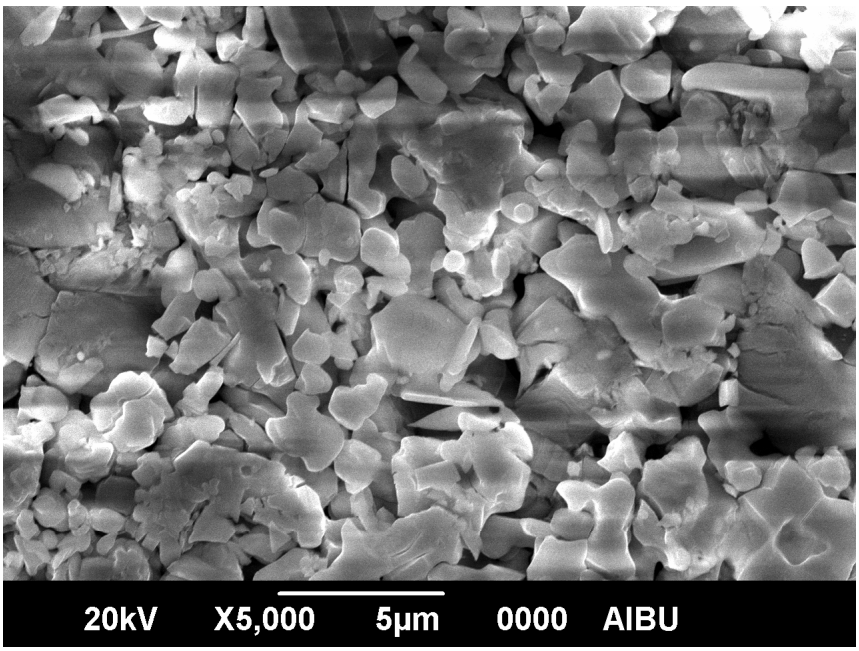


Figure 3.29 SEM image of the Li_2DyOPO_4 at 1000^oC (6h)

The EDX analysis of the products obtained showed the presence of Li, Nd, Gd, Dy, O and P elements as shown in Figure 3.30, 3.31 and 3.32.

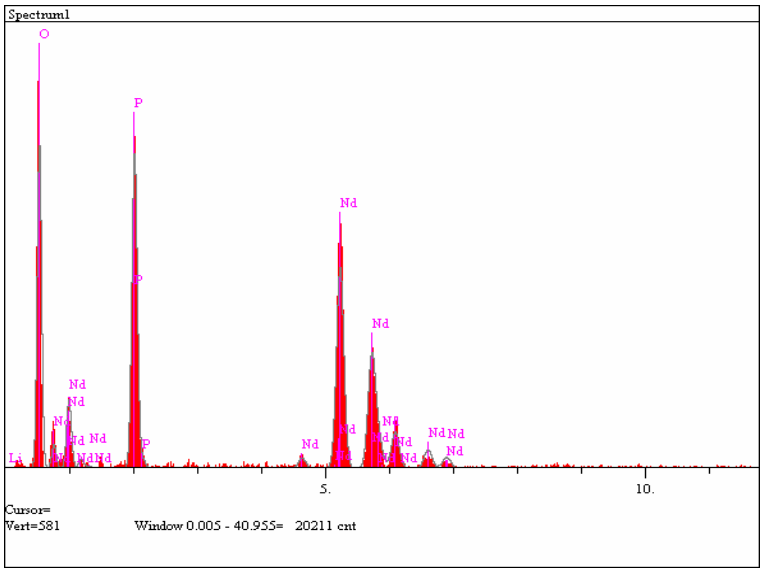


Figure 3.30 EDX Spectrum of the Products Obtained from the Reaction of $Nd_2O_{3(s)} + 2Li_2CO_{3(s)} + 2(NH_4)_2HPO_{4(s)}$ at 1000°C (6h)

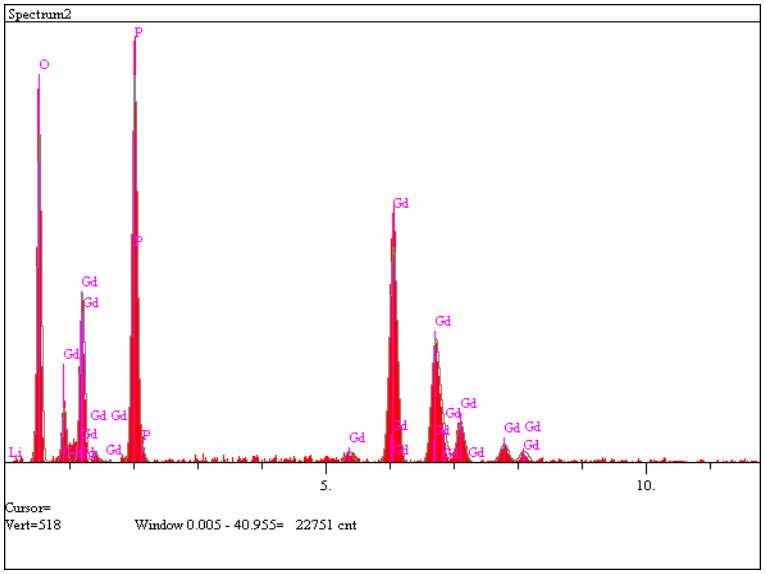


Figure 3.31 EDX Spectrum of the Products Obtained from the Reaction of $Gd_2O_{3(s)} + 2Li_2CO_{3(s)} + 2(NH_4)_2HPO_{4(s)}$ at 1000°C (18h)

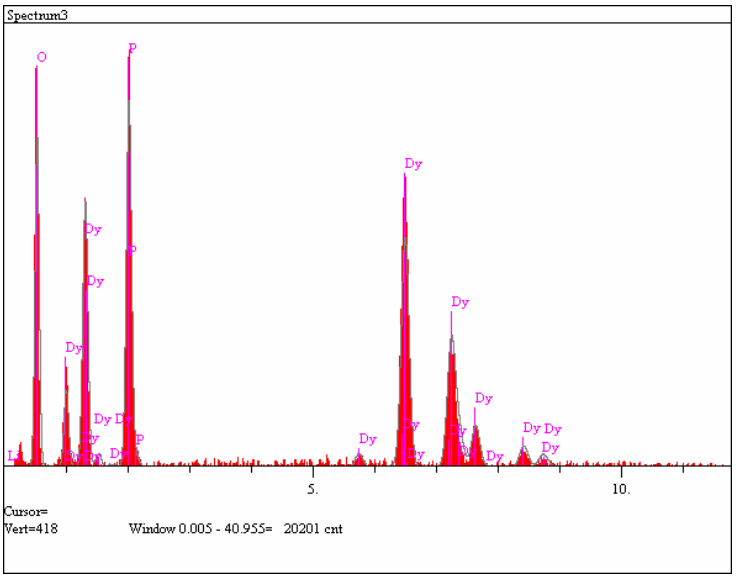


Figure 3.32 EDX Spectrum of the Products Obtained from the Reaction of $Dy_2O_{3(s)} + 2Li_2CO_{3(s)} + 2(NH_4)_2HPO_{4(s)}$ at 1000^oC (6h)

3.11 Thermal Studies (DTA-TG) of Li_2NdOPO_4, Li_2GdOPO_4 and Li_2DyOPO_4 Compounds

The DTA-TG study of Li_2NdOPO_4 and Li_2GdOPO_4 indicated that these compounds are thermodynamically stable up to 1100^oC as shown in Figure 3.33 and 3.34. After that temperature these compounds decomposed to form lanthanide orthophosphates, $LnPO_4$. However, it was observed that Li_2DyOPO_4 was stable up to 1400^oC as shown in figure 3.35.

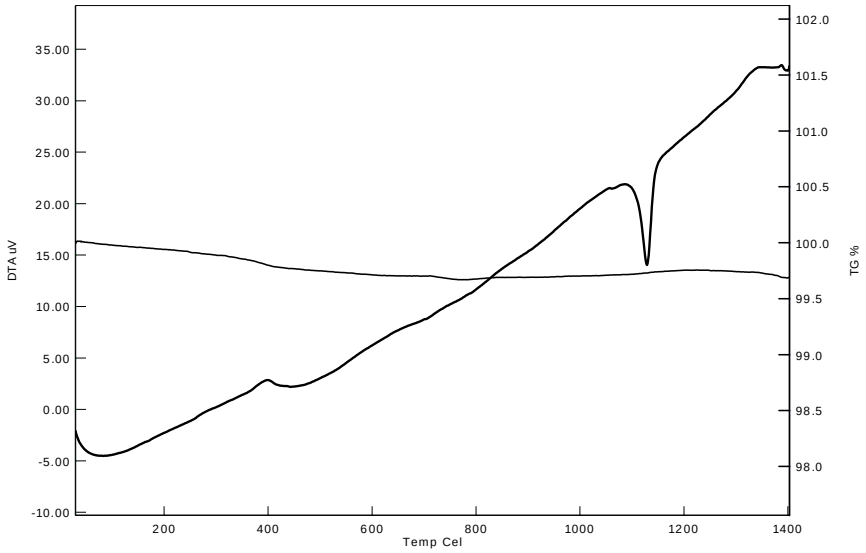


Figure 3.33 DTA-TG of the Product Obtained at 1000°C (6h) Through the Solid-State Reaction of $Nd_2O_{3(s)} + 2Li_2CO_{3(s)} + 2(NH_4)_2HPO_{4(s)}$

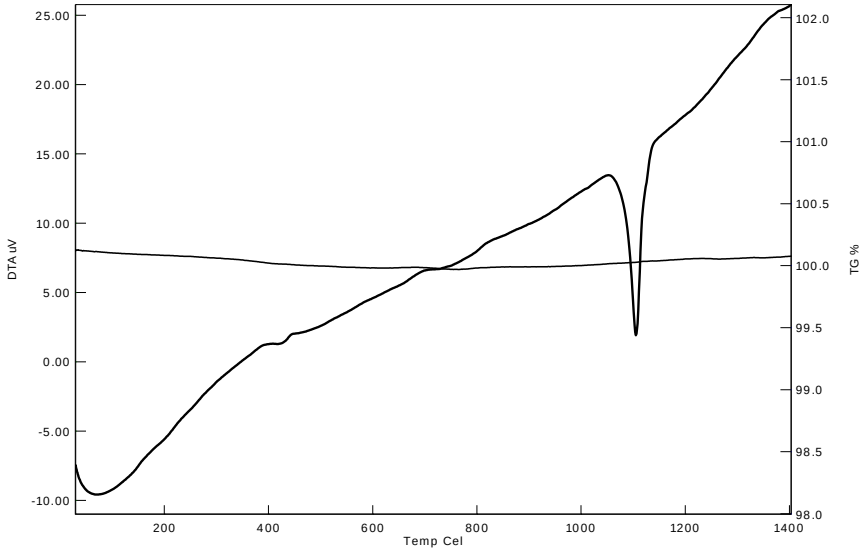


Figure 3.34 DTA-TG of the Product Obtained at 1000°C (18h) Through the Solid-State Reaction of $Gd_2O_{3(s)} + 2Li_2CO_{3(s)} + 2(NH_4)_2HPO_{4(s)}$

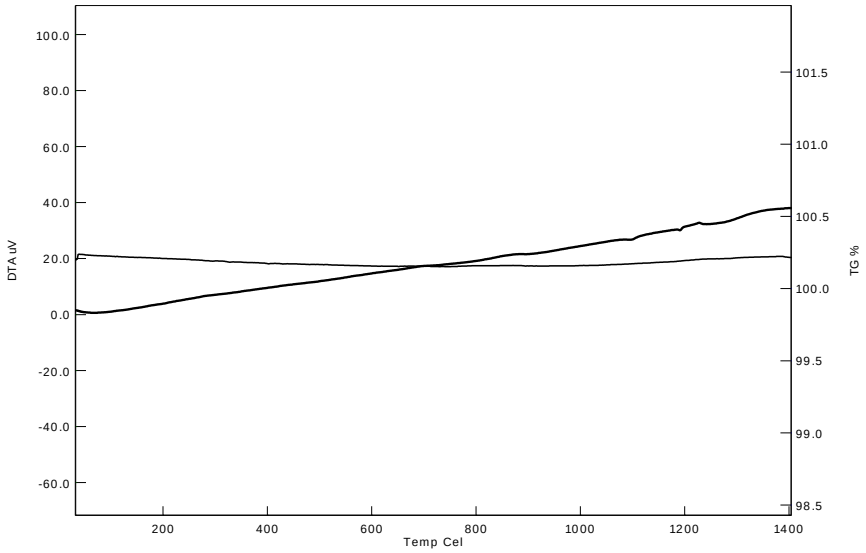


Figure 3.35 DTA-TG of the Product Obtained at 1000^{o}C (6h) Through the Solid-State Reaction of $Dy_2O_{3(s)} + 2Li_2CO_{3(s)} + 2(NH_4)_2HPO_{4(s)}$

3.12 Solid- State Reactions of $Ln_2O_{3(s)} + Li_2CO_{3(s)} + Na_2CO_{3(s)} + 2(NH_4)_2HPO_{4(s)}$ (Nd, Gd, Dy)

In this work, solid state reactions of three different rare earths were proposed to synthesize the compounds, $LiNaLnOPO_4$, Ln_2O_3 (Nd, Gd, Dy), which were not reported in the literature. The 1:1:1:2 mixture of Ln_2O_3 (Nd, Gd, Dy), Li_2CO_3, Na_2CO_3 and $(NH_4)_2HPO_4$ were heated at 800-1100^{o}C for 6 hours. The expected reaction is:

$$Ln_2O_{3(s)} + Li_2CO_{3(s)} + Na_2CO_{3(s)} + 2(NH_4)_2HPO_{4(s)} \rightarrow \mathbf{2LiNaLnOPO_{4(s)}} + 2CO_{2(g)} + 4NH_{3(g)} + 3H_2O_{(g)}$$

3.12.1 X-ray Powder Diffraction Studies for Nd, Gd and Dy Compounds

The X-ray diffraction patterns of the products obtained at different temperatures are given in Figure 3.36. In the analysis of XRD pattern of the product obtained at 800^{o}C (12h) and at 900^{o}C(6h) Nd_2O_3 (ICDD No: 21-0579), $NdPO_4$ (ICDD No: 78-1026), Nd_3PO_7 (ICDD No: 33-0938), Li_3PO_4 (ICDD No: 84-0046) and $NdPO_4$ (ICDD No: 78-1026), Nd_3PO_7 (ICDD No:33-0938), Li_2NaPO_4 (ICDD No: 45-1348), $Na_3Nd(PO_4)_2$ (ICDD No: 38-0058) were observed respectively. At 1000^{o}C, $Na_3Nd\ (PO_4)_2$, Li_2NaPO_4 and Nd_3PO_7 reacted, resulting in a new product not reported in the literature, which was presumed to be $LiNaNdOPO_4$ (with a color of dark blue). The crystal symmetry of this new compound was found to be orthorhombic with the refined unit cell parameters of a= 14.903(8), b= 10.861(3), c= 13.247(1) Å [123].The powder data of this compound is given in Table 3.9. Examination of the table 3.9 revealed that there is a close relation between the product at 1000^{o}C and Na_2NdOPO_4 [86]. So that these compounds seem to be isostructural.

At 1100^{o}C, the decomposition of lithium sodium neodymium oxyphosphate ($LiNaNdOPO_4$) to neodymium orthophosphate and some condensed phosphates was observed.

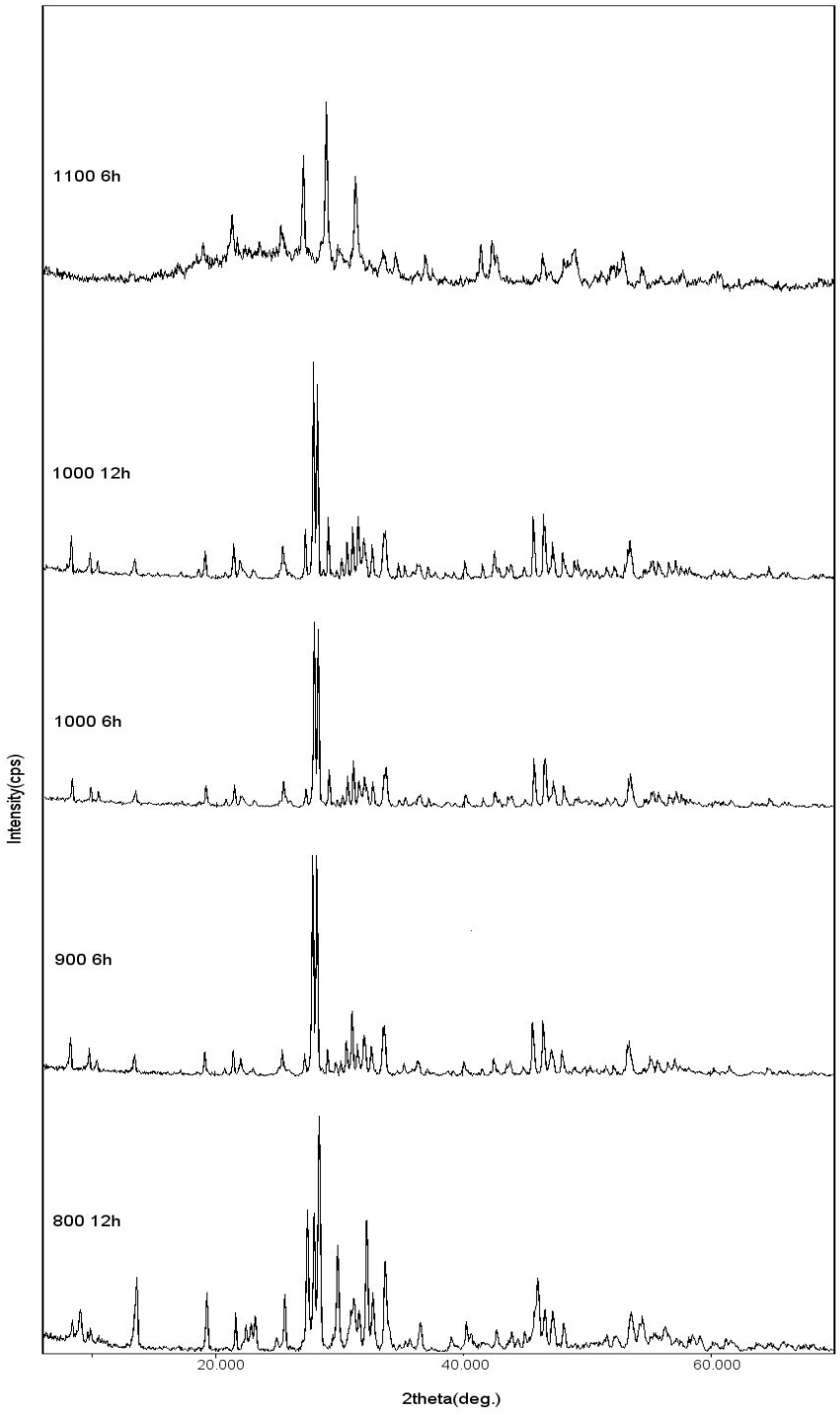


Figure 3.36 X-ray Powder Diffraction Patterns of the Products Obtained of the Solid State Reaction of $Nd_2O_{3(s)} + Li_2CO_{3(s)} + Na_2CO_{3(s)} + 2(NH_4)_2HPO_{4(s)}$ at 800 -1100^oC

Table 3.9 X-ray Powder Diffraction Data of Orthorhombic Structure of $LiNaNdOPO_4$ (1000^oC-12h)

I/I_o	h k l	d_{obs}	d_{calc}
21	0 1 0	10.6184	10.8613
14	1 1 0	8.9996	8.7777
10	0 1 1	8.4827	8.3991
11	0 0 2	6.5826	6.6235
5	1 2 0	5.1631	5.1025
6	1 2 1	4.7563	4.7615
14	3 0 1	4.6332	4.6516
18	2 2 1	4.1411	4.1662
10	1 2 2	4.0515	4.0421
16	0 3 1	3.5037	3.4924
24	2 3 0	3.2734	3.2565
100	3 2 2	3.1974	3.2072
90	2 3 1	3.1619	3.1623
29	4 2 0	3.0702	3.0723
11	5 0 0	2.9995	2.9808
18	2 3 2	2.9210	2.9224
25	5 1 0	2.8788	2.8745
30	4 0 3	2.8413	2.8476
20	0 3 3	2.7997	2.7997
17	1 3 3	2.7428	2.7516
22	3 1 4	2.6681	2.6710
23	0 4 1	2.6589	2.6600
9	0 1 5	2.5801	2.5739
8	4 3 1	2.5447	2.5480
8	3 2 4	2.4767	2.4574
7	6 1 0	2.4200	2.4214
5	4 2 4	2.3804	2.3807
4	3 0 5	2.3340	2.3377
5	5 3 0	2.2940	2.3012
9	5 2 3	2.2989	2.2488

8	5 3 2	2.1731	2.1737
14	6 1 3	2.1262	2.1232
7	1 4 4	2.0787	2.0792
8	2 5 1	2.0607	2.0601
7	3 0 6	2.0171	2.0176
30	6 0 4	1.9861	1.9871
31	6 1 4	1.9529	1.9547
25	5 1 5	1.9474	1.9481
18	5 4 2	1.9240	1.9210
14	0 0 7	1.8931	1.8924
8	0 3 6	1.8842	1.8850
10	6 3 3	1.8589	1.8581
10	1 1 7	1.8490	1.8499
6	0 6 5	1.8118	1.8121
5	1 6 0	1.7965	1.7970
7	5 1 6	1.7515	1.7510
8	4 5 3	1.7263	1.7271
15	6 2 5	1.7179	1.7189
19	0 4 6	1.7125	1.7130
6	0 5 5	1.6806	1.6798
10	7 0 5	1.6593	1.6596
10	6 0 6	1.6489	1.6502
8	9 1 1	1.6253	1.6247

Figure 3.37 shows the XRD pattern of the $LiNaGdOPO_4$ (with a color of white-cream) prepared at 1000^{o}C (12h). This pattern was found to be isomorphous with $LiNaNdOPO_4$. The new product, $LiNaGdOPO_4$, was indexed in the orthorhombic crystal system with the refined unit cell parameters of a= 14.745(0), b= 10.651(6), c= 13.096(8) Å [123]. XRD data for this compound was reported in Table 3.10.

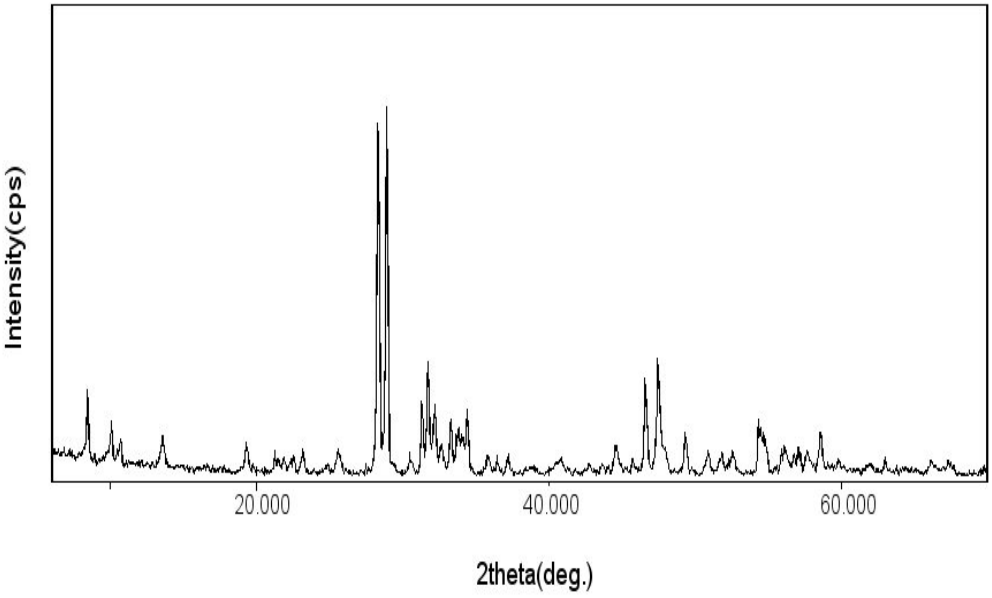


Figure 3.37 X-ray Powder Diffraction Pattern of Orthorhombic $LiNaGdOPO_4$ at 1000^oC (12h)

Table 3.10 X-ray Powder Diffraction Data of Orthorhombic Structure of $LiNaGdOPO_4$ (1000^oC-12h)

I/I_o	h k l	d_{obs}	d_{calc}
24	0 1 0	10.4925	10.6516
16	1 1 0	8.7854	8.6344
11	0 1 1	8.2767	8.2636
12	0 0 2	6.5151	6.5484
10	3 0 1	4.6046	4.6016
7	1 0 3	4.1757	4.1860
6	0 1 3	4.0625	4.0395
8	1 1 3	3.8373	3.8959
9	3 2 1	3.4768	3.4819
97	3 2 2	3.1488	3.1627
100	4 1 2	3.0869	3.0755
7	5 0 0	2.9303	2.9490

21	5 1 0	2.8572	2.8421
33	4 0 3	2.8176	2.8165
21	3 2 3	2.7810	2.7829
9	1 2 4	2.7428	2.7406
16	5 0 2	2.6915	2.6889
14	3 1 4	2.6467	2.6399
12	3 2 2	2.6331	2.6349
19	5 1 2	2.6063	2.6071
7	2 4 0	2.5048	2.5045
6	2 4 1	2.4610	2.4600
7	6 0 1	2.4150	2.4153
5	4 3 3	2.2088	2.2065
9	2 3 5	2.0282	2.0266
6	4 2 5	1.9836	1.9819
27	2 2 6	1.9482	1.9480
32	0 5 3	1.9168	1.9145
13	1 3 6	1.8462	1.8449
8	6 0 5	1.7918	1.7922
8	1 6 0	1.7616	1.7625
8	3 3 6	1.7391	1.7392
16	0 4 6	1.6874	1.6881
13	8 1 3	1.6766	1.6768
8	1 5 5	1.6424	1.6424
9	9 0 0	1.6386	1.6383
7	7 1 5	1.6216	1.6223
9	6 1 6	1.6133	1.6132
8	3 4 6	1.5964	1.5966
13	5 3 6	1.5740	1.5729
6	7 4 3	1.5448	1.5451
5	4 0 8	1.4956	1.4962
6	6 1 7	1.4742	1.4743
6	9 2 4	1.4116	1.4127
6	9 0 5	1.3897	1.3890

The XRD patterns of the products produced through the solid state reaction of Dy_2O_3, Na_2CO_3, Li_2CO_3 and $2(NH_4)_2HPO_4$ were given in figure 3.38. In the X-ray powder diffraction data of the reaction products at 800°C, Dy_2O_3 (ICDD No: 86-1327) and $DyPO_4$ (ICDD No: 74-0774) lines were observed. Besides these products, Li_3PO_4 was observed in the XRD pattern with the increasing temperature (900°C). At 1000°C, oxyphosphate of the type of $LiNaDyOPO_4$ (with a color of dark cream) was found in the X-ray diffraction data. Table 3.11 gives the X-ray powder data of this product obtained from the reactions of $Dy_2O_{3(s)}$ + $Na_2CO_{3(s)}$ + $Li_2CO_{3(s)}$ + $2(NH_4)_2HPO_{4(s)}$ at 1000°C. The new product, $LiNaDyOPO_4$ was indexed in the orthorhombic crystal system with the refined unit cell parameters of a= 14.622(2), b= 10.581(0), c= 13.018(2) Å [123]. At 1100°C, lithium sodium dysprosium oxyphosphate ($LiNaDyOPO_4$) melted but did not decomposed.

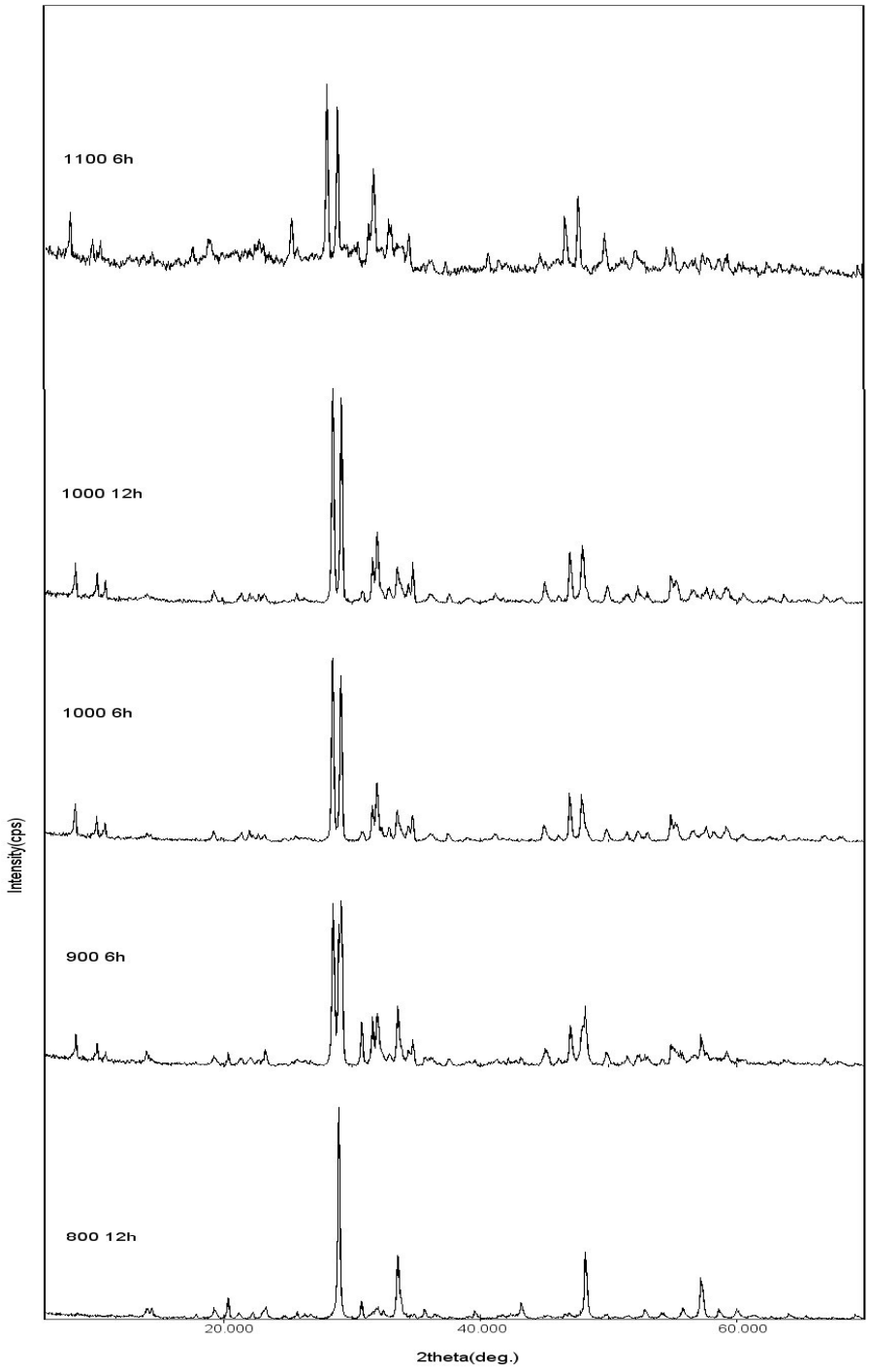


Figure 3.38 X-ray Powder Diffraction Patterns of the Products Obtained of the Solid State Reaction of $Dy_2O_{3(s)} + Li_2CO_{3(s)} + Na_2CO_{3(s)} + 2(NH_4)_2HPO_{4(s}$ at 800 -1100^oC.

Table 3.11 X-ray Powder Diffraction Data of Orthorhombic Structure of $LiNaDyOPO_4$ (1000^oC-6h)

I/I_o	h k l	d_{obs}	d_{calc}
19	0 1 0	10.5175	10.5810
15	1 1 0	8.7680	8.5721
12	0 1 1	8.2306	8.2109
7	1 2 1	4.6093	4.6471
7	1 0 3	4.1564	4.1601
6	0 1 3	4.0369	4.0149
6	3 0 2	3.9140	3.9015
6	1 1 3	3.8406	3.8716
6	3 2 1	3.4635	3.4560
100	3 2 2	3.1314	3.1400
97	4 1 2	3.0599	3.0518
7	5 0 0	2.8969	2.9244
22	5 1 0	2.8255	2.8188
34	4 0 3	2.7980	2.7957
8	1 2 4	2.7250	2.7235
18	5 0 2	2.6712	2.6676
10	0 0 5	2.6049	2.6036
20	5 1 2	2.5802	2.5866
6	2 4 0	2.4887	2.4874
6	0 3 4	2.3914	2.3918
6	4 3 3	2.1903	2.1909
4	2 4 3	2.1592	2.1580
3	0 4 4	2.0562	2.0527
12	5 2 4	2.0111	2.0118
5	4 2 5	1.9690	1.9685
25	2 2 6	1.9317	1.9358
27	3 4 4	1.8946	1.8918
10	5 2 5	1.8247	1.8252
6	3 5 3	1.7724	1.7719
9	0 6 1	1.7483	1.7475

6	1 2 7	1.7410	1.7420
6	2 5 4	1.7251	1.7241
14	8 2 2	1.6681	1.6698
12	7 3 3	1.6609	1.6605
7	8 3 0	1.6221	1.6228
6	9 1 0	1.6061	1.6059
9	4 5 4	1.5969	1.5961
8	4 2 7	1.5838	1.5817
5	8 1 4	1.5755	1.5759
9	5 3 6	1.5609	1.5622
8	0 2 8	1.5552	1.5554
6	3 1 8	1.5350	1.5274
4	2 5 6	1.4835	1.4834
6	0 6 5	1.4601	1.4601

3.12.2 IR Studies for $LiNaLnOPO_4$ (Ln: Nd, Gd, Dy) Compounds

As shown in Figures 3.39, 3.40 and 3.41 the infrared spectra of the products were obtained by the reactions of $Ln_2O_{3(s)}$ (Nd, Gd, Dy) + $Li_2CO_{3(s)}$+ $Na_2CO_{3(s)}$ +2$(NH_4)_2HPO_{4(s)}$ (for neodymium and dysprosium at 800-1100^oC, for gadolinium at 800-1000^oC).

At low temperatures (800-900), the vibrational bands due to Ln_2O_3, $LnPO_4$, Ln_3PO_7, (Ln: Nd, Gd, Dy), [86] Na_3PO_4 and Li_2NaPO_4 were observed. At high temperatures (1000^oC), the IR absorption bands according to Ln_3PO_7, $Na_3Ln(PO_4)_2$ and Ln_2O_3 disappeared whereas the vibrational modes belong to $LiNaLnOPO_4$ (Ln: Nd, Gd, Dy), appeared. Table 3.12 shows the assignment for the vibrational frequencies of the products at 1000^oC.

Table 3.12 The assignments of IR Absorption Bands for the Compounds of $LiNaNdOPO_4$, $LiNaGdOPO_4$ and $LiNaDyOPO_4$ at 1000^oC.

Assignment	**$LiNaNdOPO_4$**	**$LiNaGdOPO_4$**	**$LiNaDyOPO_4$**
υ_3 (F_2)	1120, 1091, 1045, 1025, 985, 958	1139, 1095, 1045, 1029, 986, 970	1170, 1140, 1104, 1033, 970
υ_1 (A_1)	923, 912	929, 916	922, 918
υ_4(F_2)	605, 592, 545	603, 580, 548	605, 584, 546
υ_2(E)	430	425	418

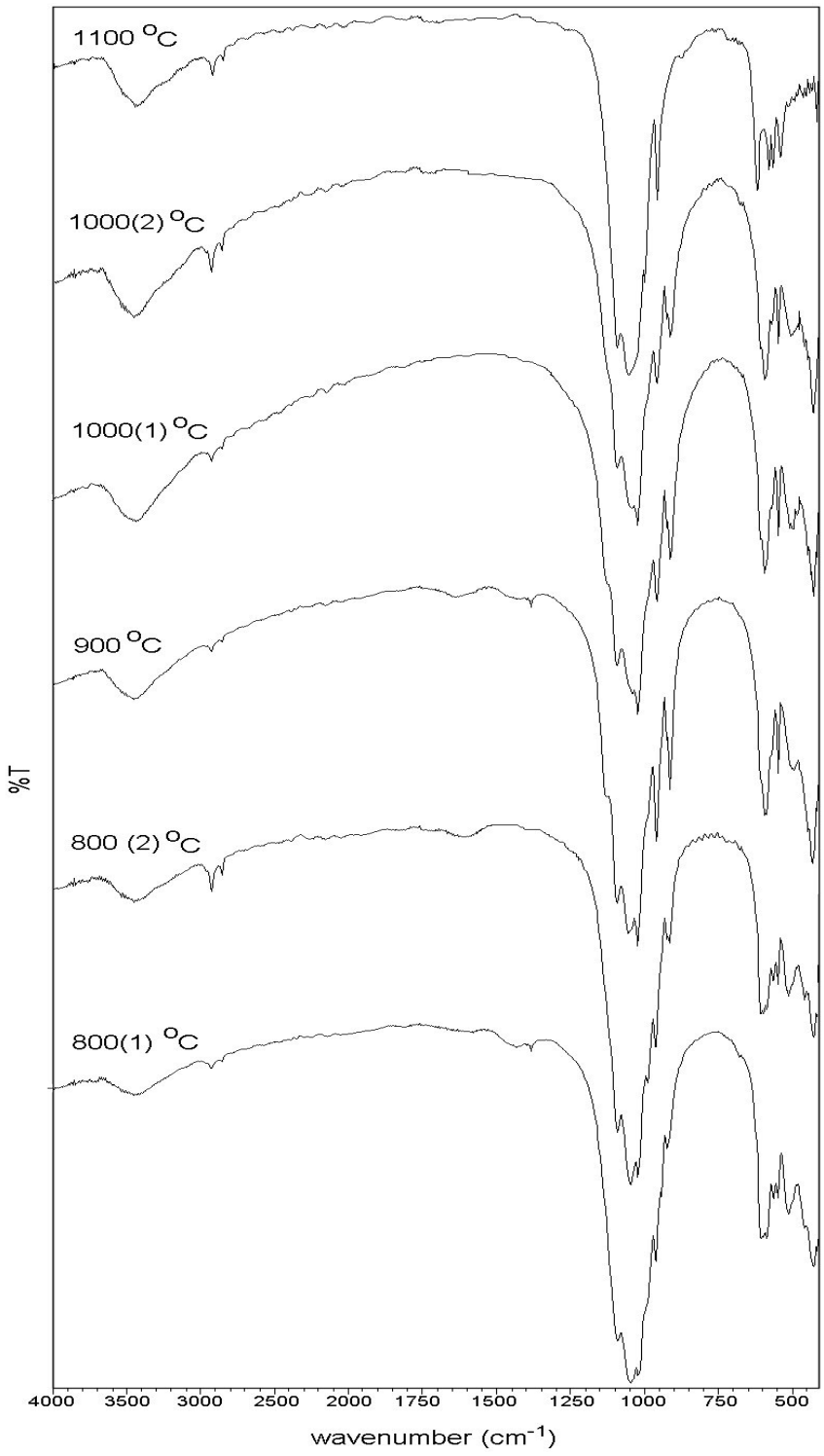


Figure 3.39 IR Spectra of the Products of the Solid-State Reactions of $Nd_2O_{3(s)}$ + $Li_2CO_{3(s)}$ + $Na_2CO_{3(s)}$ +2$(NH_4)_2HPO_{4(s)}$ at 800 - 1100^oC

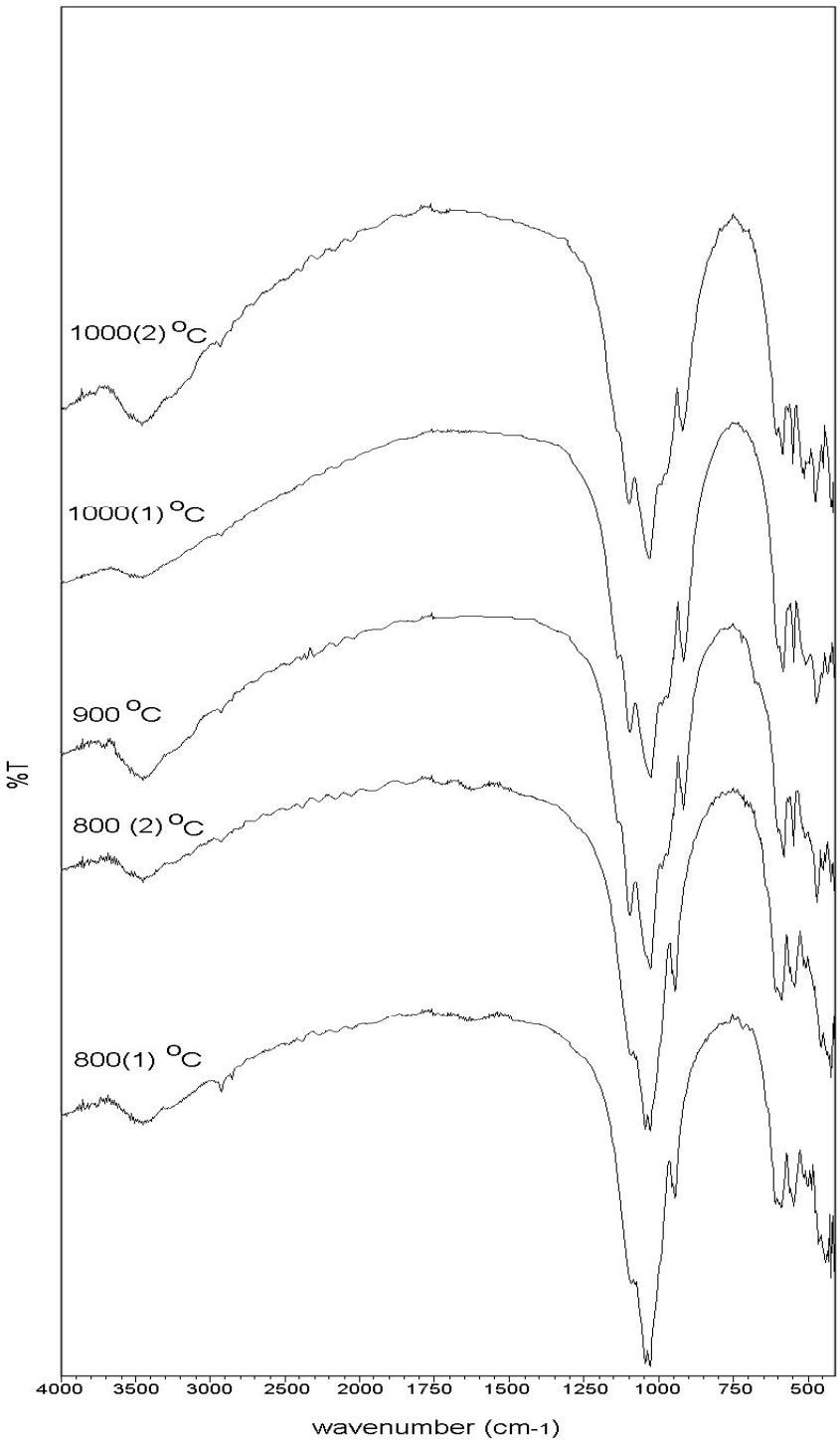


Figure 3.40 IR Spectra of the Products of the Solid-State Reactions of $Gd_2O_{3(s)}$ + $Li_2CO_{3(s)}$ + $Na_2CO_{3(s)}$ +2$(NH_4)_2HPO_{4(s)}$ at 800 - 1000^oC

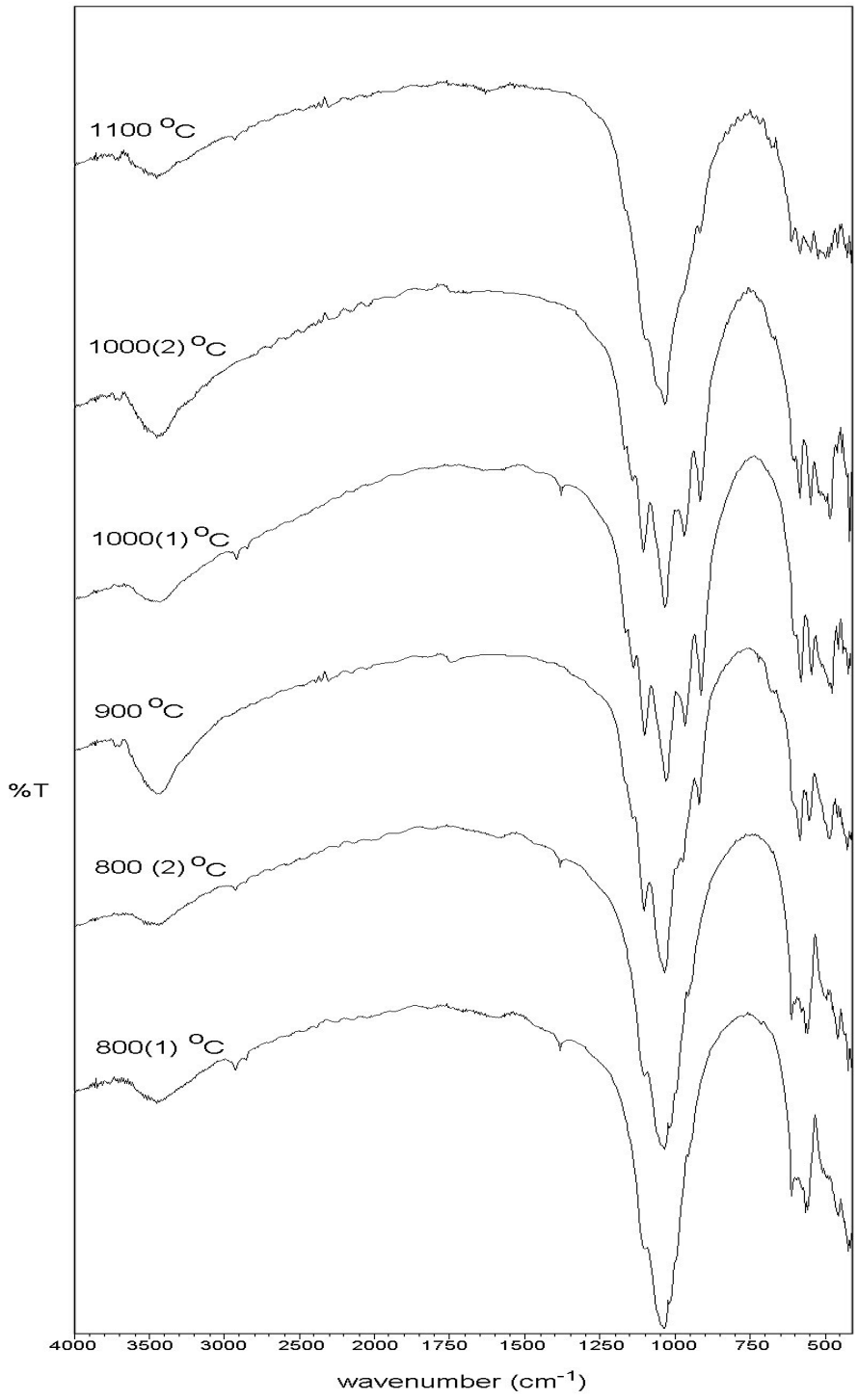


Figure 3.41 IR Spectra of the Products of the Solid-State Reactions of $Dy_2O_{3(s)}$ + $Li_2CO_{3(s)}$ + $Na_2CO_{3(s)}$ + $2(NH_4)_2HPO_{4(s)}$ at 800 - 1100^oC

3.13 SEM and EDX Analysis of $LiNaLnOPO_4$ (Ln: Nd,Gd,Dy) Compounds

The particle size and the morphology of $LiNaLnOPO_4$ (Ln: Nd, Gd, Dy) samples were investigated using SEM, as given in Figure 3.42, 3.43, 3.44 respectively. SEM images showed that the uniformity exists between the specimens of sample shape and particle size and have an irregularly grained powder.

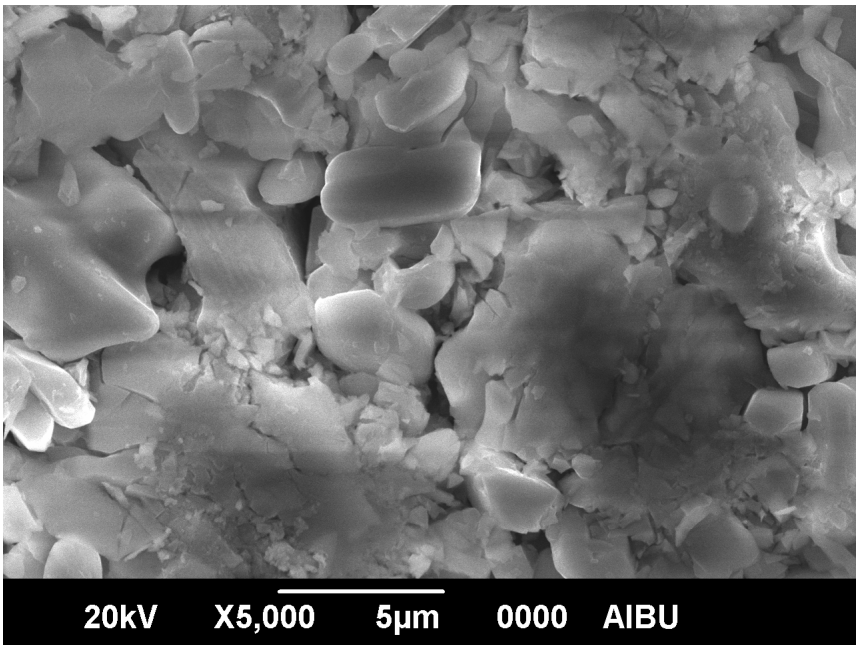


Figure 3.42 SEM image of the $LiNaNdOPO_4$ at 1000^oC (12h)

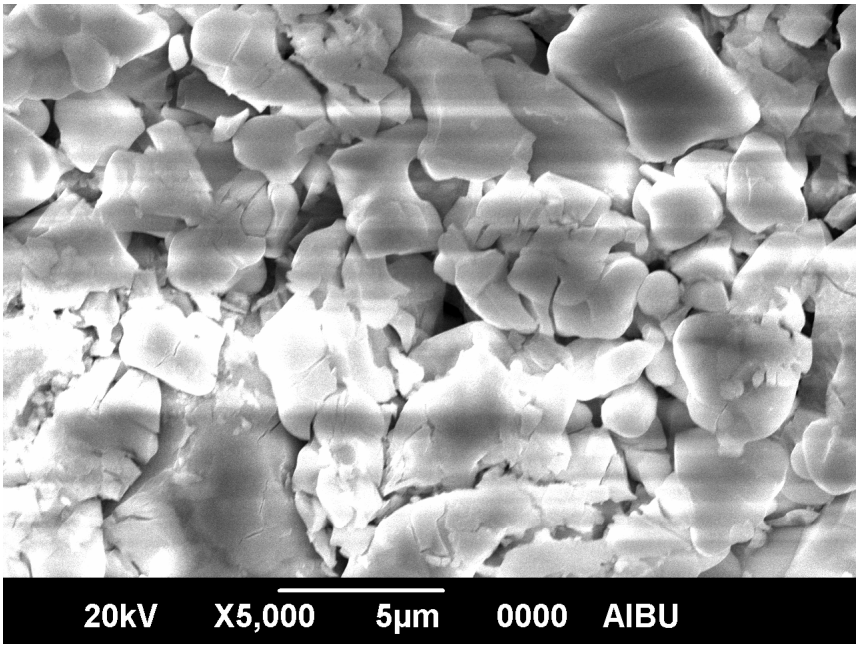


Figure 3.43 SEM image of the $LiNaGdOPO_4$ at 1000^oC (12h)

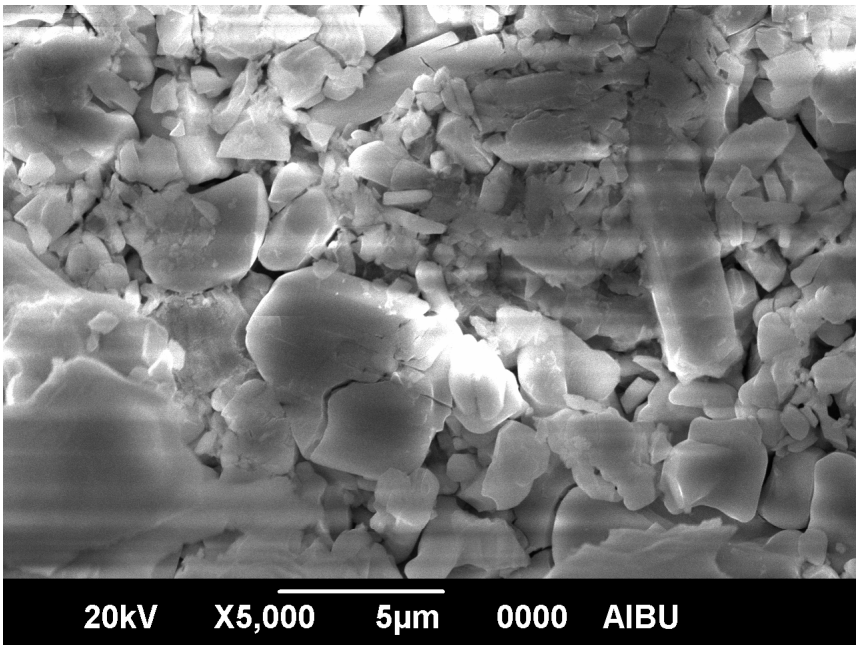


Figure 3.44 SEM image of the $LiNaDyOPO_4$ at 1000^oC (6h)

The EDX analysis of the products showed the presence of Li, Na, Nd, Gd, Dy, O and P elements as shown in Figure 3.45, 3.46 and 3.47.

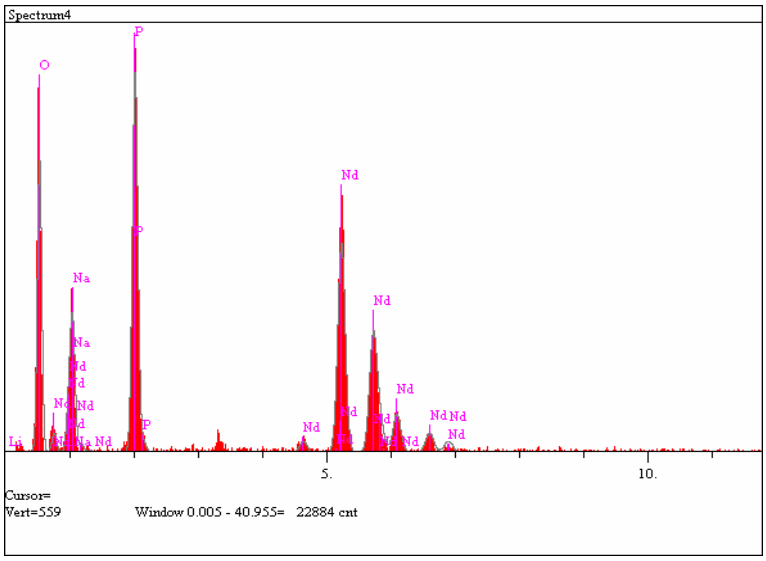


Figure 3.45 EDX Spectrum of the Products Obtained from the Reaction of $Nd_2O_{3(s)} + Li_2CO_{3(s)} + Na_2CO_{3(s)} + 2(NH_4)_2HPO_{4(s)}$ at 1000°C (12h)

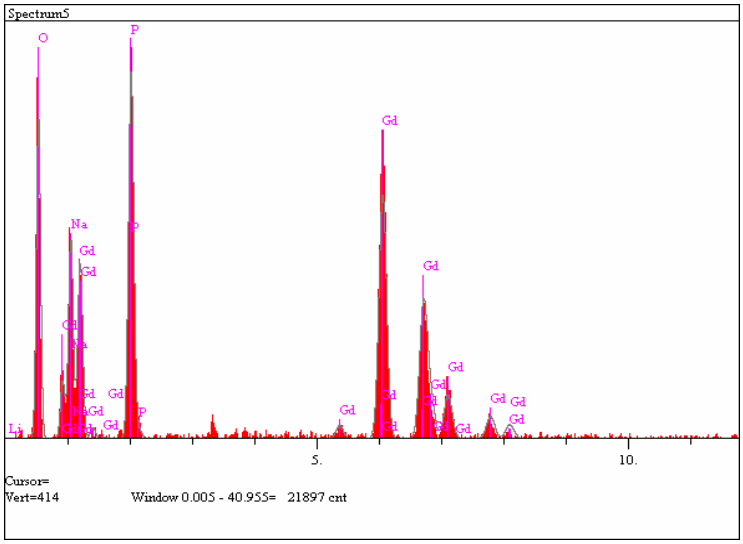


Figure 3.46 EDX Spectrum of the Products Obtained from the Reaction of $Gd_2O_{3(s)} + Li_2CO_{3(s)} + Na_2CO_{3(s)} + 2(NH_4)_2HPO_{4(s)}$ at 1000°C (12h)

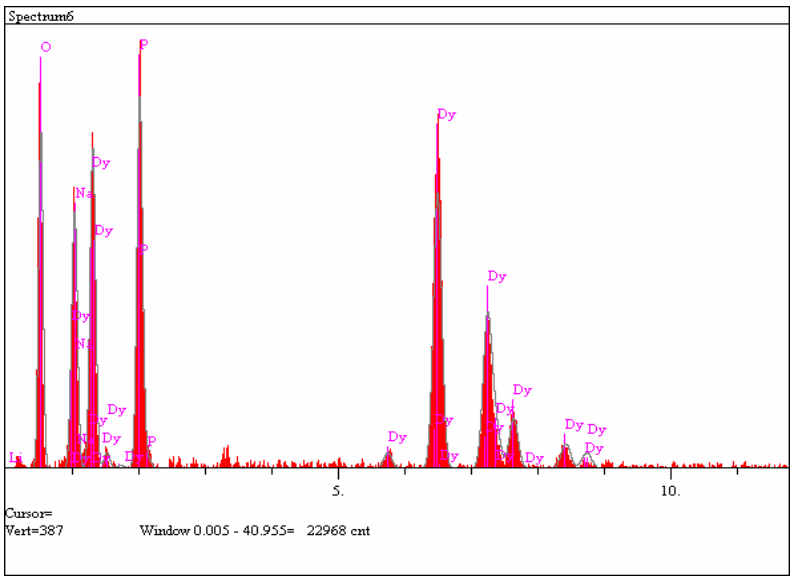


Figure 3.47 EDX Spectrum of the Products Obtained from the Reaction of $Dy_2O_{3(s)} + Li_2CO_{3(s)} + Na_2CO_{3(s)} + 2(NH_4)_2HPO_{4(s)}$ at 1000^oC (6h)

3.14 Thermal Studies (DTA-TG) of $LiNaNdOPO_4$, $LiNaGdOPO_4$ and $LiNaDyOPO_4$ Compounds

The DTA-TG studies of the compounds $LiNaNdOPO_4$, $LiNaGdOPO_4$ and $LiNaDyOPO_4$ indicated that these compounds are thermodynamically stable up to 1400^oC as shown in Figure 3.48, 3.49 and 3.50.

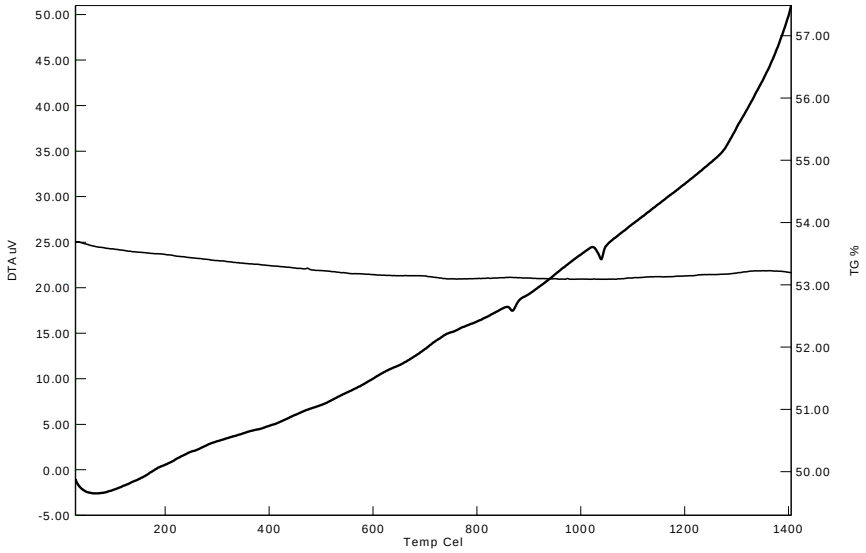


Figure 3.48 DTA-TG of the Product Obtained at 1000°C (12h) Through the Solid-State Reaction of $Nd_2O_{3(s)} + Li_2CO_{3(s)} + Na_2CO_{3(s)} + 2(NH_4)_2HPO_{4(s)}$

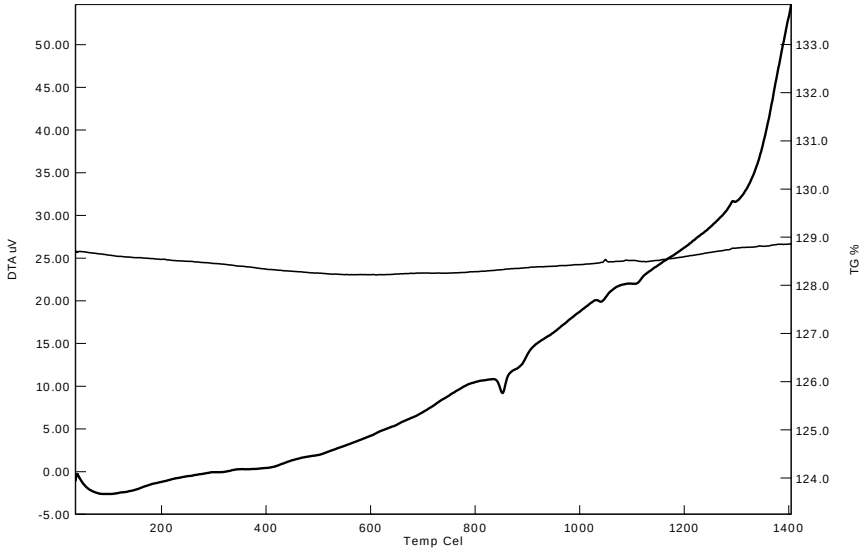


Figure 3.49 DTA-TG of the Product Obtained at 1000°C (12h) Through the Solid-State Reaction of $Gd_2O_{3(s)} + Li_2CO_{3(s)} + Na_2CO_{3(s)} + 2(NH_4)_2HPO_{4(s)}$

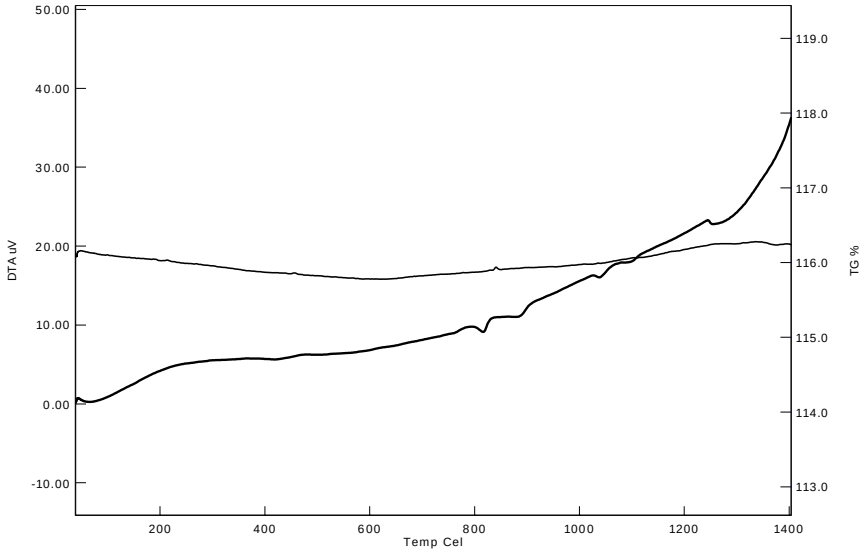


Figure 3.50 DTA-TG of the Product Obtained at 1000°C (6h) Through the Solid-State Reaction of $Dy_2O_{3(s)} + Li_2CO_{3(s)} + Na_2CO_{3(s)} + 2(NH_4)_2HPO_{4(s)}$

3.15 Solid- State Reactions of $Ln_2O_{3(s)} + 6CaHPO_4.2H_2O_{(s)} + 2CaCO_{3(s)}$ (Nd, Gd, Dy)

In this part of the thesis, the reactions were performed among 700-1000°C for 8 hours and at 1100-1300°C for 12 hours. The proposed reaction is:

$$Ln_2O_{3(s)}\ (Nd, Gd, Dy) + 6CaHPO_4.2H_2O_{(s)} + 2CaCO_{3(s)} \rightarrow \mathbf{Ca_8Ln_2(PO_4)_6O_2} + 2CO_{2(g)} + 15H_2O_{(g)}$$

3.15.1 X-ray Powder Diffraction Study of the Products

The products obtained at different temperatures were subjected to X-ray powder diffraction analysis after each heating process. The X-ray diffraction patterns observed for Nd compound are given in Figure 3.51. In the analysis of XRD pattern of the products obtained; at between 700-800°C cubic Nd_2O_3 (ICDD No: 65-3184),

monoclinic $NdPO_4$ (ICDD No: 78-1026), hexagonal β-$Ca_3(PO_4)_2$ (whitlockite ICDD No: 09-0169) and at 900^oC, additional to these lines, hexagonal $Ca_8Nd_2(PO_4)_6O_2$ (ICDD No:32-0175) were observed. At 1000^oC, the intensities of the lines of $Ca_8Nd_2(PO_4)_6O_2$ began to increase as the lines of Nd_2O_3 disappeared completely. Prolonged heating of the products at 1100^oC (12h and grinding) hexagonal $Ca_8Nd_2(PO_4)_6O_2$ lines were observed and the intensities of the lines of $NdPO_4$, β-$Ca_3(PO_4)_2$ began to decrease. At 1100-1300^oC, examination of the XRD pattern showed that the diffraction lines belong to hexagonal $Ca_8Nd_2(PO_4)_6O_2$ become weaker and the intensities of the lines of $NdPO_4$, β-$Ca_3(PO_4)_2$ began to increase.

Therefore, the final reaction could be written as follows:

$$Nd_2O_3 + 12CaHPO_4.2H_2O + 4CaCO_3 \rightarrow Ca_8Nd_2(PO_4)_6O_2 + 2\,Ca_3(PO_4)_2 + 2NdPO_4 + 2CaO + 4CO_2 + 30H_2O$$

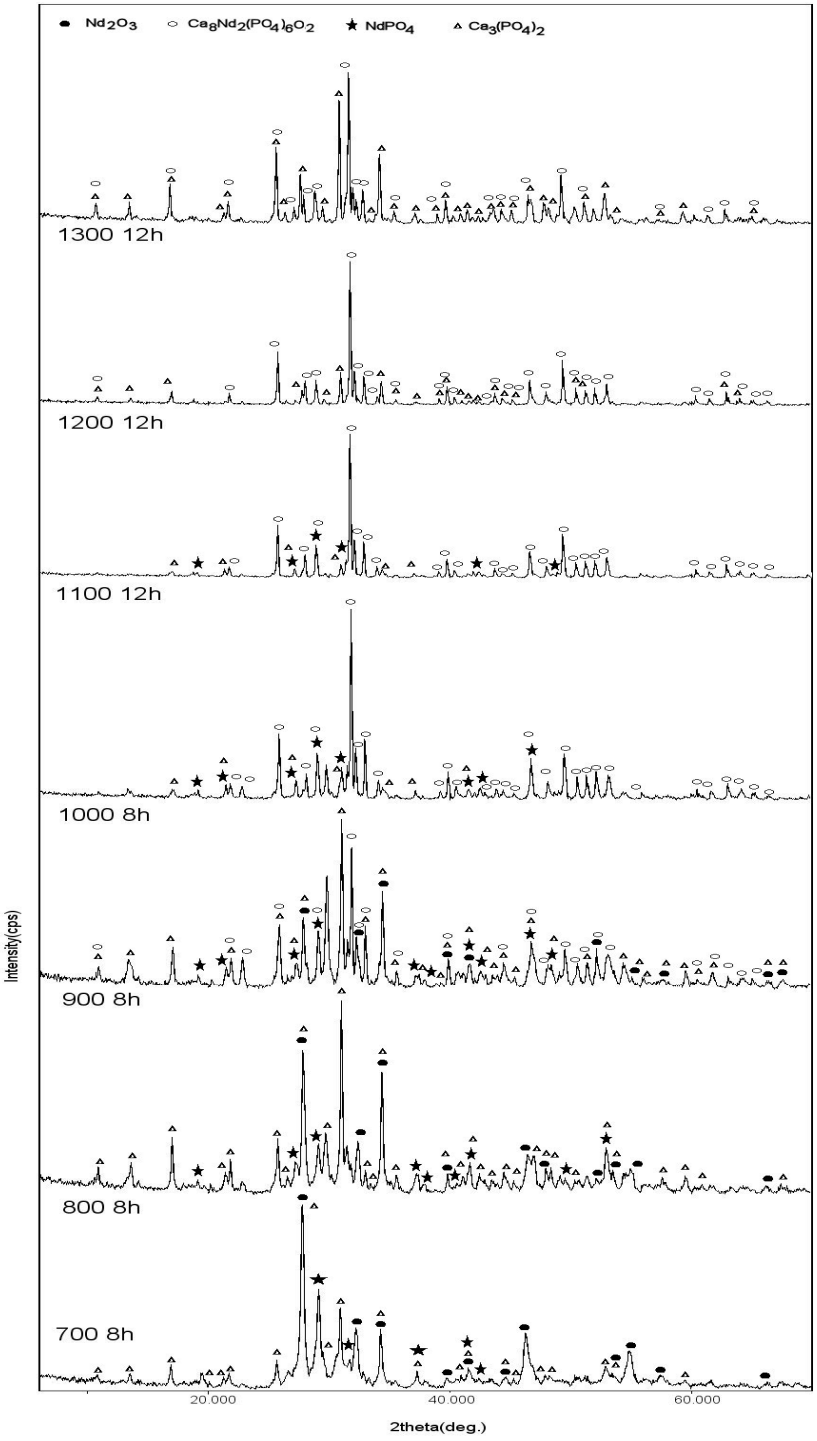


Figure 3.51 X-ray Powder Diffraction Patterns of the Products Obtained of the Solid State Reaction of $Nd_2O_{3(s)}$+ $6CaHPO_4.2H_2O_{(s)}$ + $2CaCO_{3(s)}$ at 700-1300^oC.

The X-ray diffraction patterns observed for Gd compound are given in Figure 3.52. When the X-ray powder diffraction pattern of the products were investigated at low temperature (700-800^{o}C), the lines of cubic Gd_2O_3 (ICDD No: 65-3181) as main product and hexagonal β-$Ca_3(PO_4)_2$ (whitlockite ICDD No: 09-0169) were observed. At 900^{o}C additional to these lines, monoclinic $GdPO_4$(ICDD No: 32-0386) was also observed. While the lines belong to Gd_2O_3 substantially decreased at 1000^{o}C, d-spacings for cubic $Ca_3Gd(PO_4)_3$ (ICDD No: 29-0325), hexagonal β-$Ca_3(PO_4)_2$ (whitlockite ICDD No: 09-0169), and $Ca_8Gd_2(PO_4)_6O_2$ (ICDD No: 32-0163) began to observe. Besides these lines seen at 1000^{o}C, d-spacings belong to monoclinic Gd_3PO_7 (ICDD No: 34-1066) were detected and the lines for cubic $Ca_3Gd(PO_4)_3$ were disappeared after heating process about 12hr at 1100^{o}C. While the intensities of d-lines for $Ca_8Gd_2(PO_4)_6O_2$ (ICDD No: 32-0163) increased, the lines for hexagonal β-$Ca_3(PO_4)_2$ and monoclinic Gd_3PO_7 lines decreased at 1200^{o}C. It was observed that there was an increase in intensities of the lines of cubic $Ca_3Gd(PO_4)_3$ and hexagonal β-$Ca_3(PO_4)_2$ whereas the intensities of hexagonal $Ca_8Gd_2(PO_4)_6O_2$ decreased at 1300^{o}C(12h).

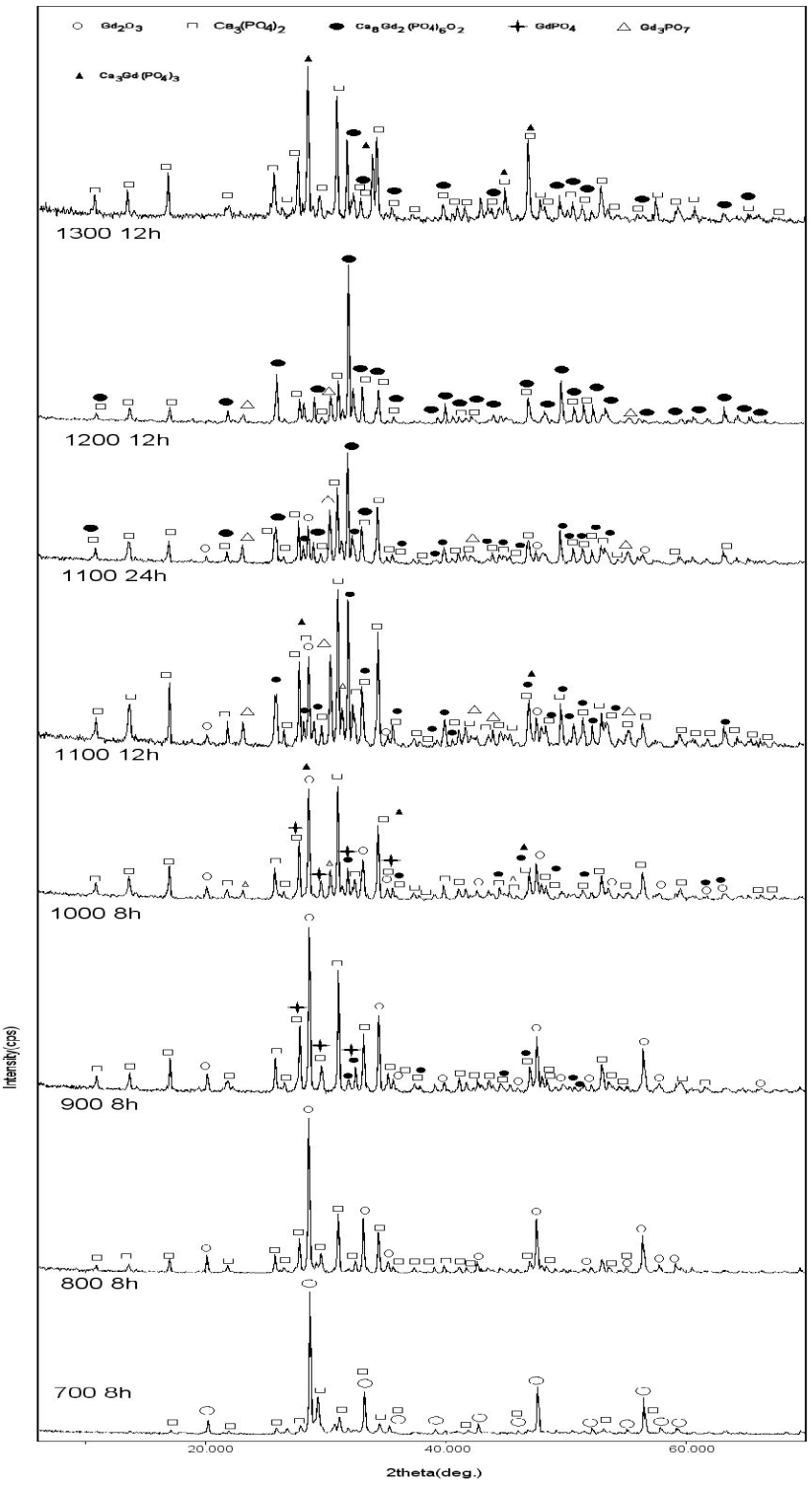


Figure 3.52 X-ray Powder Diffraction Patterns of the Products Obtained of the Solid State Reaction of $Gd_2O_{3(s)} + 6CaHPO_4.2H_2O_{(s)} + 2CaCO_{3(s)}$ at 700-1300^oC.

The X-ray diffraction patterns observed for Dy compound are given in Figure 3.53. In the analysis of XRD pattern of the products obtained at among 700-1000^{o}C, cubic Dy_2O_3 (ICDD No: 86-1327), hexagonal β-$Ca_3(PO_4)_2$ (whitlockite ICDD No: 09-0169), and $Ca_9Dy(PO_4)_7$ (ICDD No:49-1086) were observed. At 1100^{o}C (24h and grinding), additional to these lines, the d-spacings belong to $Ca_8Dy_2(PO_4)_6O_2$ were observed. At 1200 and 1300^{o}C, examination of the XRD pattern showed that the diffraction lines belong to $Ca_8Dy_2(PO_4)_6O_2$ become weak and the intensities of the lines of $Ca_9Dy(PO_4)_7$ and β-$Ca_3(PO_4)_2$ began to increase.

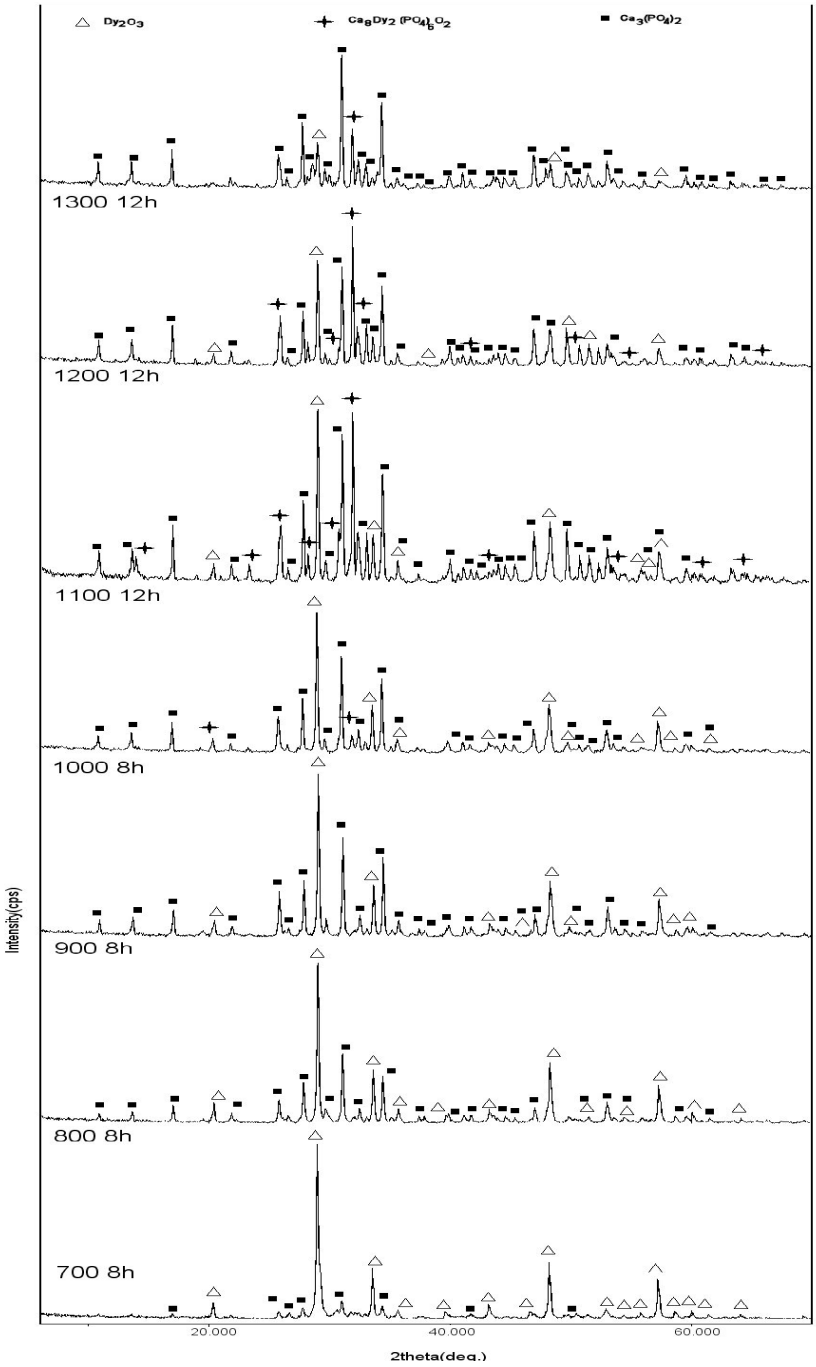


Figure 3.53 X-ray Powder Diffraction Patterns of the Products Obtained of the Solid State Reaction of $Dy_2O_{3(s)} + 6CaHPO_4.2H_2O_{(s)} + 2CaCO_{3(s)}$ at 700-1300^oC.

3.15.2 IR Spectra of the Products

The IR spectrum observed for Nd, Gd and Dy compounds are given in Figure 3.54 – 3.56 respectively. The IR data and assignments of the products indicated that υ_3 (F_2) and υ_1 (A_1) bands of stretching vibrations of P-O bonds were observed at 1100, 1048, 1016, and 960 cm^{-1} for Nd-compound, at 1100, 1048, 1014 and 960 cm^{-1} for Gd-compound, at 1100, 1046, 1013 and 962 cm^{-1} for Dy-compound respectively. The bands observed at 601, 569 cm^{-1}; 603, 570, 553 cm^{-1}; 605, 572, 553 cm^{-1} were ascribed to υ_4 (F_2) of δ(O-P-O) for Nd, Gd, and Dy-compound, respectively. The band at ~ 450 cm^{-1} (υ_2(E)) was attributed to deformation of PO_4^{3-} ion for the Nd, Gd, Dy-compounds [119].

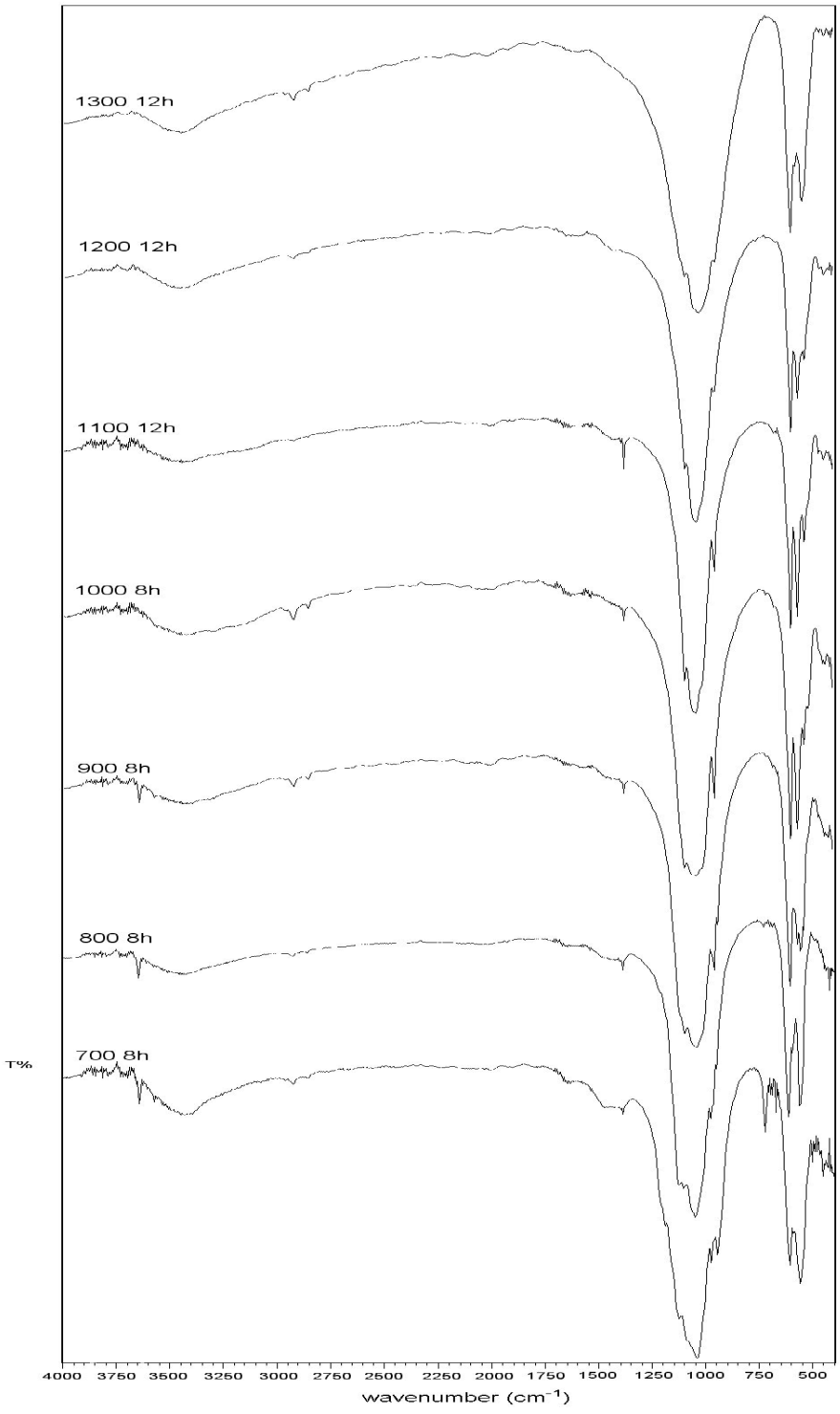


Figure 3.54 IR Spectra of the Products of the Solid-State Reactions of $Nd_2O_{3(s)}$+6$CaHPO_4.2H_2O_{(s)}$+ 2$CaCO_{3(s)}$ at 700 - 1300^oC

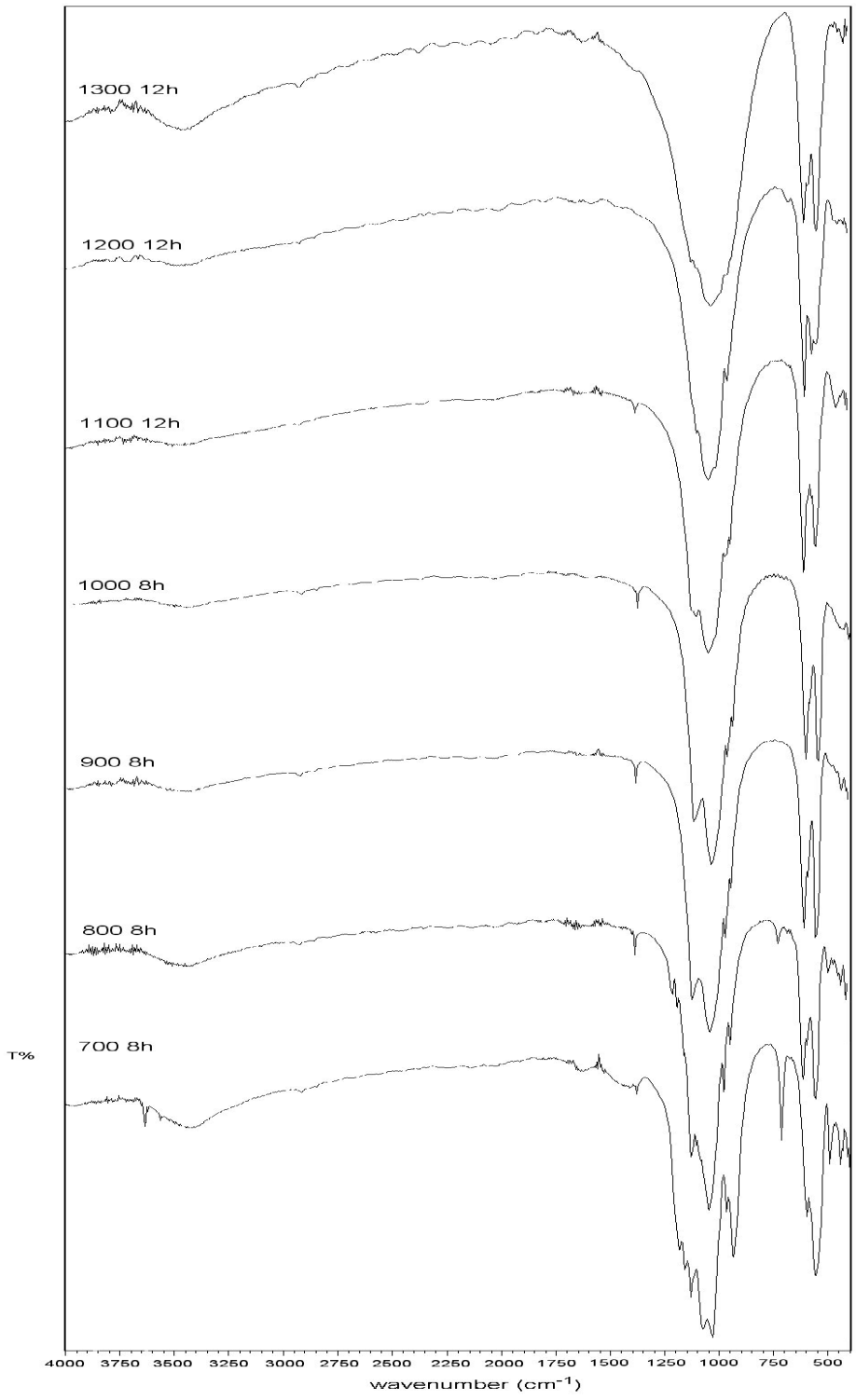


Figure 3.55 IR Spectra of the Products of the Solid-State Reactions of $Gd_2O_{3(s)}$+6$CaHPO_4.2H_2O_{(s)}$+ 2$CaCO_{3(s)}$ at 700 - 1300^oC

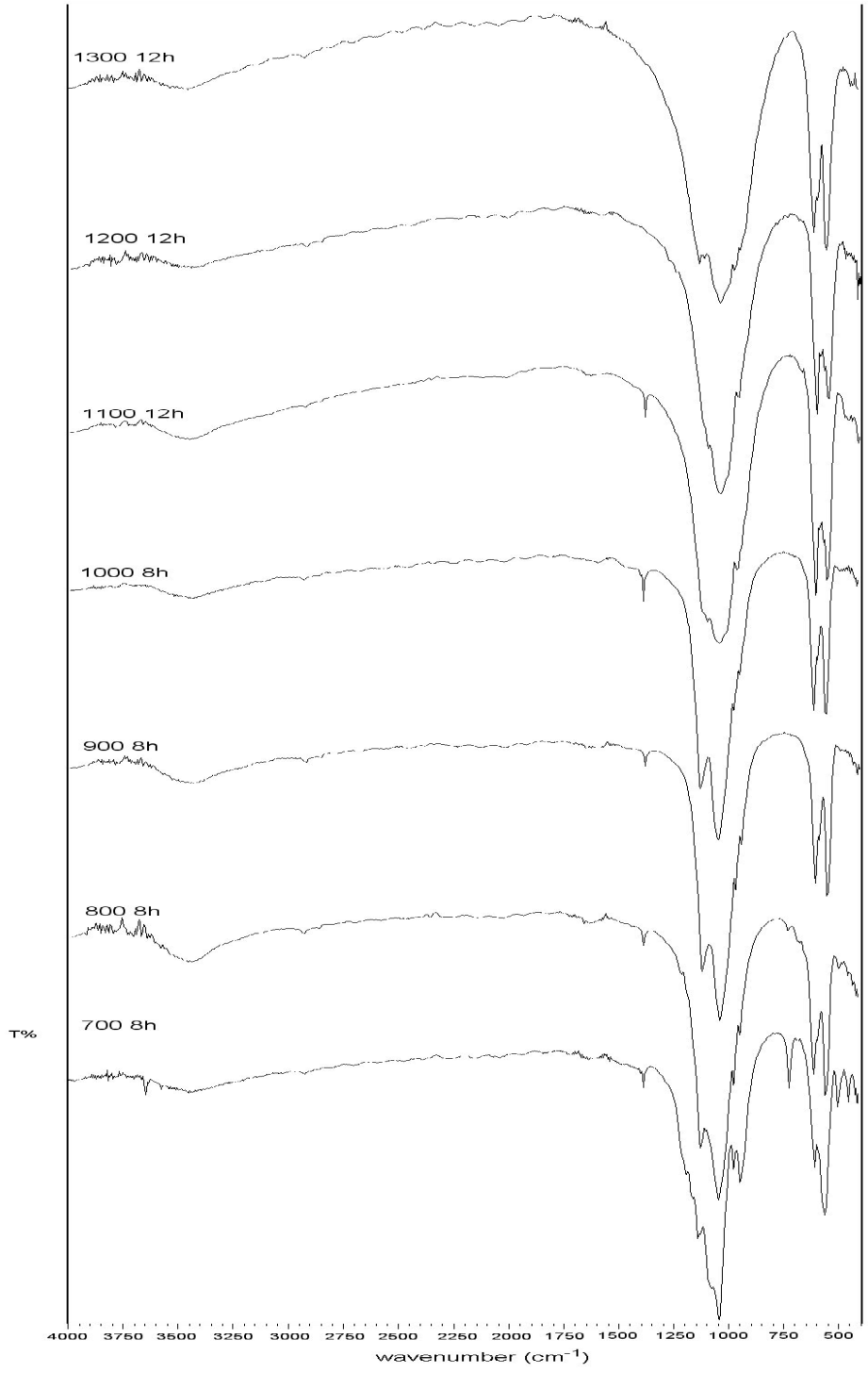


Figure 3.56 IR Spectra of the Products of the Solid-State Reactions of $Dy_2O_{3(s)}$+6$CaHPO_4.2H_2O_{(s)}$+ 2$CaCO_{3(s)}$ at 700- 1300^oC

3.16 Solid State Reactions of $2Nd_2O_3 + B_2O_3 + 2(NH_4)_2HPO_4$

In the last part of this thesis, the reactions were performed at 500-1300°C. The following equation is suggested:

$$2Nd_2O_3 + B_2O_3 + 2(NH_4)_2HPO_4 \longrightarrow 2Nd_2(BO_3)(PO_4) + 4NH_3 + 3H_2O$$

3.16.1 X-ray Powder Diffraction Study of the Products

The X-ray patterns of the products are shown in Figure 3.57 at different temperatures;

At 500 and 600°C, the lines belong to Nd_2O_3 (JCPDS Card No: 41-1089) were observed as the main product.

At 800°C, additional to the lines of Nd_2O_3 (JCPDS Card No: 41-1089), d-spacings of monazite, monoclinic $NdPO_4$ (JCPDS Card No: 78-1026) were observed.

At 900°C, the d-values of $NdPO_4$ became clear, whereas the d-values of aragonite, orthorhombic $NdBO_3$ [9] begun to appear and the lines of the starting substances substantially decreased.

At 1000°C, while the lines of Nd_2O_3 disappeared completely, the intensities of the lines of $NdBO_3$ and $NdPO_4$ began to increase.

As the temperature increased above 1100°C, only the d-values belong to aragonite, orthorhombic $NdBO_3$ [9] and monazite, monoclinic $NdPO_4$ compounds were observed.

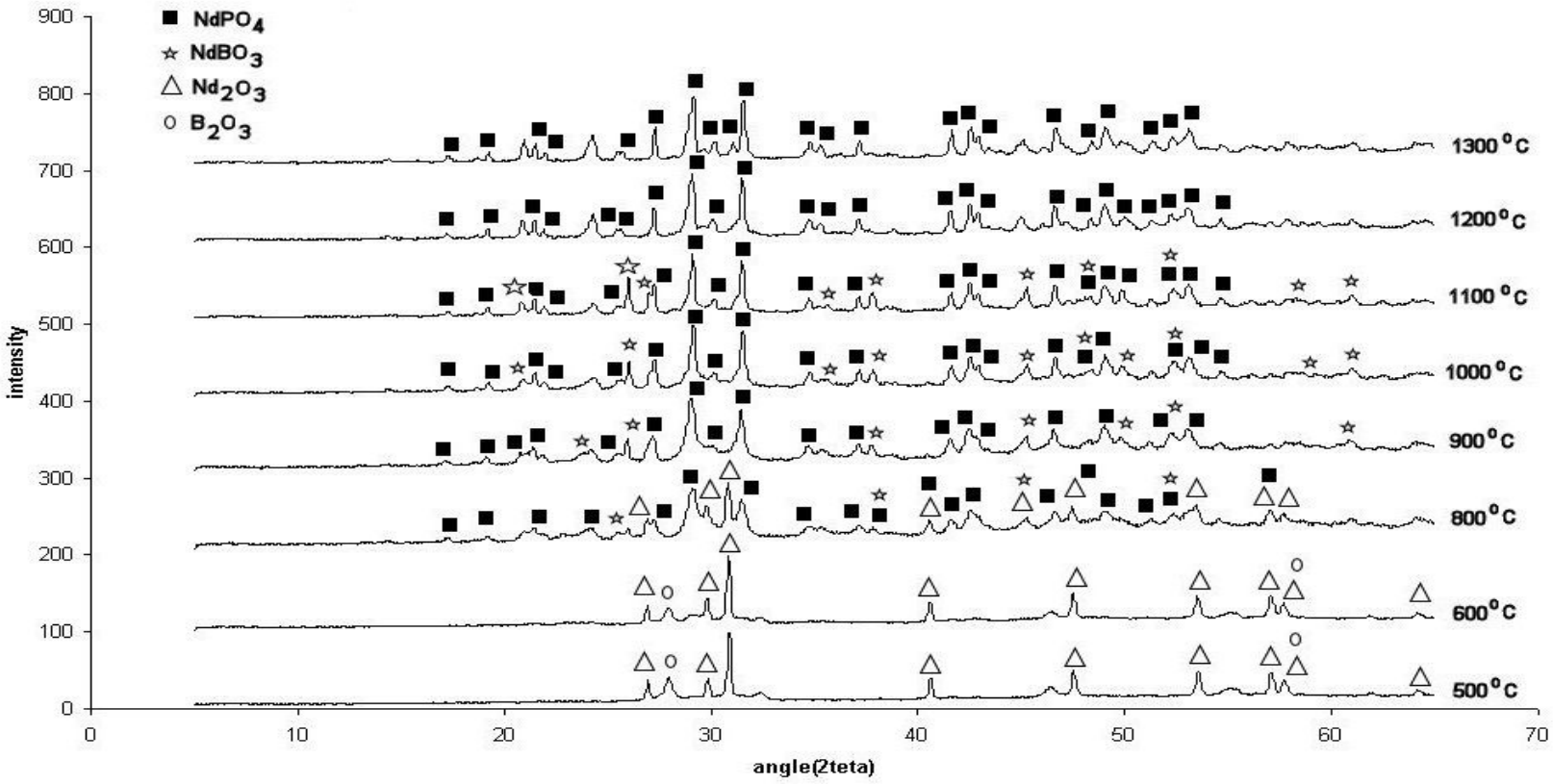


Figure 3.57 The X-ray Powder Diffraction Patterns of the Products Obtained of the Solid-State Reactions of $2Nd_2O_3 + B_2O_3 + 2(NH_4)_2HPO_4$ at 500-1300 ^oC

3.16.2 IR Spectra of the Products at Different Temperatures

The IR spectra of the products obtained at different temperatures are given in figure 3.58. Based on these data;

i) When the IR spectra of the products at low temperatures (500-600^{o}C) were analyzed, the absorption bands of Nd_2O_3 which was the starting material with the vibration bands of PO_4^{3-} anion which was obtained after the evaporation of H_2O and NH_3 gases from diammonium hydrogen phosphate compound and vibrational frequencies of N-H in ammonium and O-H in water were observed [124]. At higher temperatures (over 800^{o}C) it was observed the disappearance of N-H and O-H bands together with Nd_2O_3 bands.

ii) The infrared absorption bands of tetrahedral PO_4^{3-} anion in monazite, monoclinic $NdPO_4$ were observed over 800^{o}C. IR absorption frequencies of PO_4^{3-} units of rare earth orthophosphates were previously studied by Hezel and Ross [125]. According to the stretching frequencies of tetrahedral PO_4^{3-} anion;

ν_3 (asymmetric stretching) at 1110-1010 cm^{-1};

ν_1 (symmetric stretching) at 965 cm^{-1}

ν_4 (in-plane bending) at 635-540 cm^{-1},

ν_2 (out-of-plane bending) at 494 cm^{-1} were obtained.

iii) As it is known, boron atoms form three coordination in borates with aragonite structure [126]. Consequently, the IR bands of B-O bonds were observed especially at 100-850 cm^{-1} region. In this study, the vibrational bands of aragonite type of borates were observed at the following frequencies.

ν_3 : (asymmetric stretching) at 1307 cm^{-1}

ν_2: (out-of-plane bending) at 732 cm^{-1}

ν_4: (in-plane bending) at 670-500 cm^{-1}

ν_1: (symmetric stretching) at 950 cm^{-1} around.

The most important deformation band, ν_2 which separates aragonite borates from vaterite borates was observed as a fairly intense band at 732cm^{-1} region. This band could not be observed in vaterite, hexagonal borates [127, 128].

On the other hand, since there was no any absorption band observed around 785 cm^{-1}, it was decided that B-O-P bond was not formed.

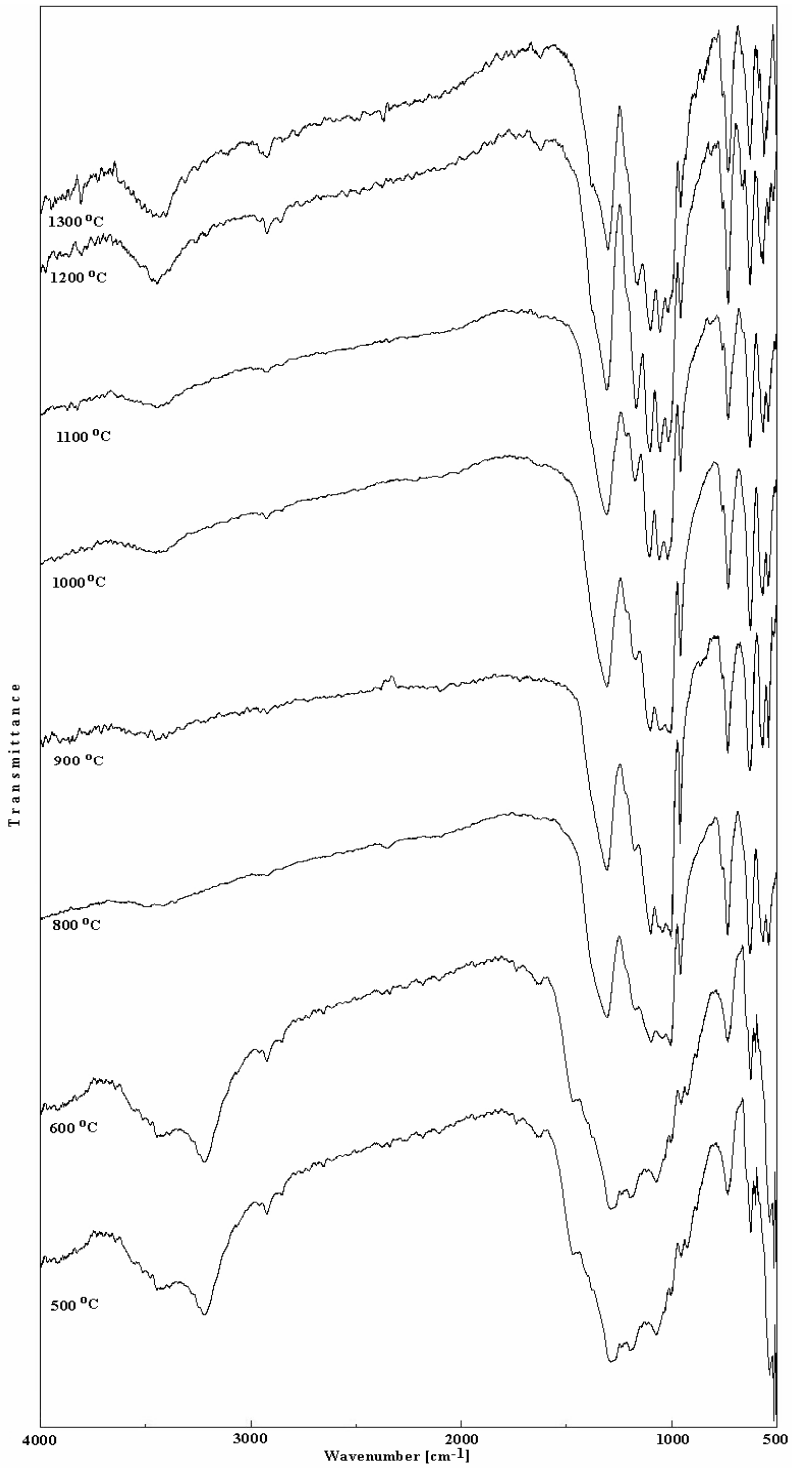


Figure 3.58 IR Spectra of the Products of the Solid-State Reactions of $2Nd_2O_3 + B_2O_3 + 2(NH_4)_2HPO_4$ at 500-1300^oC

3.17 Solid-State Reactions of $2Gd_2O_3 + B_2O_3 + 2(NH_4)_2HPO_4$

In that section, 2 moles of Gd_2O_3 were mixed with 1 mole of B_2O_3 and 2 moles of $(NH_4)_2HPO_4$ and the reactions were performed at different temperatures and reaction times, according to the following proposed reaction,

$$2Gd_2O_3 + B_2O_3 + 2(NH_4)_2HPO_4 \longrightarrow 2Gd_2(BO_3)(PO_4) + 4NH_3 + 3H_2O \quad \text{(rxn1)}$$

Characterization of the intermediate products was studied with X-ray powder diffraction and IR spectroscopy methods.

3.17.1 X-ray Powder Diffraction Study of the Products

The XRD pattern of the products prepared at different temperatures through the reaction of Gd_2O_3 with B_2O_3 and $(NH_4)_2HPO_4$ are given in figure 3.59. According to XRD patterns, the lines of Gd_2O_3 (JCPDS Card No: 12-797) were observed as the main product at low temperatures (500-600^oC).

At 800^oC, additional to the lines of Gd_2O_3, d-values of monazite, monoclinic $GdPO_4$ with low intensities [129, 130] have also been seen.

At 900^oC, while the lines of Gd_2O_3 decreased, the intensities of the lines of monazite monoclinic $GdPO_4$ increased and the existance of d-values of vaterite hexagonal $GdBO_3$ (JCPDS Card No: 74-1932) was detected.

By combining the results up to that point, the following equation could be written;

$$2Gd_2O_3 + B_2O_3 + 2(NH_4)_2HPO_4 \longrightarrow 2GdBO_3 + 2GdPO_4 + 4NH_3 + 3H_2O$$

When the XRD patterns of the products above 1000^{o}C (figure 3.59) were investigated, it was appointed that the lines of Gd_2O_3 completely disappeared but the diffraction lines of monazite (monoclinic) $GdPO_4$ and vaterite (hexagonal) $GdBO_3$ compounds become dominant. Consequently, it was found that the product composed of two components that can be formulated as $GdBO_3$.$GdPO_4$.

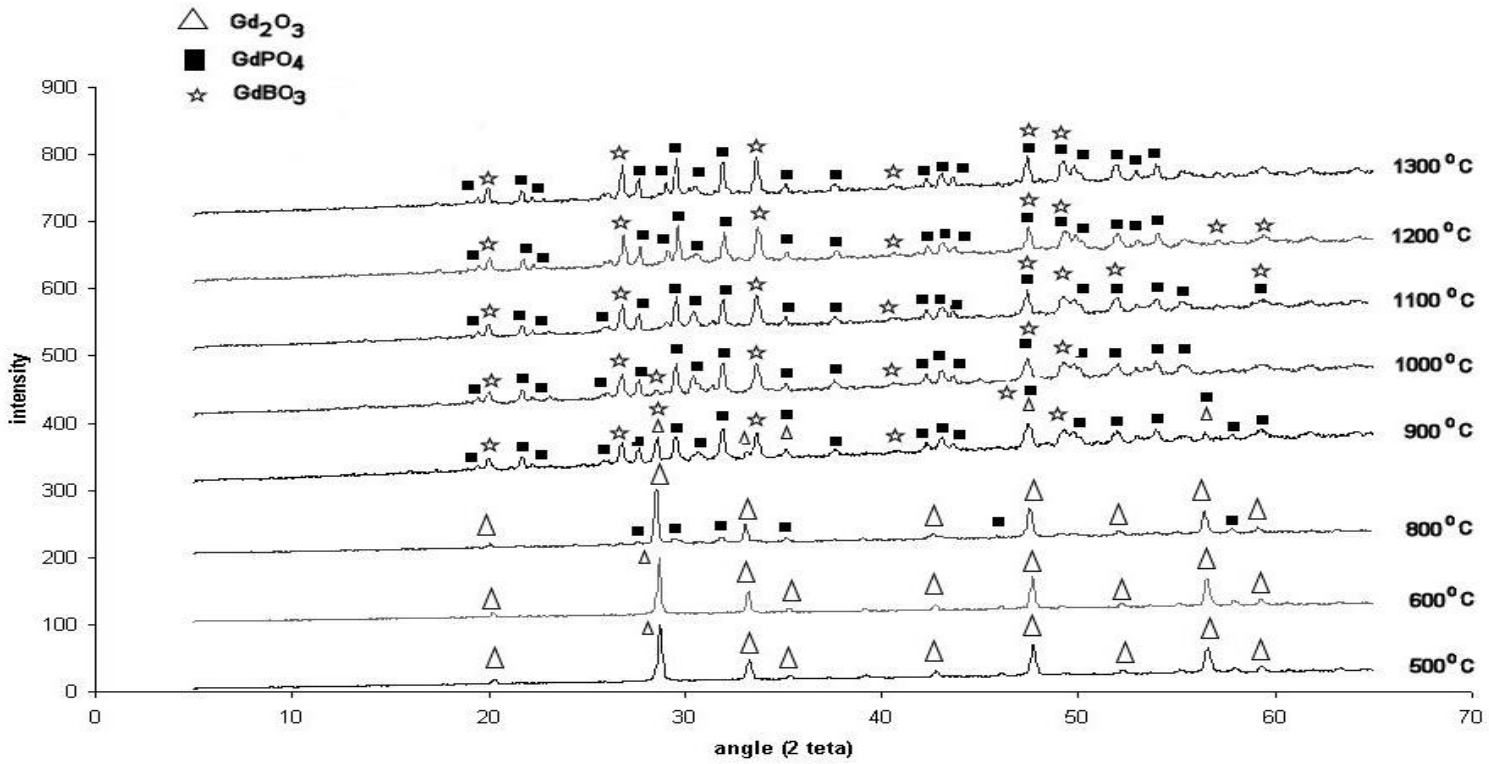


Figure 3.59 The X-ray Powder Diffraction Patterns of the Solid-State Reactions of $2Gd_2O_3 + B_2O_3 + 2(NH_4)_2HPO_4$ at 500-1300^{o}C

3.17.2 IR Spectra of the Products at Different Temperatures

IR spectra of the products obtained at different temperatures are given in figure 3.60. Accordingly, when the IR spectra of the products at low temperatures (500-600^{o}C) were analyzed, the IR absorption frequencies of Gd_2O_3 [124] which is the starting material and the vibrational bands of PO_4^{3-} anion were observed parallel to XRD data.

At 800 and 900^{o}C, while the bands of Gd_2O_3 disappeared, the vibrational bands of PO_4^{3-} units in monazite, monoclinic $GdPO_4$ [125] and the bands of isolated planar, triangle BO_3^{3-} unit in $GdBO_3$ compound were observed.

When the IR spectra of the products over 1000^{o}C were observed, there is no infrared absorption band at 1150cm^{-1}, consequently it was detected that tetrahedral B atom was not present as BO_4 units.

Moreover, it was observed that IR data of $LnBO_3$ compounds in vaterite [128] form at 1052, 1013, 910, 871, 850, 700 and 567cm^{-1} as the vibrational frequencies of B-O bonds in BO_3 units.

On the other hand, it was confirmed that the absence of B-O-P bond since any infrared absorption band could not be observed around 785-750cm^{-1}. As a result, it could be said that the triangle BO_3 and tetrahedral PO_4 units were assigned for the products obtained over 1000^{o}C. Accordingly, well-matching with the XRD results, the formula of the borophosphate compound at 1300^{o}C was determined as $GdBO_3.GdPO_4$.

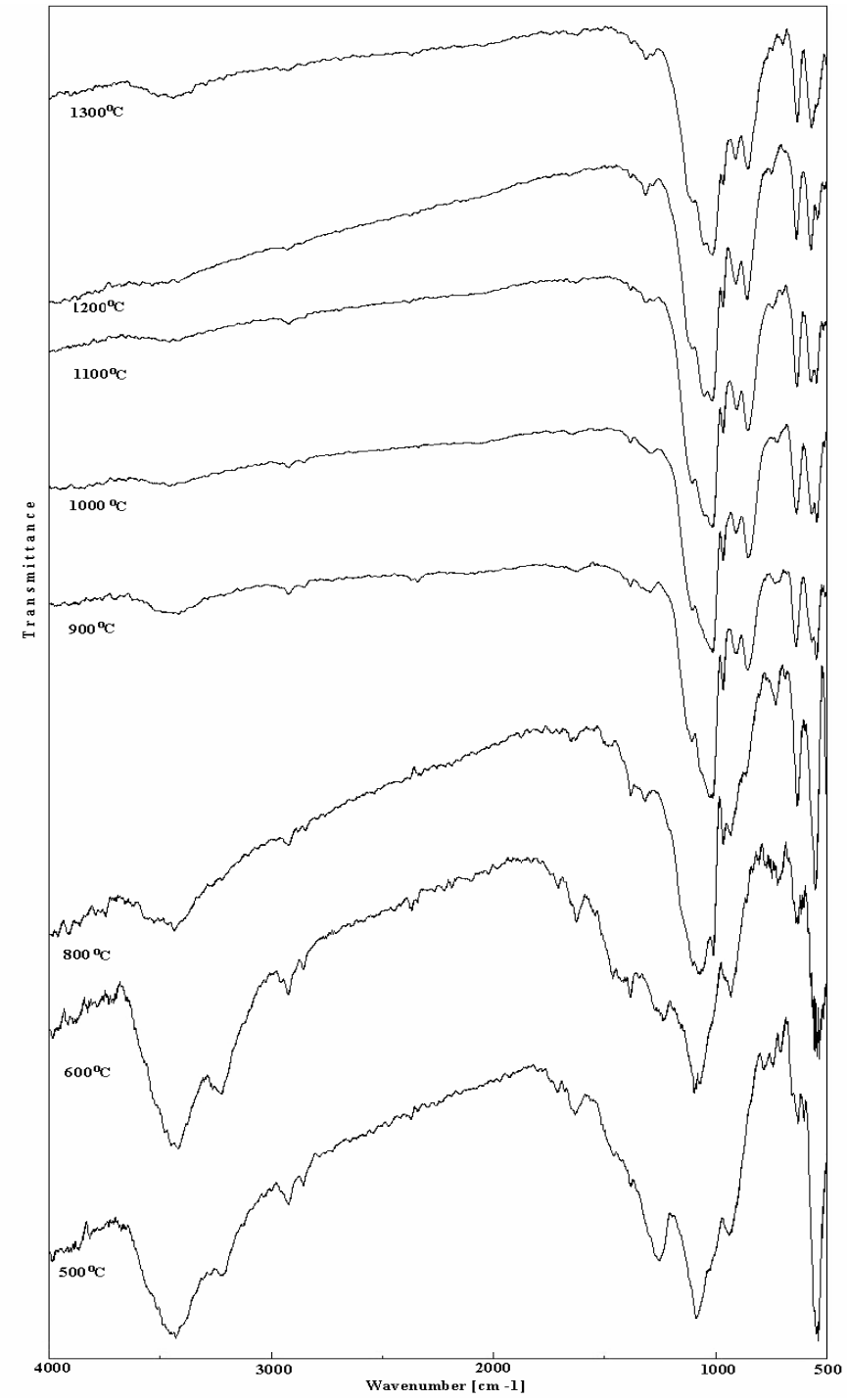


Figure 3.60 IR Spectra of the Products of the Solid-State Reactions of $2Gd_2O_3 + B_2O_3 + 2(NH_4)_2HPO_4$ at 500-1300^oC

3.18. Solid State Reactions of $2Dy_2O_3 + B_2O_3 + 2(NH_4)_2HPO_4$

In the last part of this thesis, the reactions were performed at 500-1300°C. The following equation is suggested:

$$2Dy_2O_3 + B_2O_3 + 2(NH_4)_2HPO_4 \longrightarrow 2Dy_2(BO_3)(PO_4) + 4NH_3 + 3H_2O$$

3.18.1 X-ray Powder Diffraction Study of the Products

When the X-ray powder diffraction patterns of the products (Figure 3.61) were investigated at low temperatures (500-600°C), the lines belong to Dy_2O_3 (JCPDS Card No: 21-0314) were observed as the main product.

At 800°C, additional to the lines of Dy_2O_3, the diffraction lines due to xenotime, tetragonal $DyPO_4$ [129, 130] and vaterite, hexagonal $DyBO_3$ [126] with low intensities were observed.

At 900°C, it was observed that the intensities of the lines of (figure 3:61) $DyPO_4$ and $DyBO_3$ increased whereas the intensities of lines of Dy_2O_3 decreased.

As the temperature rised to 1000, 1100, 1200°C, any diffraction line for Dy_2O_3 was not observed, only the d-values belong to vaterite hexagonal $DyBO_3$ and xenotime, tetragonal $DyPO_4$ were observed.

Consequently, it was found product composed of two components that can be formulated as $DyBO_3.DyPO_4$. The xenotime $DyPO_4$ and vaterite $DyBO_3$ components were indexed as tetragonal and hexagonal crystal system. Unit cell parameters with the h k l values are given Table 3.13 and table 3.14.

Table 3.13 X-ray Powder Diffraction Pattern of $DyPO_4$ Indexed in Tetragonal System and Unit Cell Parameters of a= 6.912, c= 6.041Å

Experimental data of xenotime (tetragonal) $DyPO_4$			JCPDS Card No: 77-1296 data xenotime (tetragonal) $DyPO_4$	
I / Io	**$d_{observed}$**	**$d_{calculated}$**	**d**	**h k l**
34	4.55	4.55	4.55	1 0 1
100	3.45	3.46	3.46	2 0 0
25	2.753	2.753	2.751	2 1 1
44	2.569	2.570	2.569	1 1 2
22	2.443	2.444	2.443	2 2 0
9	2.274	2.274	2.274	2 0 2
30	2.152	2.153	2.152	3 0 1
19	1.934	1.9336	1.933	1 0 3
48	1.770	1.7709	1.770	3 1 2
26	1.728	1.7281	1.727	4 0 0
16	1.689	1.6873	1.6870	2 1 3

Table 3.14 X-ray Powder Diffraction Pattern Indexed in Hexagonal System and Unit Cell Parameters of $DyBO_3$ given as a= 3.793, c= 8.847 Å

Experimental data of Hexagonal $DyBO_3$			JCPDS Card No: 74-1933 data hexagonal $DyBO_3$	
I / I_o	**$d_{observed}$**	**$d_{calculated}$**	**d**	**h k l**
19	4.43	4.42	4.424	0 0 2
37	3.288	3.288	3.285	1 0 0
32	3.076	3.079	3.079	1 0 1
46	2.635	2.637	2.637	1 0 2
17	1.899	1.897	1.896	1 1 0
35	1.830	1.834	1.835	1 0 4
14	1.643	1.643	1.642	2 0 0
25	1.545	1.540	1.540	2 0 2

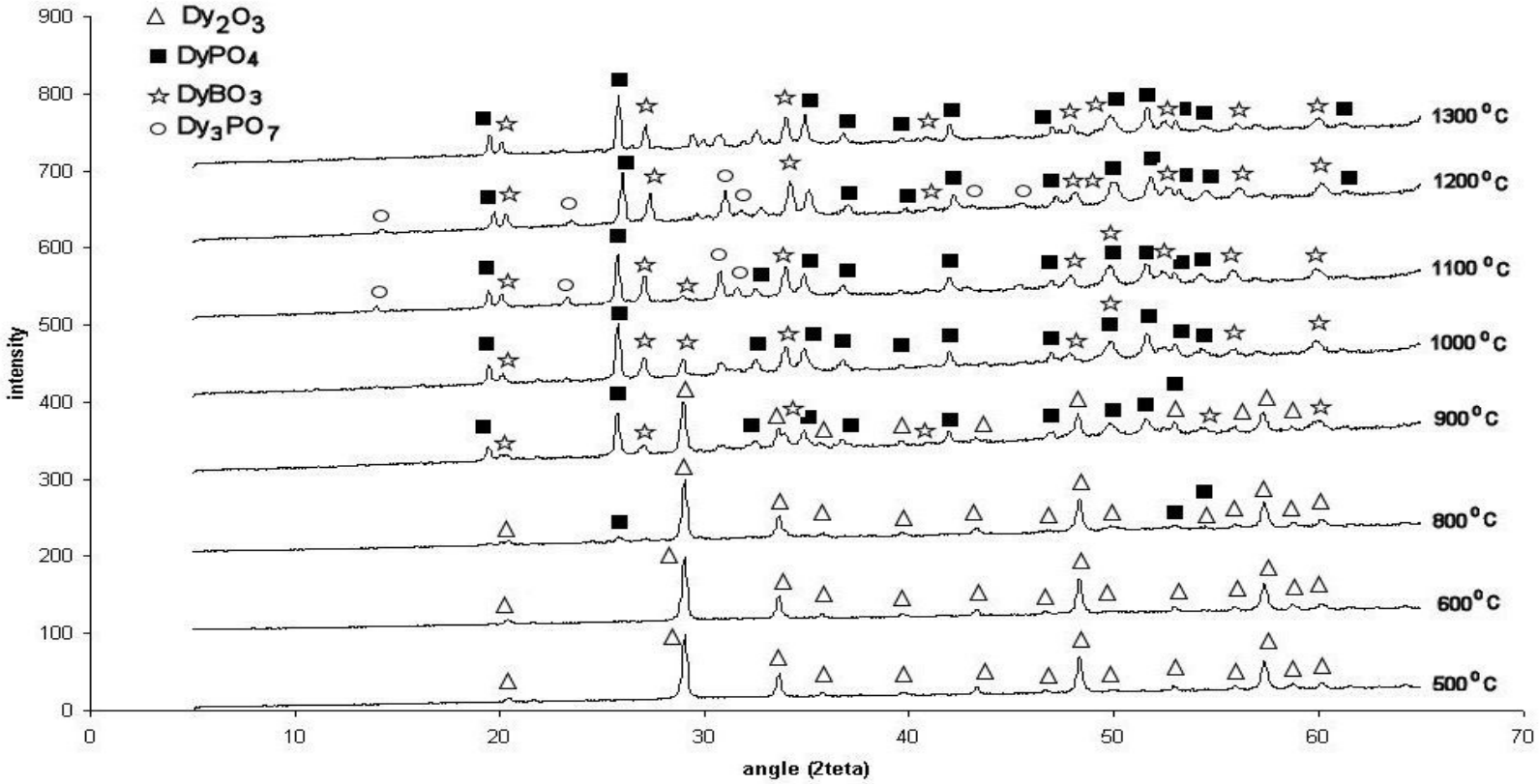


Figure 3.61 The X-ray Powder Diffraction Patterns of the Products Obtained of the Solid-State Reactions of $2Dy_2O_3 + B_2O_3 + 2(NH_4)_2HPO_4$ at 500-1300^oC

3.18.2 IR Spectra of the Products at Different Temperatures

The Infrared spectra of the products obtained at different temperatures are given in figure 3.62. When the infrared spectra of the products prepared at low temperatures were investigated, the vibration bands due to Dy_2O_3 [124] and PO_4^{3-} anion were assigned, as the temperature increased (800-900^oC), the disappearance of the bands of Dy_2O_3 was detected.

When the IR spectra of the products obtained over 1000^oC were analyzed, the bands for B-O bonds in vaterite hexagonal $DyBO_3$ which is composed of planar BO_3 units [126] and for P-O bonds in xenotime tetragonal structure of $DyPO_4$ which is composed of tetrahedral PO_4 units were observed. The frequencies and assignments for these absorption bands as;

ν_3: (asymmetric stretching) at 1025 cm^{-1}

ν_2: (out-of-plane bending) at 495 cm^{-1}

ν_4: (in-plane bending) at 643-521cm^{-1}

ν_1: (symmetric stretching) at 950 cm^{-1} were determined [131].

Therefore, similar to gadolinium and neodymium materials, it was determined that the product composed of two components that can be formulated as $DyBO_3$.$DyPO_4$ as a result of investigation of IR and XRD data.

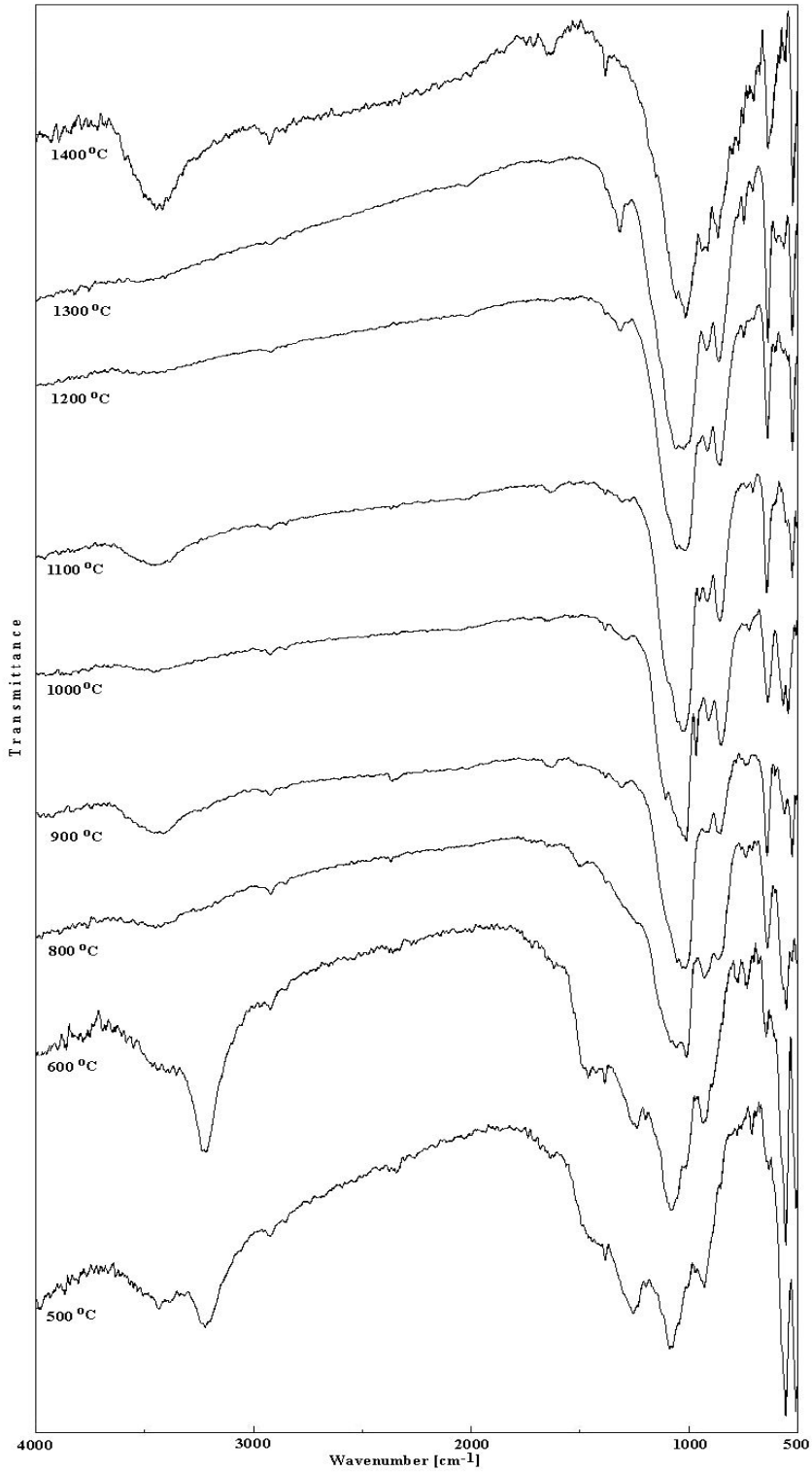


Figure 3.62 IR Spectra of the Products of the Solid-State Reactions of $2Dy_2O_3$ + B_2O_3 + $2(NH_4)_2HPO_4$ at 500-1400^oC

3.19 Thermal Studies of the Products

Thermogravimetric-differential (TG / DTA) thermal analysis curves of the product of neodymium borate phosphate at 1200^{o}C are given at figure 3.63. According to this figure, when the DTA curves were examined, an endothermic curve was observed around 200^{o}C due to the result of the absorption of moisture of the products.

Since any variation was not observed for IR and XRD data, it was assumed that the structure was recognized and re-crystallized because of the detection of an endothermic DTA curve at 1045^{o}C.

The endothermic DTA curve at 1430^{o}C indicated that the melting point of gadolinium phosphate compound in the mixed material. Since the melting of $GdBO_3$ is at 1580^{o}C [132], it could not be possible to observe in that range.

In gadolinium and dysprosium compounds, similar thermal analysis curves were obtained for mixed material (figure 3.64 and figure 3.65).

According to TG curves of those three materials, it was detected that the masses of these products increase by increasing temperature. However the reason has not been found yet.

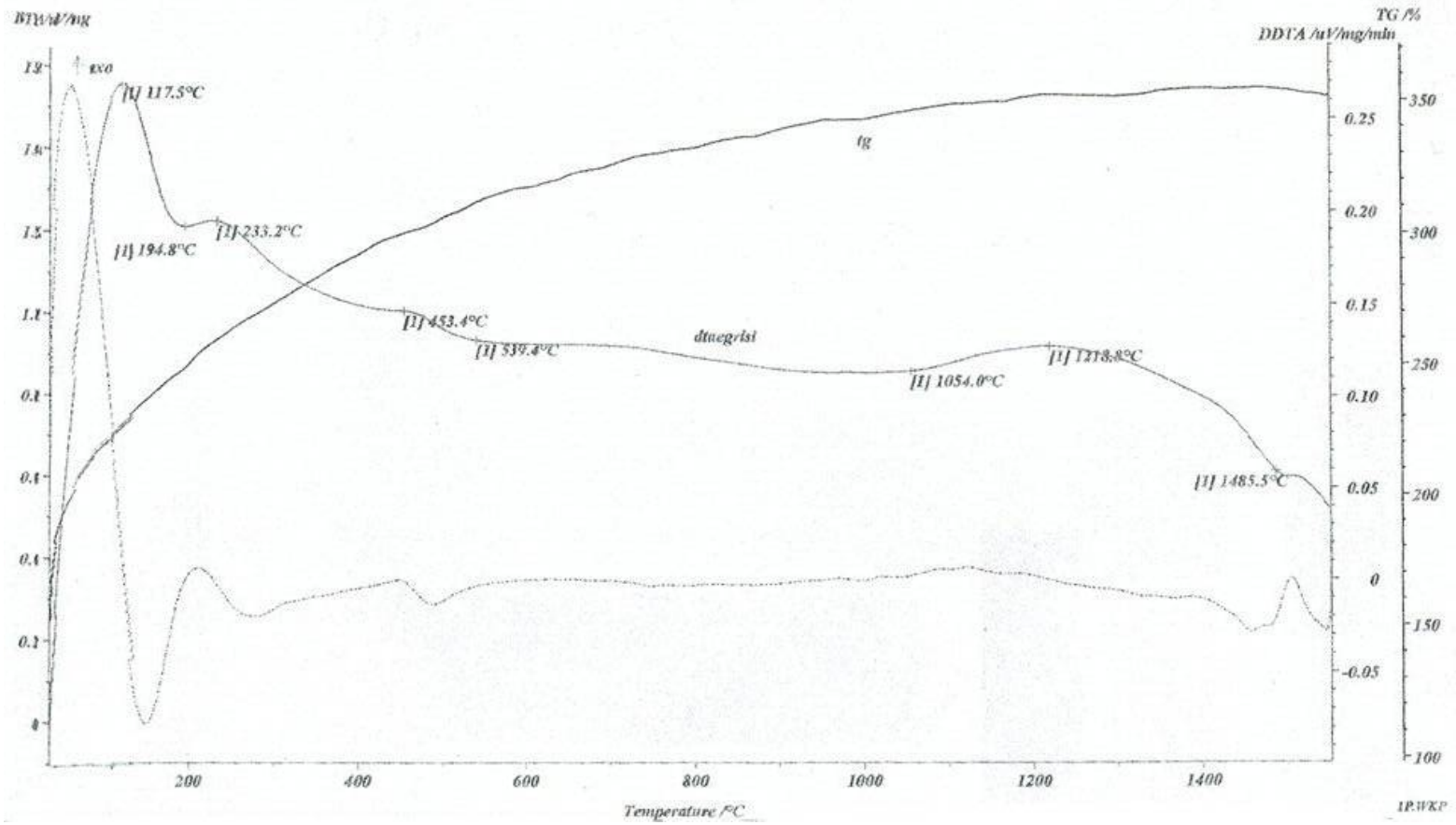


Figure 3.63 DTA-TG (Thermal Analysis) Curve of the Solid-State Reactions of $2Nd_2O_3 + B_2O_3 + 2(NH_4)_2HPO_4$ at 1200^{o}C

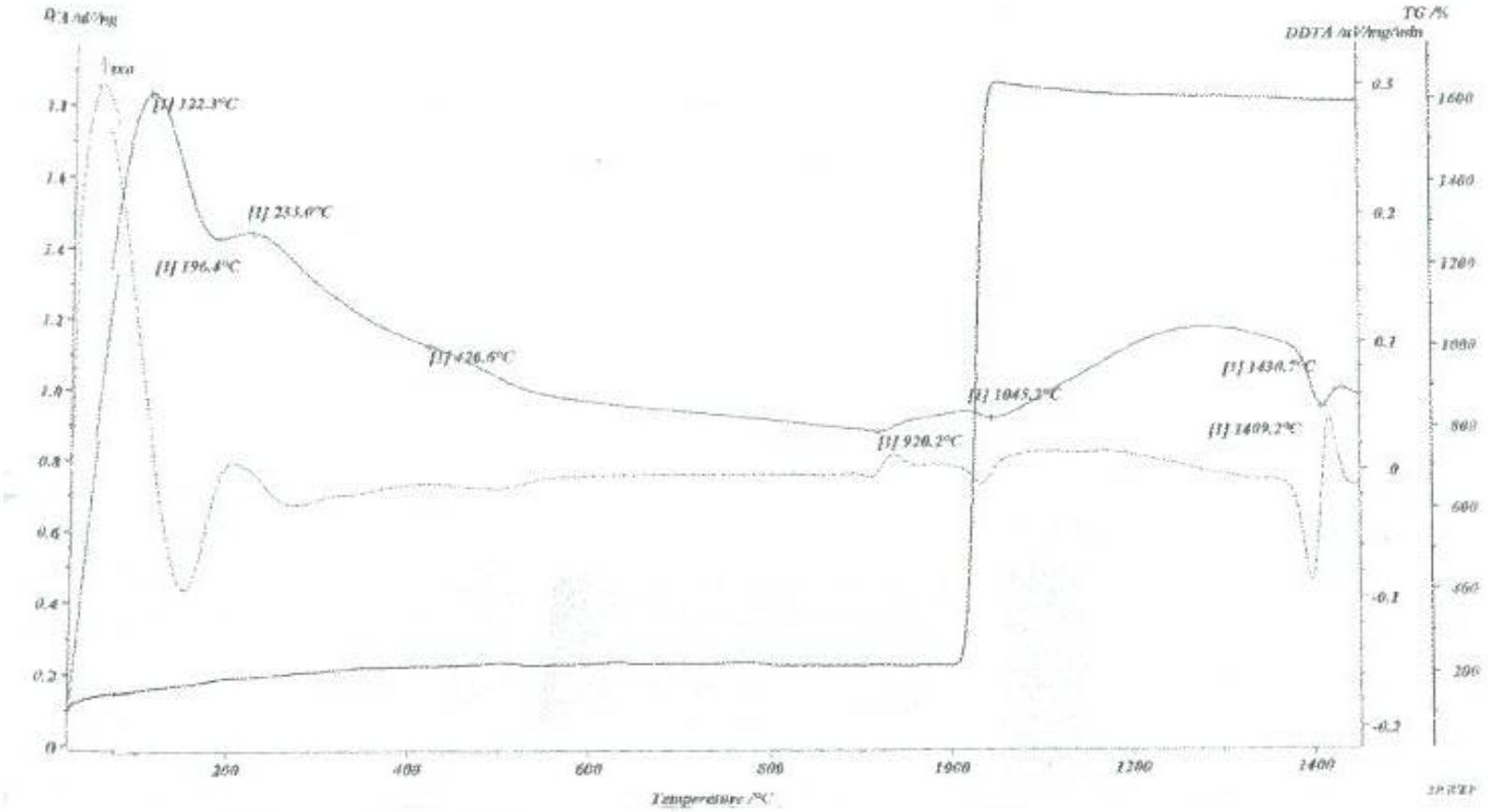


Figure 3.64 DTA-TG (Thermal Analysis) Curve of the Solid-State Reactions of $2Gd_2O_3 + B_2O_3 + 2(NH_4)_2HPO_4$ at 1200^{o}C

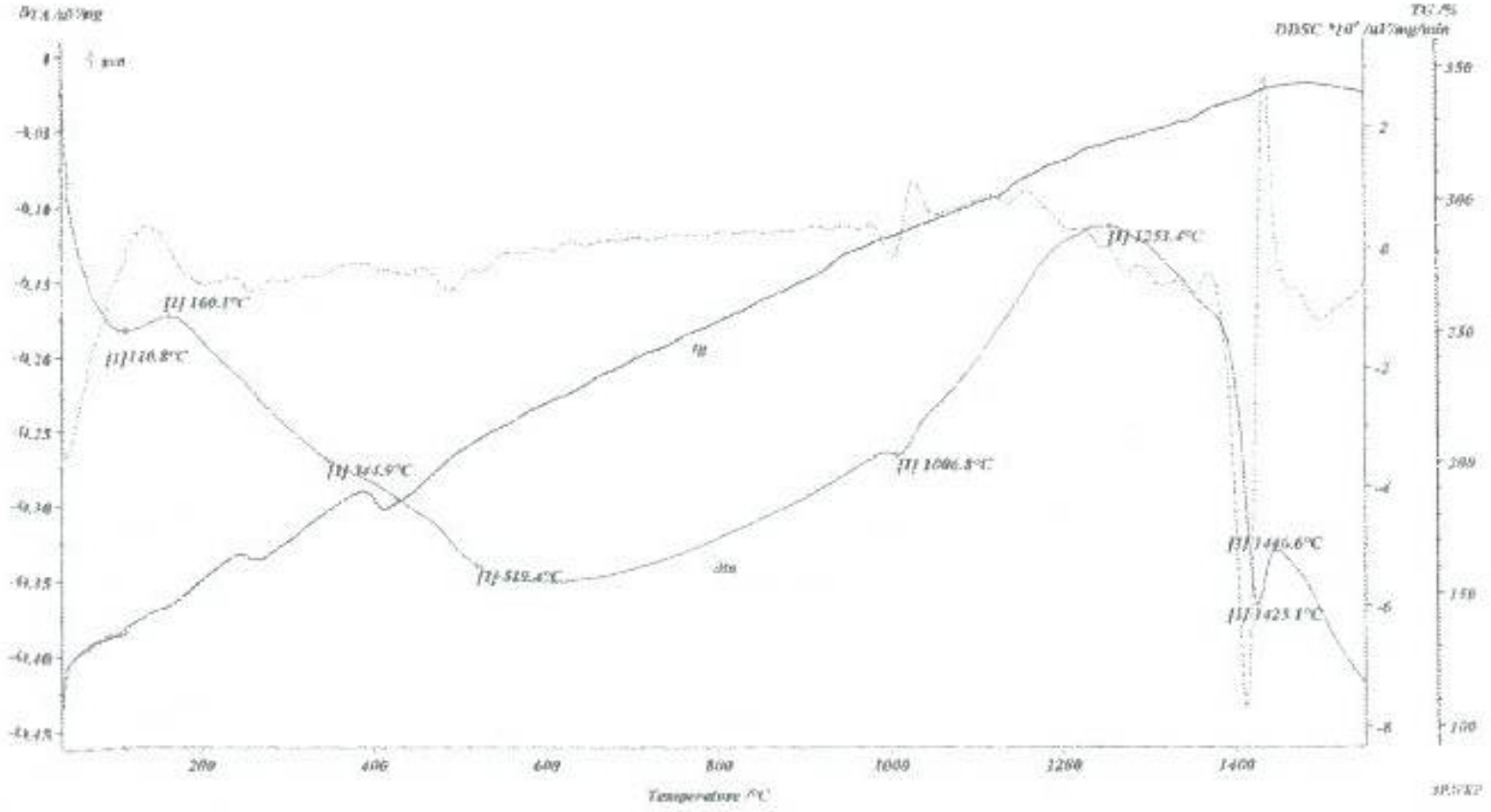


Figure 3.65 DTA-TG (Thermal Analysis) Curve of the Solid-State Reactions of $2Gd_2O_3 + B_2O_3 + 2(NH_4)_2HPO_4$ at 1200°C

CHAPTER 4

GENERAL REVIEW AND CONCLUSION

The aim of this work was to synthesize some new magnesium transition metal borates, lithium rare earth oxyphosphates, lithium sodium rare earth oxyphosphates, calcium rare earth oxyapatites and rare earth borates phosphates which were not reported previously. For this purpose various solid state reactions were performed. Investigation of the XRD and IR data and theoretical attempts to obtain the structural data such as Miller indices, unit cell parameters and spectra-structural correlation led to the following conclusions.

1) Novel magnesium transition metal orthoborate compounds, formulated as $MgNi_2(BO_3)_2$, $MgCo_2(BO_3)_2$, $Mg_2Ni(BO_3)_2$ and $Mg_2Co(BO_3)_2$ were synthesized through the following reactions;

$$2Ni(NO_3)_2\,6.H_2O_{(s)} + MgO_{(s)} + 2H_3BO_{3(s)} \rightarrow \mathbf{MgNi_2(BO_3)_{2(s)}} + 4NO_{2(g)} + 15H_2O_{(g)} + O_{2(g)}$$

$$2Co(NO_3)_2\,6.H_2O_{(s)} + MgO_{(s)} + 2H_3BO_{3(s)} \rightarrow \mathbf{MgCo_2(BO_3)_{2(s)}} + 4NO_{2(g)} + 15H_2O_{(g)} + O_{2(g)}$$

$$Ni(NO_3)_2.6H_2O_{(s)} + 2MgO_{(s)} + 2H_3BO_{3(s)} \rightarrow \mathbf{Mg_2Ni(BO_3)_{2(s)}} + 2NO_{2(g)} + 9H_2O_{(g)} + 1/2\,O_{2(g)}$$

$$Co(NO_3)_2.6H_2O_{(s)} + 2MgO_{(s)} + 2H_3BO_{3(s)} \rightarrow \mathbf{Mg_2Co(BO_3)_{2(s)}} + 2NO_{2(g)} + 9H_2O_{(g)} + 1/2O_{2(g)}$$

Indexing of the XRD data of the products obtained from the above reactions showed that $MgNi_2(BO_3)_2$, $MgCo_2(BO_3)_2$, $Mg_2Ni(BO_3)_2$ and $Mg_2Co(BO_3)_2$ crystallizes in the orthorhombic system with the refined unit cell parameters of a= 5.393(9), b= 8.350(2), c= 4.462(3); a= 5.442(2), b= 8.428(0), c= 4.517(4); a= 5.398(9), b= 8.400(4), c= 4.490(7); a= 5.423(2), b= 8.425(9), c= 4.509(4)Å respectively, and space group P*nmn*. It was found that the crystal system is isostructural with the compounds of $M_3(BO_3)_2$ (M: Mg, Co and Ni) in kotoite structure which were reported by Effenberger [50]. The TG-DTA curves indicate that there is no weight loss and endothermic or exothermic peak from 20 to 1000^oC. It could be concluded that these compounds are thermodynamically stable within these ranges.

2) The oxyphosphates, Na_2NdOPO_4, Na_2GdOPO_4, Na_2DyOPO_4 were synthesized previously from different solid state reactions [86]. In this part of this thesis, the lithium rare earth oxyphosphates, Li_2LnOPO_4 (Ln: Nd, Gd and Dy) were prepared at 1000^oC from the following solid state reactions;

$$Ln_2O_{3(s)} + 2Li_2CO_{3(s)} + 2(NH_4)_2HPO_4(s) \rightarrow \mathbf{2Li_2LnOPO_{4(s)}} + 4NH_{3(g)} + 2CO_{2(g)} + 3H_2O_{(g)}$$

The indexing of the data showed that Li_2NdOPO_4, Li_2GdOPO_4, Li_2DyOPO_4 crystallizes in the orthorhombic system with the refined unit cell parameters of a=14.865(1), b=10.734(2), c=13.231(1); a=14.686(3), b=10.634(5) c=13.047(9); a=14.554(1), b=10.589(8), c= 12.926(2) Å respectively.

3) In the fourth part of the present study, lithium sodium rare earth oxyphosphates $LiNaLnOPO_4$ (Ln: Nd, Gd and Dy) which were not reported before, were prepared through the following solid state reaction at 1000°C.

$$Ln_2O_{3(s)} + Li_2CO_{3(s)} + Na_2CO_{3(s)} + 2(NH_4)_2HPO_{4(s)} \rightarrow \mathbf{2LiNaLnOPO_{4(s)}} + 2CO_{2(g)} + 4NH_{3(g)} + 3H_2O_{(g)}$$

Investigations of the X-ray, IR, DTA and theoretical attempts indicated that $LiNaNdOPO_4$, $LiNaGdOPO_4$, $LiNaDyOPO_4$, have orthorhombic crystal structure with the refined unit cell parameters a=14.903(8), b=10.861(3), c=13.247(1); a =14.745(0), b=10.651(6), c=13.096(8); a= 4.622(2), b=10.581(0), c= 13.018(2) Å respectively.

Examination of these parameters showed that these oxyphosphates were isomorphous with the orthorhombic Li_2LnOPO_4 (Ln: Nd, Gd, Dy) prepared in this work and also Na_2LnOPO_4 (Ln: Nd, Gd, Dy) reported previously [86, 99, 100].

In the DTA curve it is found that Li_2LnOPO_4 and $LiNaLnOPO_4$ (Ln: Nd, Gd, Dy) compounds are stable up to 1100°C however these products decompose into $LnPO_4$ and some unidentified phosphates at around 1100°C.

As a result it is also seen that the refined cell parameters of these oxyphosphates decrease from the neodymium compound to dysprosium oxyphosphate as expected according to lanthanide contraction.

4) The oxyapatites, $Ca_8Ln_2(PO_4)_6O_2$ (Ln: Nd, Gd, Dy) were reported previously through the solid state reactions of Ln_2O_3 with $(NH_4)_2HPO_4$, $CaCO_3$ using 1:6:8 molar ratio at 1100°C for 35 and 40 hours [119]. In the last part of this study,

$Ca_8Ln_2(PO_4)_6O_2$ (Ln: Nd, Gd, Dy) were attempted to prepare by using different solid state reactions of Ln_2O_3 with $CaHPO_4$ and $CaCO_3$ using 1:6:2 molar ratio at different temperatures performing short reaction period of time. The following conclusions were done;

a) It was observed that the oxyapatite compounds of three rare earth metal (Ln: Nd, Gd, Dy) which are formulated with $Ca_8Ln_2(PO_4)_6O_2$ were not obtained as a single phase.

b) in neodymium compound, hexagonal $Ca_8Nd_2(PO_4)_6O_2$, monoclinic $NdPO_4$, and hexagonal β-$Ca_3(PO_4)_2$,

c) in gadolinium compound, hexagonal $Ca_8Gd_2(PO_4)_6O_2$, cubic $Ca_3Gd(PO_4)_3$, and hexagonal β-$Ca_3(PO_4)_2$,

d) in dysprosium compound, $Ca_8Dy_2(PO_4)_6O_2$, hexagonal β-$Ca_3(PO_4)_2$ were observed.

5) In this study, in order to form borophosphate compounds of rare earth metals $Ln_2(BO_3)(PO_4)$ (Ln: Nd, Gd and Dy) through the solid state reactions of Ln_2O_3, B_2O_3 and $(NH_4)_2HPO_4$ studied at 2:1:2 mol ratio at different temperatures and reaction periods. The products were analyzed with XRD, IR and thermal analysis (TG/DTA).

According to studies, by examining XRD data, IR and DTA, the following results were obtained:

a) Examining the XRD data, it was decided that the boratephosphate compounds of the three rare earth metals which can be formulated with $LnBO_3.LnPO_4$, were obtained as mixed phase materials.

b) The IR data of the products showed that tetrahedral PO_4 contains P-O bonds, planar triangle BO_3 contains B-O bonds but there was not B-O-P bond formation.

c) Differential Thermal Analysis indicates that there is no weight loss and exothermic or endothermic peak from 20 to 1450^{o}C was observed.

REFERENCES

1. Muetterties, E.L. 1967. The Chemistry of Boron and Its Compounds *John Wiley Pub., Newyork.*

2. Kıstler R., Helvacı C., Boron and Borates. kisi.deu.edu.tr/cahit helvacı/ boron

3. Kılıç, A.M., 2004. Importance of Boron Mine for Turkey and Place in the Future. *Proceedings of the 2nd International Boron Symposium, Eskişehir*, (23-25 September 2004) p. 34.

4. Ullmann's Encyclopedia of Industrial Chemistry, 2002. *Sixth Edition, WILEY-VCH, Boron Compounds.*

5. Anonymous1.WEB, 2007.http://www.webelements.com/webelements/ elements/text/B

6. Heller, G., 1986. A Survey of Structural Types of Borates and Polyborates Chemistry and Material Science. Vol 131, 39-98.

7. Evans, R.C. 1964. Introduction to Crystal Chemistry. *Cambridge University Press.*

8. Goldschmidt, V.M., and Hauptmann, H. 1931-1932. Isomorphie Von Boraten und Karbonaten.*Nachr. Ges. Wiss. Gott. Math. Phys. KI.*, 53-72.

9. Levin, E.M., Roth, R.S., and Martin, J.B. 1961. Polymorphism of ABO_3 Type Rare Earth Borates. *Am. Mineral*. 46: 9-10, 1030-1055.

10. Weidelt, J., and Bambauer, H.U. 1968**.** Cerium borate isostructural with aragonite. *Naturwissenschaften*. 55 (7): 342.

11. Abdullaev G.K., Dzhafarov G.G., Mamedov Kh.C., 1976. Azerbaidzhanskii Khim. Zh., 3, 117-120.

12. Bohlhoff, R., Bambauer, H.U., and Hoffman, W.1971. *Z. Kristallogr.* 133: 386.

13. Goryunova A., 2003, Üniversitat zu Köln, Beitrag zur Kristallchemie und Kristallsynthese binaer Seltenerdborate vom Typ SEB3O6 und SEBO3. *PhD. Thesis.*

14. Nakatsuka A., Ohtaka O., Arima H., Nakayama N., Mizota T., 2006. Aragonite-type lanthanum orthoborate, $LaBO_3$. *Acta Cryst*. E62, i103-i105.

15. Corbel G., Leblanc M., Antic-Fidancev E., Lemaitre-Blaise M., Krupa J.C.,1999. Luminescence analysis and subsequent revision of the crystal structure oftriclinic L- $EuBO_3$. *J. Alloys Comp*., 287, 71-78.

16. Palkina K. K., Kuznetsov V. G., Butman L. A., Dzhurinskii B. F., 1976 *2Russ. J. Coord. Chem.,* 2, 286-289.

17. Huppertz H., 2001. Multianvil High-Pressure Synthesis and Crystal Structure of b-$YbBO_3$. *Z. Naturforsch.,* 56 b, 697–703.

18. Emme H., Huppertz H., 2004. High pressure synthesis of υ-$DyBO_3$.*Acta Cryst.*, C60, i117-i119.

19. Noirault S., Joubert O., Caldes M.T., Piffard Y., 2006. High-temperature form of neodymium orthoborate, $NdBO_3$. *Acta Cryst.,* E62, i228-i230.

20. Chaminade, J.P., Garcia, A., Pouchard, M., and Fouassier, C.1990. Crystal growth and characterization of $InBO_3$: Tb^{3+} . *J. Crystal Growth*, 99: 799-804.

21. Cox, J., and Keszler, D.A.1994. $InBO_3$. *Acta Crystallogr. Sect.*, C50: 1857-1859.

22. Biedl, A., Frondel, C., and Ito, J. 1966. New type of ferric iron tourmaline. *Amer. Mineral*. 51, 1501-1505.

23. Meyer H.J., Skokan A., 1971. Ytterbiumborat mit Calcit-Struktur. *Naturwissenschaften,* 58, 566.

24. Tukia M., Hölsa J., Lastusaari M., Niittykoski J., 2005. Eu^{+} doped rare earth orthoborates, RBO_3 (R= Y, La and Gd), obtained by combustion synthesis. *Optical Materials*, 27, 1516-1522.

25. Felten E.J., 1961. Preparation and properties of some rare earth borates. *Journal of Inorganic Nuclear Chemistry,* 19, 61-64.

26. Henkels A.E., Schaak R.E., 2008. Syntheses of nanocrystalline $REBO_3$ (RE= Y, Nd, Sm, Eu, Gd, Ho) and YBO_3: Eu using a borohydride-based solution precursor route. *J. Solid State Chem.,* 181, 3264-3268.

27. Iwai, M., Kobayeshi, T., Furaya, H., Wari, Y., Sasaki, T., 1997. Crystal growth and optical characterization of rare-earth (Re) calcium oxyborate $ReCa_4O(BO_3)_3$ (Re = Y or Gd) as new nonlinear optical material . *Jan. J. Appl. Phys.*, 36:3A, L276-L279.

28. Zhang, Y., Chen, X.L., Liang, J.K., Cao, Y.G., Xu, T.2001. Phase relations in the system La_2O_3–CaO–B_2O_3. *J. Alloys Comp.*, 315: 198-202.

29. Zhang, Y., Chen, X.L., Liang, J.K., Xu, T. 2002. Synthesis and structural study of new rare earth sodium borates $Na_3Ln(BO_3)_2$ (Ln=Y, Gd). *J. Alloys Comp*., 333: 72-75.

30. Zhang, Y., Chen, X.L., Liang, J.K. 2001. Phase relations in the $MgO–Ga_2O_3–B_2O_3$ system and the crystal structure of $MgGaBO_4$. *J. Alloys Comp*., 319: 247-252

31. He, M., Chen, X.L., Lan. Y.C., Li, H. 2001. Ab Initio Structure Determination of New Compound $LiAlB_2O_5$. *J. Solid State Chem.*, 156: 181-184.

32. Mascetti, J., Vlasse, M., Fouessier, C.1981. The crystal chemistry of the new rare-earth sodium borates $Na_3Ln(BO_3)_2$(Ln = La, Nd). *J. Solid State Chem.*, 39: 288-293.

33. Weir, C.E., Lippincott, E.R.1961. Infrared studies of aragonite, calcite, and vaterite type structures in the borates, carbonates, and nitrates. *J. Res. NBS.*, 65A: 173.

34. Hart, P.B. and Smallwood S.E.F, 1962. An examination of the Infra-red spectra of borate Anions**.** *J. Inorg. Nucl. Chem* Vol: 24, 1047-1056.

35. Takeuchi, Y., 1952. The crystal structure of magnesium pyroborate. Acta Crystallogr. 5, 574-581.

36. Mrose, m.E., Fleischer M., 1963. The probable identity of magnioborite with suanite. Am. Mineral. 48, 915-924.

37. Öztaş, N.A., and Erdoğan, H., 2009. Syntheses and Characterization of Magnesium Pyroborate by Solution Combustion and Conventional Ceramic Methods: A Comparative Study. *Z. Annorg. Allg. Chem.*, 635, 1626-1632.

38. Rulmont A., and Almou M., 1989. Vibrational Spectra of Metaborates with Infinite Chain Structure. *Spectrochimica Acta* Vol:45A, No: 5, 603-610.

39. Herzberg G. 1949. Molecular Spectra and Molecular Structure II. Infrared and Raman Spectra of Polyatomic Molecules, Van Nostrand , *New York.*

40. Watanabe, T., Kato, A., Matsumato, T., and Ito, J., 1963. Jimboite $Mn(BO_3)_2$, a new mineral from the Kaso mine, Tochigi Prefecture, *Japan. Proc. Jpn. Acad.* 39, 170-175.

41. Suknev, V.S. 1969. Infrared Spectra of High-Temperature Borates Containing Simple Radicals. *J.Applied Spectroscopy*. Vol:11, No:6, 1531-1535.

42. Pardo, J., Martinez-Ripoll, M., and Blanco-Garcia, S.,1974. The Crystal Structure of Nickel Orthoborate, $Ni_3(BO_3)_2$, *Acta Crystallogr. Sect. B.*, Vol 30, 37-40.

43. Tekin, B., Güler, H., 2008. Synthesis and Crystal Structure of Dicobalt Nickel Orthoborate, $Co_2Ni(BO_3)_2$. *Materials Chemistry and Physics,* Vol 108, Issue 1, 88-91.

44. Güler, H., Tekin, B.,2009. Synthesis and Crystal Structure $CoNi_2(BO_3)_2$. *Inorg. Materials* Vol 45, No 5, 538-542.

45. Waugh, L.T., 1968. *Structural Chemistry and Molecular Biology,*Vol 1, 731-749.

46. Weir, C.E and Schroeder, R.A., 1964. *J.Res. Natl. Bur. Stand.* 68A, 465-487.

47. Götz, W., 1963. Raumgruppenbestimmung des Nickelborates $Ni_3(BO_3)_2$ *Naturwissenschaften*, 50, 567.

48. Berger, S.V. 1949. The Crystal Structure of the Isomorphous Orthoborates of Cobalt and Magnesium, *Acta Chem. Scand*. 3, 660-675.

49. Bandareva O.S., Simanov, M.A., Belov, N.B., 1978. The Crystal Structure of Synthetic Jimbolite, $Mn_3(BO_3)_2$, *Sov. Phys. Crystallogr*., Vol 23, 272-273.

50. Effenberger, H. and Perttlik, F**.,** 1984. Verfeinerung der Kristallstrukturen der Isotypen Verbindungen $M_3(BO_3)_2$ mit M= Mg, Co and Ni (Strukturtyp:Kotoit), *Z. Kristallogr.*, vol.66, 129-140.

51. Pompetzki M., Albert B., 2004. Ein ionenleitendes Natriumnickelborat, $Na_2Ni_2B_{12}O_{21}$, mit offener Kanalstruktur, *Z. Anorg. Allg. Chem.* 630, 2550.

52. Hofmann, K. A., Höschele, K., 1914. Das Magnesiumchlorid als Mineralisator, miteinem Beitrag zur Spektrochemie der ktrochemie der seltenen Erden. Berichte *d. D. Chem. Gesellschaft* 47, 238-247.

53. Sadanaga, R., Nishimura, T., and Watanabe, T., 1965. The Structure of Jimbolite, $Mn(BO_3)_2$ and Relationship With The Structure of Kotoite . *Mineral J.* 4, 380-388.

54. Richter L., Müller, F., 1980. Zur Strucktur Von $Sr_3B_2O_6$. *Z. Anorg. Allg. Chem*, 467, 123-125.

55. Smith, R.W., Keszler, D.A., 1989. Syntheses an Crystal Structures of the α and β forms of the Orthoborate $Sr_2Cu(BO_3)_2$. *J. of Solid State Chem.* 81, 305-313.

56. Smith, R.W., Keszler, D.A., 1991. Sythesis, Structure and Properties of the Orthoborate $SrCu_2(BO_3)_2$. *J. of Solid State Chem.* 93, 430-435.

57. Smith, R.W., Keszler, D.A., 1990. Structure of $Ba_2Cu(BO_3)_2$. *Acta Cryst.C* 46: 370-372.

58. Verstegen, J.M.P.J., 1974. The Luminescence of Tb^{2+} in Borates of the Composition $X_2Z(BO_3)_2$. *J. Electrochim. Soc.* 121, 1631.

59. Pabst, A., 1974. Synthesis, Properties and Structure of $K_2Co(CO_3)_2$ Buetschliite. *Amer. Mineral.* Vol 59, 353-358.

60. Milton C., Axelrod. J., 1947. Fused wood-ash stones: Fairchildite (n.s.p) $K_2CO_3.CaCO_3$, buetschliite.(n.s.p) $3K_2CO_3.2CaCO_3.6H_2O$ and calcite, $CaCO_3$, their essential constituents. *Am. Mineral.* 32, 607-624.

61. Akella, A., Keszler, D.A., 1995. Structure and Eu^{2+} luminescence of dibarium magnesium orthoborate. *Mater. Research Bull.* 30, 105.

62. Akella, A., Keszler, D.A., 1995. *Main Group Metal. Chem.,* 18, 35.

63. Sarkar S., Schaffers K.I., Keszler D. A, unpublished results.

64. Diaz A., Keszler D.A., 1997. Eu^{2+} Luminescence in the Borates $X_2Z(BO_3)_2$. *Chem. Mater.,* 9, 2071-2077.

65. Ying, S., Jingkui, Li., and Zhang, H., Quanlin, L., et al.1998. Crystal Structure and Thermal Decomposition Studies of Barium Borophosphates, $BaBPO_5$. *J. of Solid State Chem*., 135: 43-51.

66. Levesseur, A., Olazcuaga, R., Kbala, M., Zahir, M., Hagenmuller, P., and Couzi, M. 1981. Etudes electrique et Raman des verres des systemes B_2O_3---M_2O---M_3PO_4 (M=Li, Na). *Solid State Ionics.* 2: 205-213.

67. Ramamoorthy, P., Rockett, T.J.1974. Phase Relations in the System $CaO-B_2O_3-P_2O_5$ at 900°C . *J. American Ceramic Society.* 57: 501-502.

68. Bauer, H. 1965. Über eine Reihe isotyper Erdalkaliboratphosphate und -arsenate vom Typus 2 $MeO{\cdot}X_2O_5{\cdot}B_2O_3$.*Zeitschrift für Anorganishe und Allgemeine Chemie*, 337: 183-190.

69. Bauer, H.1966. Über eine Reihe isotyper Erdalkaliboratphosphate und -arsenate vom Typus $2MeO \cdot X_2O_5 \cdot B_2O_3$. II. Die Verbindungen $2BaO \cdot P_2O_5B_2O_3$ und $2BaO \cdot As_2O_5 \cdot B_2O_3$. *Zeitschrift für Anorganishe und Allgemeine Chemie*, 345: 225-229.

70. Kniep R., Gözel, G., Eisenmann ,B., Röhr, C., Asbrand, M., Kızılyallı, M. 1994. Borophosphates - A Neglected Class of Compounds: Crystal Structures of $M^{II}[BPO_5]$ (M^{II}: Ca, Sr) and $Ba_3[BP_3O_{12}]$. *Angew. Chem. Int. Ed. Engl*., 33(7): 749.

71. Gözel, G.1993. Preparation and Structural Investigation of Alkaline-Earth Borophosphates, *Ph.D. Thesis*, METU, Ankara.

72. Baykal, A., Kızılyallı, M., Gozel, G., Toprak, M., Kniep, R. 2000. Synthesis of Strontium Borophosphate, $SrBPO_5$ by Solid State and Hydrothermal Methods and Characterization . *Cry. Res. Technol.,* 35(3): 247-254.

73. Baykal, A., Gozel, G., Kızılyallı, M., Toprak, M., Kniep, R. 2000. X-ray Powder Diffraction and IR Study Of Calcium Borophosphate, $CaBPO_5$. *Turk. J. Chem.,* 24: 381-388.

74. Pushcharovsky D.Y., Gobetchia E.R., Pasero M., Merlino S., Dimitrova O.V. 2002. Hydrothermal Synthesis and Crystal Structures of Li, Ba-nanoborate, $LiBaB_9O_{15}$, and Ba-borophosphate, $BaBPO_5$. *J. Alloys and Compounds*, 339: 70-75.

75. Pan S., Wu, Y., Fu, P., Zhang, G., Wang,G., Guan, X., Chen, C. 2002. The Growth of $BaBPO_5$ Crystals from $Li_4P_2O_7$. Flux . *J. Crystal Growth*, 236: 613-616.

76. Liebertz, J., and Stähr, S. 1982. Zur Tieftemperaturphase von BaB_2O_4. *Zeitschrift* K*ristallographie,* 160,135.

77. Bluhm, K., and Park, C.H. 1997. Synthesis and Crystal Structure of the Borate-Phosphate: α-$Zn_3(BO_3)(PO_4)$. *Zeitschrift für Naturforschung*, 52b: 102.

78. Wang, G., Wu, Y., Fu, P., Liang, X., Xu, L., Chen, C. 2002. Crystal growth and properties of β-Zn_3BPO_7. *Chem. Mater.,* 14: 2044-2047.

79. Yılmaz, A., Bu, X., Kızılyallı, M., Kniep, R., et al. 2001. Cobalt Borate Phosphate $Co_3[BPO_7]$, Synthesis and Characterization. *J.of Solid State Chem.,* 156 (2): 281-285.

80. Hauf, C., Friedrich, T., Kniep, R., 1995. Crystal structure of pentasodium catena-(diborato-triphosphate), $Na_5[B_2P_3O_{13}]$. *Z. Kristallogr*. 210(6): 446.

81. Bontchev, R.P., Sevov, S.C. 1996. $Co_5BP_3O_{14}$: The First Borophosphate with Planar BO_3 Groups Connected to PO_4 Tetrahedra. *Inorg. Chem*. 35, 6910-6911.

82. Bluhm, K., and Park, C.H.1995. Synthesis and Crystal Structure of Trilead-Diphosphato-Borate-Phosphate, a Compound with a $1/(infinity)((PO_4)_2BPO_4)_6$ Anion. *Zeitschrift für Naturforschung*, B 50 (11): 1617-1622.

83. Kniep, R**.,** Schafer, G., Engelhandt, H. 1999. $K[ZnBP_2O_8]$ and $A[ZnBP_2O_8]$ ($A=NH_4^+$, Rb^+, Cs^+): Zincoborophosphates as a New Class of Compounds with Tetrahedral Framework Structures**.** *Angew. Chem. Int. Ed.* 38 (24), 3641-3644.

84. Shi, Y., Liang, J., Zhang, Hao., et.al.1997. X-ray Powder Diffraction and Vibrational Spectra Studies of Rare Earth Borophosphates, $Ln_7O_6(BO_3)(PO_4)_2$ Ln= La, Nd, Gd and Dy). *Journal of Solid State Chem.* 129, 45-52.

85. Ma, H.W., Liang J.K., et.al.2004.Ab inito structure determination of new compound $Ba(BO_3)(PO_4)$. J.of Solid State Chem. 177, 3454-3459.

86. The detail references can be found in M.S. Thesis of Demirözü S. 2003

87. Gopal, R., Calvo, C., 1972. Crystal structure of βVPO_5. *J. Solid State Chem*. 5, 432.

88. R'Kho, C., Vanderborre, M.T., et.al.1986. Spectroscopic study of colloidal $VOPO_4 \cdot 2H_2O$. *J. Solid State Chem*. 63, 202-215.

89. Serra, D.L., Hwu, S., 1992. *J. Acta Crystal*. C28, 733-735.

90. Kierkegaard, P., Longo, J. M., 1970. A Refinement of the Crystal Structure of $MoOPO_4$. *Acta Chemica Scandinavica*, 24, 427-432.

91. Levin, E., M, Roth, R.S., 1970. The system niobium pentoxide-phosphorus pentoxide. *J. Solid State Chem*, 2, 250.

92. Kinomura, N., Hirose, M., Kumada, N., Muto, F., 1988. Preparation of a new tungsten(V) phosphate and its polymorph. *J. Solid State Chem*. 77, 156-161.

93. Piffard, Y., Oyetola, S., Verbaere, A., Tournoux, M., 1986. Synthesis, thermal stability, and crystal structure of antimony(V) phosphate SbOPO4. *J. Solid State Chem*. 63, 81-85.

94. Masse, R., Grenier, J.C., 1971. *Bull. Soc. Fr. Miner. Crystallogr*. 94, 437-439.

95. Nagornyi, P.G., Kapshuk, A.A., Stus N.v., et.al.1991. *Zh. Neorg. Khim*. 36 (11) 2766-2768.

96. Thomas, P.A., Glazer, A.M., Watts, B.E., 1990. Crystal structure and nonlinear optical properties of $KSnOPO_4$ and their comparison with $KTiOPO_4$. *Acta Crystallogr*. B.46, 333-343.

97. Lii, K.H., Li, C.H., Chen, T.M., 1991. Z. Kristallogr. 197 (1-2) , 67-73.

98. Benhamada, L., Grandin, A., Borel, M., et.al. 1992. C.R. Acad Sci. Ser II, 314(6), 585-589.

99. Uztetik-Amour and Kızılyallı M. 1995. Solid-State Synthesis, X-ray Powder Diffraction and IR Data of Na_2GdOPO_4. *J. Solid State Chem*.120, 275-278.

100. Gönen Z.S., Kızılyallı, M., Pamuk H.Ö., 2000. Synthesis and Characterization of Na_2GdOPO_4 and Na_2LaOPO_4. *Journal of Alloys and Compounds*, 303-304, 416-420.

101. Seyyidoğlu S., Özenbaş, M., and Yılmaz , A., 2008. Investigation of Solid State Synthesis and Characterization of Novel Sodium Rare-Earth Oxyphosphates. *Turk J. Chem.*, 32: 35-54.

102. Robertson, J.G, Fletcher, J.M.S, Skakle, A.R., 1994. Synthesis of $LiTiPO_5$ and $LiTiAsO_5$ with the α-Fe_2PO_5 Structure. *J. Solid State Chem*, 109, 53.

103. Nagornoy G., Kapshuck A.A., Stuss N.V., Slobodyani N.S., 1989. Zh, Neorg. Khim. 34, 3030.

104. Schindler, M., Joswing, W., Baur W.H., 1997. The Hydrothermal $NH_4/V/P/H_2O$ and $K/V/P/N(C_2H_5)_3/H_2O$ Systems at 473 K and the Crystal Structures of $NH_4VOPO_4$and $(NH_4)_3V_2O_3(VO)(PO_4)_2(HPO_4)$. *J. Solid State Chem* 134, 286.

105. Phillips, M.L.F., Harrison W.T., Stucky G.D., 1990. Influence of electronic configuration on the structure and optical properties of potassium tin oxide phosphate. *Inorg. Chem.*, 29, 3245.

106. Essehli, R., El Bali. B., Ehrenberg, H., et al. 2009. $Co_{0.5}TiOPO_4$: Crystal Structure, magnetic and electrochemical properties. *Material Research Bulletin*, 44, 817-821.

107. Manoun, B., Jazouli, A.El, Gravereau, P., Chaminade, J.P. 2005. Rietveld refinement of the solid solution $Li_{(1-2x)}Ni_xTiO(PO_4)$ ($0 \leq x \leq 0.50$). *Material Research Bulletin*, 40, 229-238.

108. Benmokhtar S., Jazouli A. El., Chamide, J.P., et.al. 2006. Synhesis, structure, magnetic susceptibility and Mössbauer and raman spectroscopies of the new oxyphosphate $Fe_{0.5}TiO(PO_4)$. *J. Solid State Chem.* 179, 3709-3717.

109. Benmokhtar S., Jazouli A. El., Krimi, S., Chamide, J.P., et.al. 2007. Synhesis, structure, refinement and characterization of a new oxyphosphate $Mg_{0.5}TiO(PO_4)$. *Material Research Bulletin* 42, 892-903.

110. Gravereau, P., Benmokhtar S., Chamide, J.P, Jazouli A. El., et.al. 2007. Jahn – Teller phase transition in $Cu_{0.5}TiO(PO_4)$: Powder structural charactrization of the β- variety and thermal study. *Solid State Science.* 9, 258-266.

111. Benmokhtar S., Belmal, H., Jazouli A. El., Chamide, J.P, et.al., 2007. Synhesis, structure, and physicochemical investigations of the new α- $Cu_{0.5}TiO(PO_4)$ oxyphosphate. *J. Solid State Chem.* 180, 772-779.

112. Elliot J.C., Wilson R.M., and Dowker SEP, 2002. Apatite Structures. JCPDS-International Centre for Diffraction Data, Advances in X-ray Analysis Vol.45, 172-181.

113. Elliot J.C., 1994. Structure and Chemistry of the Apatites and Other Calcium Orthophosphates, Elsevier, Amsterdam.

114. Naray- Szabo St., 1930. *Zeit. Krist.*, 75, 387-398.

115. Mehmel M., 1930. *Z. Kristallogr.*, 75, 323-331.

116. Mobasherpour I., Soulati Heshajin M., et.al. 2007. Synthesis of nanocrystalline hydroxyapatite by using precipitation method. *J of Alloys and Compounds* 430, 330-333.

117. Morgan H., Wilson R.M., et.al. 2000. Preparation and characterization of monoclinic hydroxyapatite and its precipitated carbonate apatite intermediate. *Biomaterials*, 21, 617- 627.

118. Legeros R.Z.,1991. Calcium Phosphates in Oral Biology and Medicine. Monographs in Oral Sciences. Vol 15 Myers H (ed). Basel: Karger.

119. Escobar M.E., and Baran J. E.,1982. Kristallographische Daten und Schwingungsspektren einiger Oxoapatite der Seltenen Erden des Typs $Ca_8Ln_2(PO_4)_6O_2$. *Monatshefte für Chemie* 113, 43-48.

120. Mikou M., et.al., 1985. *Ann. Chim.*, 10, 645.

121. Benmoussa H., Mikou M., and Lacout J.L., 1999. Synthesis and Physicochemical Study of New Rare-Earth Containing Vanadocalcic Oxyapatites. *Materials Research Bulletin* Vol: 34, No:9 1429-1434.

122. Teterskii, A.V., Stefanovich S.Yu.,and Turova N.Ya. 2006. Sol-Gel Synthesis of Oxygen-Ion Conductors Based on Apatite- Structure Silicates and Silicophosphates. *Inorganic Materials* Vol:42, No:3, 294-302.

123. E. Wu, " POWD, An Interactive Program For Powder Diffraction Data Interpretation and Indexing, Ver. 2.2", J. Appl. Cryst. 22, 506 (1989).

124. Ross S.D. 1972. Inorganic IR and Raman Spectra. McGraw Hill, London.

125. Hezel A and Ross S.D., 1966. Forbidden transitions in the infra-red spectra of tetrahedral anions—III. Spectra-structure correlations in perchlorates, sulphates and phosphates of the formula MXO_4 . *Spectrochimica Acta*, 22, 1949.

126. Chadeyron G., El-Ghozzi M., Mahiou R., Arbus A., 1997. Revised Structure of the Orthoborate YBO_3. *J. Solid State Chem.*,128, 261-266.

127. Denning J.H. and Ross S.D. 1972. The vibrational spectra and structures of some rare-earth borates. *Spectrochim. Acta* A28, 1775.

128. Lemanceau S., Bertrand-Chadeyron G., et al., 1999. Synthesis and Characterization of H-*Ln*BO_3 Orthoborates (*Ln*=La, Nd, Sm, and Eu). *J. Solid State Chem.,* 148, 229-285.

129. Kızılyallı M., 1973. The Chemistry and Structure of Rare Earth Phosphates, *Ph.D.Thesis,* London University.

130. Kızılyallı M., and Welch A. J.E., 1976. Crystal data for lanthanide orthophosphates. *J. Appl. Cryst.* 9, 413.

131. Kijkowska R., Cholewka E., Duszak B., 2003. X-ray diffraction and Ir-absorption characteristics of lanthanide orthophosphates obtained by crystallisation from phosphoric acid solution. *J. Mater. Sci.,* 38, 223-228.

132. Cohen-Adad M.Th., Aloui-Lebbou O., et al. 2000. Gadolinium and Yttrium Borates: Thermal Behavior and Structural Considerations. *J. Solid State Chem.,*154, 204-213.

CIRRICULUM VITAE

Name	**:** Sevim Demirözü ŞENOL
Permanent Address	**:** Abant İzzet Baysal University, Science & Arts Faculty, Department of Chemistry, TR-14280, Bolu, TURKEY
Degree and date to be conferred	**:** M.Sc., 2003
Place-Date of Birth	**:** Üsküdar, 11.04.1976
Secondory education	**:** Kadıköy İntaş High School, İstanbul, 1993

Collegiate institutions attended	**Dates**	**Degree**	**Date of degree**
Abant İzzet Baysal University	1995-1999	B.Sc.	June, 1999
Abant İzzet Baysal University	2000-2003	M.Sc.	February, 2003
Abant İzzet Baysal University	2004-2010	Ph.D.	August, 2010

Publications:

1. A. Uztetik Morkan, I. Morkan, S. Demirözü-Senol, and H. Güler, "Intermediate products in solid-state reactions of gadolinium oxide and ammonium dihydrogen phosphate", Cryst. Res. Technol. 42, 1007-1013, 2007.

Communications to national scientific meetings

1. "Na_2DyOPO_4 Bileşiğinin Sentezi Ve Karakterizasyonu" S. Demirözü, A. Uztetik-Morkan, İ. Morkan, M. Kızılyallı, XV. Ulusal Kimya Kongresi, Boğaziçi Üniversitesi- İstanbul, 4-7 Eylül 2001.

2. "Nd_2O_3'ın Na_2HPO_4 İle Katı Hal Reaksiyonlarının XRD, IR Ve Termal Analiz Yöntemleriyle İncelenmesi" S. Demirözü , A. Uztetik-Morkan, İ. Morkan, M. Kızılyallı, XVI. Ulusal Kimya Kongresi, Selçuk Üniversitesi- Konya, 10-13 Eylül 2002.

3. "Disprosyum Oksitin Disodyum Hidrojenfosfat İle Katı Hal IR ve DTA Yöntemleriyle İncelenmesi", S. Demirözü , A. Uztetik-Morkan, İ. Morkan, M. Kızılyallı, XVII. Ulusal Kimya Kongresi, İstanbul Üniversitesi- İstanbul,7-10 Eylül 2003.

4. "Katı Hal Yöntemleriyle Bazı Lantanit Borfosfatların Sentezi ve Karakterizasyonu", S. Demirözü Senol, G. Özen Kahveci, A. Uztetik Morkan, XIX. Ulusal Kimya Kongresi, Kuşadası, 30 Eylül-4 Ekim, 2005.

5. "$NaDyP_2O_7.5H_2O$ Bileşiğinin Hazırlanması, XRD, IR Ve Termal Yöntemlerle İncelenmesi" G. Özen Kahveci, S. Demirözü Senol, A. Uztetik Morkan, XX. Ulusal Kimya Kongresi, Erciyes Üniversitesi-Kayseri, 4-8 Eylül, 2006.

6. "Neodmiyum Borfosfat Bileşiğinin Katı Hal Yöntemiyle Hazırlanması ve XRD, IR ile Karakterizasyonu", S. Demirözü Senol, G. Özen Kahveci, A. Uztetik Morkan, XX. Ulusal Kimya Kongresi, Erciyes Üniversitesi-Kayseri, 4-8 Eylül, 2006.

7. "Bazı Yeni Lantanit Metalleri Borfosfatlarının Katı-Hal Yöntemiyle Sentezi Ve Karakterizasyonu" G. Özen Kahveci, S. Demirözü Senol, A. Uztetik Morkan, 23. Ulusal Kimya Kongresi, Cumhuriyet Üniversitesi-Sivas, 16-20 Haziran 2009.

8. "Sodyum Erbiyum Pirofosfat'ın Sentezi ve Karakterizasyonu" G. Özen Kahveci, S. Demirözü Senol, A. Uztetik Morkan ve İzzet Morkan, XXIV. Kimya Kongresi, Zonguldak Kara Elmas Üniversitesi-Zonguldak, 29 Haziran-2 Temmuz 2010.

9. "Apatit Tipinde $Ca_8Nd_2(PO_4)6O_2$ Bileşiğinin Yeni bir Yöntemle Sentezi ve Karakterizasyonu", S. Demirözü Senol, G. Özen Kahveci, A. Uztetik Morkan, XXIV. Kimya Kongresi, Zonguldak Kara Elmas Üniversitesi-Zonguldak, 29 Haziran-2 Temmuz 2010.

Communications to international scientific meetings

1. "Solid-State Synthesis and Characterization of a New Form of Na_2DyOPO_4 ", S. Demirozu Senol, A. Uztetik Morkan, 235th American-Chemical-Society National Meeting, New Orleans, LA, USA. April, 06-10, 2008.

2. "Synthesis and Characterization of Rare Earth Oxoapatite, $Ca_8Ln_2(PO_4)_6O_2$ (Ln: Gd, Dy)" S. Demirözü Senol, G. Özen Kahveci, A. Uztetik Morkan, 9th Conference on Solid State Chemistry, September 2010 in Prague.

3. " Solid-State Synthesis and Characterization of Novel Xenotime Type Rare-Earth Borophosphate, $LnBP_2O_8$", G. Özen Kahveci, S. Demirözü Senol, A. Uztetik Morkan and İzzet Morkan, 9th Conference on Solid State Chemistry, September 2010 in Prague.

Position held

Research Asisstant- Department of Chemistry, AIBU, Bolu, Turkey July 1999-present.